DISSERTATION

N-LINKED GLYCOSYLATION IS FUNDAMENTALLY LINKED TO THE SURFACE EXPRESSION OF NEUROLIGINS

Submitted by

Thomas Cast

Department of Biochemistry and Molecular Biology

In partial fulfillment of the requirements

For the Degree of Doctor of Philosophy

Colorado State University

Fort Collins, Colorado

Summer 2023

Doctoral Committee:

Advisor: Soham Chanda

Jennifer DeLuca
Santiago DiPietro
Stuart Tobet

Copyright by Thomas Peter Cast 2023

All Rights Reserved

ABSTRACT

N-LINKED GLYCOSYLATION IS FUNDAMENTALLY LINKED TO THE SURFACE EXPRESSION OF NEUROLIGINS

N-linked glycosylation is one of the most prevalent forms of post-translational modification, decorating secreted and cell-surface transmembrane proteins as they are trafficked along the secretory pathway. While well-characterized in most tissues, non-canonical N-glycan diversification has been reported to occur in the central nervous system. Chapter 2 of this dissertation describes the importance of N-linked glycosylation for the neuroligin family of synaptic cell-adhesion molecules (NLGN1-4). NLGNs play a crucial role in regulating synaptic transmission strength by recruiting neurotransmitter receptors to synapses. Mutation of N-glycosylated residues increased retention of each NLGN isoform in the endoplasmic reticulum (ER), consequentially reducing their ability to interact with presynapses. Pharmacological inhibition of various stages of the N-glycan maturation pathway further revealed that only the initial transfer of the polysaccharide is essential for the surface expression of NLGN proteins.

Chapter 3 characterizes a missense mutation identified in the NLGN4 gene of a patient with autism. This mutation, p.Arg101Gln (R101Q), is directly upstream of a conserved N-linked glycosylation site, which played a universal role for the surface localization of each NLGN isoform. Biochemical and cellular analysis revealed the NLGN4-R101Q variant to be immaturely glycosylated and mistrafficked, retained in the ER similarly to N-glycan site mutants. In neurons, the mistrafficked R101Q variant failed to reproduce the excitatory synaptogenic effects of NLGN4-WT, indicating an overall loss-of-function phenotype. Further, equivalent RQ mutations introduced in other NLGN isoforms mimicked the glycoprotein maturation and surface expression defects. Together, these findings reveal a profound overall significance of N-glycans for NLGNs and the conserved role of a specific N-linked glycosylation site for promoting the forward trafficking of NLGN protein.

ACKNOWLEDGEMENTS

I have so many people to thank for helping me complete this program. First and foremost is my advisor, Soham Chanda. Thank you for having me as the first graduate student in your lab and for showing me the rigorous work required to be a successful scientist. You quite literally taught me everything I know about science, and I will carry the lessons I learned from you throughout my scientific career. I will support my ideas with evidence and consideration, and stand up for myself and my well-being when it is right to do so.

To my committee, Santiago di Pietro, Stu Tobet, and Jake DeLuca, thank you for the support throughout these years and encouraging my independent understanding of my projects. To Santiago, for intriguing discussion in the joint journal club, and sharing of reagents across the hall, thank you. To Jake, I can't overstate how grateful I am for your career advice and consideration for my success as a scientist. And to Stu, thank you for your very, very low tolerance for nonsense. In both your neurodevelopment class and grant writing class, I learned to cut unnecessary fluff in order to make key details shine.

To Jim Bamburg and Laurie Minamide, thank you for being two of the most welcoming people I have ever met. Jim, rotating in your lab was my first experience in a graduate-level lab setting, and I learned so much about how to independently approach experiments. Attending your journal club throughout my time at CSU taught me how to ask the right questions of a scientific paper, and I eventually picked a good one to share! Laurie, I will never forget Winter of 2018, when you made me a blueberry cake for my birthday after you heard I don't like chocolate, having known me for about 3 months. Thank you both so much. To Alisa Shaw, thank you for showing me (more than once) how to order and manage reagents. Your assistance in Chapter 3, especially toward the dimerization assay, was instrumental in the success of these projects.

Thank you to all the members of the BMB department, and especially Steven Markus for your help figuring out how to purify a transmembrane protein. No big surprise, but it's not easy. Thank you to Andrea Ambrosio as well, for help finding reagents and emotional support when helping me figure out how to approach assays. To the BMB students, especially my cohort of Drew Tonsager, Amanda Kuerzi, Gabe Galindo, and Aldy Liman, we may not be the most social cohort, but we have it where it counts. Thanks for all the support and opportunities to talk about

our research. To past and current members of the Chanda Lab, Scott Burlingham, Orion Benner, Etta Carricaburu, Lily Lubow, and Daniel Boesch, thank you for all the fun and great discussions in the lab. Scott especially, your edits to this dissertation in particular were invaluable, thank you! Orion, it was truly a blast mentoring you these past few years, and thank you for your help collecting data for Chapter 2. Ban Alkurdi, Ambika Basu, and Lindsay Peterkin, thanks for the support and great times in and out of the MRB building.

To my friends in Denver and Seattle: Will Clawson, Kase Wille, Bobbi Erhart, Eric Silva, Jacob Yee, Ben Ely, Peter Bugos, Jack Strobel, Maddie Birchfield, Blake Troska, Christina Canino, Dylan Graff, Elizabeth Stewart, and Morgan Bergerud. I know you don't always get what I'm talking about, but I've loved explaining my research to you all. Thank you for your support! To Ashley and Aleksei, my friends from Gonzaga who somehow also ended up in Denver, I'm looking forward to spending more time with you and discussing all the science we're doing!

To my dad, also called Tom Cast, my mom Amy, and my siblings Frank and Jamie, thank you for your support as I tackled this whole endeavor. Sharing Fort Collins with you all has been a treat, and this will have to continue to be a vacation spot in the future! I love you all.

Last, and absolutely most definitely not least, I owe the biggest thanks to my best friend, partner in life, current fiancé and future wife, Madison Rose. Thank you for your trust and patience, even when "10 minutes" in the lab means 30, "30 minutes" means an hour, and "just one hour" means at least three. Your unwavering support is what made all this possible, and I can't wait for our future together! I love you. Also, can't forget our dog, Miles, the smartest dog in the world.

TABLE OF CONTENTS

ABSTRACT ii
ACKNOWLEDGEMENTS iii
CHAPTER 1: INTRODUCTION 1

1.1 Synaptic Cell Adhesion Molecules Regulate Synaptic and Sub-synaptic Organization 1
1.2 NLGN Proteins Maintain Synaptic Levels of Ionotropic Receptors 4
1.3 Molecular Characteristics and Post-translational Modification of NLGN Proteins 7
1.4 Mechanisms of N-linked Glycosylation 9
1.5 N-linked Glycosylation in the Central Nervous System 11

CHAPTER 2: N-LINKED GLYCOSYLATION CRITICALLY MODULATES SURFACE LOCALIZATION OF NLGN PROTEINS 13

2.1 Introduction 13
2.2 Materials and Methods 15
2.3 Results 24

2.3.1 Regulation of Endogenous NLGN Glycan Maturation 24
2.3.2 Contribution of N-glycan Sites to NLGN Glycoprotein Maturation and Stability 28
2.3.3 N-linked Glycosylation Promotes NLGN Export from the ER 34
2.3.4 N-glycan-Null Mutation Reduces NLGN Proteins' Presynaptic Recruitment Through Surface Expression Defects 37
2.3.5 Conserved N-glycan Site I Universally Reduces NLGN Surface Expression and Interaction with Presynaptic Terminals 40
2.3.6 Endogenous NLGNs are Heterogeneously Glycosylated on Neuronal Cell Surfaces 44
2.3.7 High-Mannose N-glycans are Sufficient for Endogenous NLGN Surface Expression 49

2.4 Discussion 51

2.4.1 Addition of the High-Mannose N-glycan Structure in the ER Regulates NLGN Secretory Trafficking 52
2.4.2 Differential Golgi-mediated N-glycan Processing of Neuronal NLGN Glycoproteins ..53
2.4.3 Regulation of Endogenous Glycosylation May Influence NLGN Surface Expression .54

CHAPTER 3: R101Q MUTATION IMPAIRS NLGN4 GLYCOSYLATION AND REDUCES SURFACE LOCALIZATION IN HUMAN NEURONS 57

3.1 Introduction 57
3.2 Materials and Methods 59
3.3 Results 67

3.3.1 Molecular Characteristics of NLGN4-R101Q Variant 67
3.3.2 NLGN4-R101Q is Specifically Impaired in Glycan Maturation and Secretory Transport 72
3.3.3 The Effects of RQ Mutation are Conserved in Other NLGN Isoforms 74

3.3.4 R101Q Mutation Exclusively Impairs Glutamatergic Synaptogenic Effects of Overexpressed NLGN4 76
3.3.5 R101Q Mutation Reduces NLGN4-Mediated Synaptogenesis in Ngn2-induced Neurons 80
3.4 Discussion 84
3.4.1 NLGN4-R101Q Synaptogenic Properties are Impaired Through Reduced Surface Expression 84
3.4.2 RQ Mutations Reduce NLGN Glycoprotein Maturation of Each Isoform 86
CHAPTER 4: CONCLUSIONS AND FUTURE DIRECTIONS 87
4.1 Occupancy of N-glycan Site I in NLGN4-R101Q 88
4.2 Deciphering the Varied Maturation of NLGN1 in Mouse Brain 90
4.3 Influence of N-glycosylation Toward NLGN-NRXN Molecular Interaction 91
REFERENCES 95

CHAPTER 1: INTRODUCTION

1.1 Synaptic Cell Adhesion Molecules Regulate Synaptic and Sub-synaptic Organization

Synapses represent the basic information processing units of the central nervous system (CNS), incorporating intercellular electrochemical signals into broader circuits that constitute complex sensory information and thought processes, including pain, emotion, memory, and executive function (Batool et al., 2019; Südhof, 2021; Fries et al., 2023). The canonical chemical synapse is composed of three primary regions: the presynapse, postsynapse, and synaptic cleft. In the standard model of anterograde synaptic signaling, vesicles within the presynaptic cell, filled with neurotransmitter (NT) chemicals by transporter proteins, fuse to the presynaptic membrane at the active zone (AZ) of the synapse, releasing NTs into the extracellular synaptic cleft. NTs subsequently bind to and activate receptors on the postsynaptic cell surface.

Postsynaptic receptors initiate a variety of downstream effects. Among the most predominant NT receptors are ionotropic receptors, which are ligand-gated ion channels and include α-amino-3-hydroxy-5-methyl-4-isoxazolepropionic acid (AMPA)-type, N-methyl-D-aspartate (NMDA)-type, and γ-aminobutyric acid type A ($GABA_A$) receptors (Crowder et al., 1987; Johnston, 1996; Shepherd and Huganir, 2007; Lu et al., 2009; Gassmann and Bettler, 2012; Diering and Huganir, 2018). Upon NT binding, these channels open, allowing ions to flow in or out of the cell according to their respective electrochemical gradients. Activation of AMPA receptors (AMPARs), by the NT glutamate allows Na^+ ions to flow into the neuron, reducing the recipient cell's membrane potential. NMDA receptors (NMDARs) are also activated by glutamate, but at resting membrane potential, these channels are blocked by Mg^{2+} ions. Only after depolarization, typically through AMPAR-mediated Na^+ influx, is the Mg^{2+} block released, and Ca^{2+} ions allowed to flow through open NMDARs into the neuron. This further depolarizes the postsynapse and triggers Ca^{2+}-mediated signal cascades which can alter synapse strength

(Bliss and Collingridge, 1993; Huganir and Nicoll, 2013; Colgan and Yasuda, 2014). Accumulation of enough depolarization events by glutamate receptor-mediated cation influx can depolarize the postsynaptic neuron from resting potential (~ -70 mV) to ~ -50 mV, triggering action potential (AP) firing (Hodgkin and Huxley, 1952c, a, b; Stuart et al., 1997). Thus, these events are classified as excitatory synaptic transmissions. In adults, $GABA_A$ receptors ($GABA_ARs$) are considered mediators of inhibitory synaptic transmission, as they allow Cl^- influx upon activation by the NT γ-aminobutyric acid (GABA), which hyperpolarizes the postsynaptic cell away from the AP threshold (Jacob et al., 2008). However, in the developing brain, high intracellular concentrations of Cl^- cause anion efflux upon $GABA_AR$ activation, making these events excitatory for the first few weeks of life (Ben-Ari, 2002). Various other NTs and corresponding receptors exist throughout the CNS, including serotonin receptors (5-HTRs), dopamine receptors, inhibitory glycine receptors, and metabotropic G-protein coupled receptors, but throughout the CNS glutamatergic and GABAergic synapses are most abundant (Micheva et al., 2010).

Synapses are small, dynamic, and tightly regulated. The width of the protein-rich postsynaptic density (PSD), where NT receptors are concentrated, ranges from 250 to 500 nm in diameter, with the opposing presynapse separated by the ~30 nm long synaptic cleft (Heupel et al., 2008; Meyer et al., 2014). However, the nanoscale organization of synapses is far from uniform. Recent advancements in super-resolution imaging have revealed the segregation of synaptic proteins into locally concentrated regions called sub-synaptic domains (SSDs). At glutamatergic postsynapses of both rat and mouse hippocampal neurons, AMPAR SSDs are around 80 nm wide (Fukata et al., 2013; MacGillavry et al., 2013; Fukata et al., 2021). Similarly, at inhibitory synapses in rat hippocampal neurons $GABA_ARs$ cluster in SSDs of ~200 nm diameter (Crosby et al., 2019). Postsynaptic SSDs are closely aligned with presynaptic AZs, identified by vesicle fusion accessory proteins, including bassoon and RIM1, which are similarly

concentrated in SSDs, and together form a transsynaptic structure termed the nanocolumn (Südhof, 2012; Biederer et al., 2017). NT molecules released from presynaptic vesicles at the AZ begin highly concentrated; local glutamate concentration at the site of vesicle release is estimated to be 1 mM. However, NTs quickly diffuse, and consequentially the probability of stimulating NT receptors decreases with increased distance from the vesicle fusion site. According to models, AMPARs 100 nm away from a site of glutamate vesicle fusion will not be reliably activated (Xu-Friedman and Regehr, 2004; Savtchenko and Rusakov, 2014; Biederer et al., 2017). Thus, alignment of pre and postsynaptic SSDs is critical for efficient NT-mediated synaptic signaling.

Strong evidence implicates synaptic cell-adhesion molecules (SCAMs) as mediators of transsynaptic alignment. Many distinct SCAMs occupy the synaptic cleft, engaging in transsynaptic interactions that govern the molecular organization of the pre and postsynapse. Some SCAMs expressed on both the pre and postsynapse engage in homophilic interactions as observed in canonical cell-cell adhesion; these include N-Cadherins and SynCAMs (Missler et al., 2012; Sudhof, 2018). More specialized SCAMs are specifically localized to either the pre or postsynapse and interact heterophilically. Neurexins (NRXNs) are a major family of presynaptic SCAMs that act as a “central hub” of transsynaptic interaction, binding to a variety of postsynaptic SCAM families including leucine-rich repeat transmembrane proteins (LRRTMs) and neuroligins (NLGNs), as well as dystroglycan (Südhof, 2008, 2021). Early evidence for the role of these transsynaptic interactions in coordinating pre and postsynaptic morphologies was apparent in artificial synapse formation assays. Overexpressing NRXN in heterologous cells (i.e. HEK293 or COS7) and subsequently co-culturing these cells with primary neurons induces the formation of postsynaptic structures by neurons surrounding the non-neuronal cells (Graf et al., 2004). Likewise, expressing NLGNs in co-cultured heterologous cells causes presynaptic terminals to accumulate (Scheiffele et al., 2000; Ko et al., 2009). More recently, SCAMs have

been implicated in regulating the structure of, and protein recruitment into SSDs. Ramsey et al. found in 2021 that acute enzymatic cleavage of LRRTM2's extracellular domain (ECD) reduced the density of AMPARs transsynaptically aligned to AZs. Crucially, this effected was observed without any alteration in the total number of AMPARs at the whole of the postsynaptic compartment (Ramsey et al., 2021). Similarly, NLGN1, a member of the NLGN family which localizes preferentially to excitatory synapses, regulates sub-synaptic AMPAR coordination with the AZ through intracellular interactions with the postsynaptic scaffolding protein PSD-95 (Haas et al., 2018).

1.2 NLGN Proteins Maintain Synaptic Levels of Ionotropic Receptors

No particular SCAM appears to be solely responsible for synapse formation; genetic knockout studies reveal no major change in synapse numbers upon individual deletion of most SCAMs (Sudhof, 2018). However, functional consequences with regard to synaptic transmission are often associated with the loss of certain SCAMs, particularly NLGNs. The NLGN protein family consists of five isoforms: NLGN1-3, NLGN4X, and NLGN4Y. NLGN1, as mentioned, localizes to glutamatergic postsynapses, where through PSD-95 interaction it recruits diffusing AMPARs and NMDARs to postsynapses, thus directly influencing excitatory synapse strength (Irie et al., 1997; Song et al., 1999). NLGN2 primarily localizes to inhibitory GABAergic postsynapses. There, it plays a role analogous to NLGN1, interacting with GABAergic postsynaptic scaffolding molecules gephyrin and collybistin and recruiting $GABA_A$Rs to the postsynapse (Varoqueaux et al., 2004; Poulopoulos et al., 2009; Gangwar et al., 2017). NLGN3 is present at both excitatory and inhibitory postsynapses, similarly recruiting NT receptors (Budreck and Scheiffele, 2007; Yoshida et al., 2021; Wang et al., 2022). In humans, NLGN4X and NLGN4Y genes are gametologs, an X-Y chromosome pair, and despite sharing ~97% sequence similarity, NLGN4Y is poorly expressed and inefficiently trafficked to cell surfaces

(Nguyen et al., 2020). NLGN4X (also called NLGN4) localizes preferentially to glutamatergic postsynapses where it interacts with PSD-95 and AMPAR subunits (Marro et al., 2019).

While its precise role remains somewhat controversial, evidence suggests NLGN4 likely attenuates AMPAR recruitment (Zhang et al., 2009; Marro et al., 2019; Cast et al., 2021). As regulators of NT receptors, NLGNs are critical for proper synaptic functioning. Genetic knockout of NLGN1-3, while minimally affecting synapse numbers, dramatically reduces evoked postsynaptic current (PSC) amplitudes of associated synapse subtypes (Chanda et al., 2017). While NLGN1-3 are strongly conserved between humans and mice, allowing for effective modeling of the endogenous roles of these three isoforms, mouse NLGN4 is evolutionarily divergent from the human NLGN4 (Bolliger et al., 2008; Maxeiner et al., 2020; Maxeiner et al., 2022). Mouse NLGN4 (also called NLGN4-*like*) is localized to inhibitory glycinergic postsynapses (Hoon et al., 2011; Ju et al., 2014), while strong evidence suggests that human NLGN4 regulates excitatory glutamatergic postsynaptic molecules (Zhang et al., 2009; Marro et al., 2019; Cast et al., 2021).

Because NLGNs directly control NT receptor recruitment to both glutamatergic and GABAergic postsynapses, this protein family plays crucial roles in balancing the excitatory/inhibitory (E/I) ratios of neural circuits (Hu et al., 2015). The dynamic balance between E/I signals in the brain is critical for memory and decision-making tasks (Capano et al., 2015; Lam et al., 2022) and contributes toward maintaining brain wave oscillations (Isaacson and Scanziani, 2011). Altering expression of NLGN1 through transgenic overexpression or knockout shifts the E/I balance and alters spatial memory in mice (Kim et al., 2008; Dahlhaus et al., 2010). As NLGN2 recruits inhibitory NT receptors, its expression throughout the brain can also impact the E/I ratio (Durieux et al., 2016), specifically regulating fear memory, stress response, and social interactions observed in mice (Hines et al., 2008; Perova et al., 2015; Troyano-Rodriguez et al., 2019). Maintenance of E/I ratio is critical for healthy

neurodevelopment. Aberrant E/I ratios in humans are associated with neuropathologies including epilepsy (Fritschy, 2008), schizophrenia (Liu et al., 2021), and autism spectrum disorder (ASD; Bruining et al., 2020), with which NLGNs are strongly implicated.

Disrupted NLGN expression or function is associated with a number of neurological diseases. It was recently shown that NLGN1 protein is reduced in the parietal cortex and hippocampus of patients with Alzheimer's Disease (AD) and amnesiac mild cognitive impairment (Dufort-Gervais et al., 2020; Camporesi et al., 2021). Chronic injection of amyloid-β peptide into mice reduces NLGN1 protein and mRNA expression, and causes loss of spatial memory (Blundell et al., 2010; Dufort-Gervais et al., 2020). NLGN1 polymorphisms are also associated with schizophrenia (Zhang et al., 2015), and missense mutations have been identified in the NLGN2 genes of patients with schizophrenia, one major example being NLGN2-R251H (Sun et al., 2011). This mutation reduces the expression of NLGN2 protein, similar to a NLGN2 nonsense mutation identified in another patient with schizophrenia (Parente et al., 2017). A NLGN2-R251H knock-in mouse model manifests behavioral abnormalities associated with mental disorders and a severe loss of GABAergic synaptic signaling (Chen et al., 2017; Jiang et al., 2018).

The developmental disorder most commonly associated with NLGN mutations is ASD. In fact, the first genetic mutation specifically linked to autism was NLGN3-R451C (Jamain et al., 2003), which has since been extensively characterized (Comoletti, 2004; Tabuchi et al., 2007; Wang et al., 2022). This mutation causes an increase in excitatory synaptic signaling in the hippocampus but also increases inhibitory signaling in the somatosensory cortex (Etherton et al., 2011), and alters social interaction in mouse models (Burrows et al., 2015; Burrows et al., 2017; Burrows et al., 2022). Infrequently, copy-number and missense mutations in NLGN1 are associated with ASD and intellectual disability (Glessner et al., 2009; Nakanishi et al., 2017; SFARI, 2021b). However, over 50 NLGN4 mutations have been identified in patients with ASD,

including chromosomal deletion, nonsense mutations, and several missense mutations (Jamain et al., 2003; Laumonnier et al., 2004; Chocholska et al., 2006; Lawson-Yuen et al., 2008; Pampanos et al., 2009; Zhang et al., 2009; Bemben et al., 2015; Chanda et al., 2016; SFARI, 2021a).

1.3 Molecular Characteristics and Post-translational Modification of NLGN Proteins

NLGN isoforms are highly structurally conserved. They are each single-pass transmembrane proteins with an N-terminal ECD consisting of a globular acetylcholinesterase (AChE)-like domain (although enzymatically inert), followed by a disordered stalk which leads to the transmembrane domain and finally a short C-terminal intracellular domain (ICD). NLGNs constitutively form dimers through their AChE-like domains, and evidence suggests that dimerization is a requirement for the export of the proteins from the endoplasmic reticulum (ER; (Poulopoulos et al., 2012). While thought to most often form homodimers, NLGN1/NLGN3 and NLGN2/NLGN3 heterodimers are known to form (Budreck and Scheiffele, 2007; Poulopoulos et al., 2012; Shipman and Nicoll, 2012). At the synapse, each NLGN monomer interacts with a presynaptic NRXN molecule in a calcium-dependent manner (Arac et al., 2007; Fabrichny et al., 2007).

Many studies demonstrate clear roles of NLGN isoforms' ECDs and ICDs that work in concert to bestow the characteristic properties of NLGNs. NLGN1 apposition to presynapses is, unsurprisingly, dependent on its extracellular domain and unaffected by deletion of its C-terminal ICD (Mondin et al., 2011). However, without its ICD, NLGN1 dissociates from AMPAR SSDs and is unable to recruit AMPARs to postsynapses (Haas et al., 2018). Conversely and intriguingly, NLGN1-mediated recruitment of NMDARs may be dependent on its ECD, specifically its ability to interact with NRXN (Wu et al., 2019). Interestingly, all NLGN isoforms' ICDs contain conserved sequences for interaction with both the excitatory postsynaptic scaffolding protein PSD-95 and the inhibitory scaffold gephyrin. In some cases, differences in

actual affinity for these scaffolds results from specific motifs, e.g. a collybistin-binding motif found in NLGN2's ICD facilitates its recruitment of gephyrin (Poulopoulos et al., 2009). Further, deletion of the PSD-95-interacting motif from NLGN2's ICD does not affect its recruitment of $GABA_A$Rs to inhibitory synapses (Nguyen et al., 2016), which is expected as PSD-95 is largely absent from inhibitory postsynapses. In other cases, phosphorylation of intracellular residues by various kinases influences NLGN isoforms' affinity for postsynaptic proteins (Giannone et al., 2013; Antonelli et al., 2014; Bemben et al., 2014; Jeong et al., 2017). Phosphorylation of NLGN1-Y782 by tropomyosin receptor kinase B (TrkB) and TrkC is stimulated by extracellular interaction with NRXN and increases the protein's affinity for PSD-95, thus increasing AMPAR recruitment (Giannone et al., 2013; Letellier et al., 2018; Letellier et al., 2020). Likewise, phosphorylation of NLGN2 residue Y770 reduces NLGN2's interaction with gephyrin; this site is minimally phosphorylated *in vivo* (Poulopoulos et al., 2009; Nguyen et al., 2016; Letellier et al., 2018). Recent studies indicate that phosphorylation of NLGN2-Y770 may be linked to phosphorylation of a nearby tyrosine (Y714), which modulates NLGN2-gephyrin interaction and increases NLGN2 internalization into recycling endosomes by SNX27 (Halff et al., 2019; Halff et al., 2022).

Aside from phosphorylation, another fundamental post-translational modification (PTM) that NLGNs undergo is glycosylation, which is partitioned into two major classifications: N-linked and O-linked glycosylation. N-linked glycosylation begins in the endoplasmic reticulum (ER) with the transfer of a preformed oligosaccharide *en bloc* to an asparagine residue of a nascent polypeptide, as determined by the consensus sequon N-X-T/S, where X≠P (Bieberich, 2014; Taguchi et al., 2021). O-linked glycans are first added to serine or threonine residues of folded glycoproteins trafficking through the Golgi. The initial saccharide of the chain is typically N-acetylgalactosamine (GalNAc), which is then modified by the addition of other sugars producing any of the 8 known core structures (Van den Steen et al., 1998; Wilkinson and Saldova, 2020).

O-glycan chains can then be further diversified by the addition of glucose, fucose, or sialic acid residues. The heterogeneity of O-glycan structures has made structural and functional study difficult. However, terminal O-glycan moieties are important for immune self-recognition and cell-cell linkages (Vitiazeva et al., 2015; Chang et al., 2020; Wandall et al., 2021).

NLGN proteins are heavily modified by both O- and N-linked glycosylation. O-glycans decorate their stalk domain (Irie et al., 1997; Hoffman et al., 2004), while multiple N-glycan sequons are found within their AChE-like domain and appear to be critically linked to NLGN function, discussed further in Chapter 2. Early studies of NLGN1 confirmed the occupancy of its predicted N-linked glycan sites using mass spectrometry of recombinant NLGN1 expressed in HEK293 cells (Hoffman et al., 2004). Then, using surface plasmon resonance, Comoletti et al. discovered that one particular N-glycan site, residue N303, modulates recombinant NLGN1's affinity for NRXN via steric hindrance (Comoletti et al., 2003). NLGN1-N303 is located within a short alternatively spliced peptide sequence, and it was shown that alternative splicing can control NLGN1 glutamatergic synapse induction by altering its NRXN affinity (Boucard et al., 2005; Chih et al., 2006; Koehnke et al., 2010). However, the NLGN1-4 contain in total 11 N-linked glycosylation sites, and it remained unclear how these sites affect the molecular and functional features of NLGNs in a neuronal context.

1.4 Mechanisms of N-linked Glycosylation

A number of enzymes are involved in the processing and diversification of N-glycans. First, the oligosaccharyltransferase (OST) complex transfers the stereotyped immature N-linked polysaccharide to nascent polypeptides as they are translocated into the ER. The core of the immature oligosaccharide contains two sequential N-acetylglucosamine (GlcNAc) residues, followed by a triantennary mannose-rich glycan structure which is capped by three sequential glucose residues. Metazoans express two mutually exclusive catalytic subunits of the OST complex, STT3A and STT3B, which are highly conserved with monomeric archaeal and

eubacterial OSTs (Lizak et al., 2011). STT3A and STT3B are catalytically similar, but the two subunits have slightly non-overlapping roles. STT3A-containing OST complexes associate with the Sec61 translocon channel, scanning the polypeptide for the consensus sequon as it is translocated into the ER (Helenius and Aebi, 2004; Shrimal et al., 2015). Once the sequon is recognized, STT3A transfers the mannose-rich glycan chain from the lipid donor to the Asn residue. Because STT3A glycosylates unfolded polypeptide chains, its glycosylation event is considered co-translational or co-translocational.

STT3B is catalytically identical to STT3A, and its primary role is to maximize glycan occupancy by recognizing sequons skipped by STT3A (Shrimal et al., 2015; Cherepanova et al., 2016). STT3B complexes glycosylate proteins post-translationally, and contain subunits which form transient mixed disulfide bonds with cysteine residues either up or downstream from the sequon to facilitate this process. (Schulz et al., 2009; Mohorko et al., 2014). While STT3A and STT3B recognize the same N-glycan sequon and are decidedly redundant in activity, there is evidence for substrate specificity between the two; selective knockdown or knockout of either subunit does not significantly perturb the overall cellular glycome but leaves certain substrates hypoglycosylated (Shrimal et al., 2015; Cherepanova and Gilmore, 2016; Cherepanova et al., 2019). While the exact principles governing N-glycan site occupancy and STT3A/B substrate preference remain elusive, amino acid residues neighboring N-glycan acceptor sites are known to contribute toward glycosylation efficiency. Proline, for example, is strictly excluded from the +1 residue respective to the acceptor Asn due to incompatibility with the STT3 peptide recognition site (Taguchi et al., 2021). Further, as evidenced by substrate-specific effects of STT3A or B depletion (Cherepanova and Gilmore, 2016; Cherepanova et al., 2019) and N-glycan sequon optimization studies (Gavel and von Heijne, 1990; Ben-Dor et al., 2004; Huang et al., 2017), certain amino acid neighbors, e.g. an upstream aromatic residue (Murray et al., 2015), promote N-glycosylation.

Within the ER, nascent glycoproteins are sequestered by calnexin (CNX) and/or calreticulin (CALR) until properly folded, following which terminal glucose residues are removed from the oligosaccharide and the protein is translocated to the Golgi apparatus (Helenius and Aebi, 2004; Ferris et al., 2014; Xu and Ng, 2015). There, N-glycans undergo additional modification through sequential cleavage and transfer of saccharides by glycosidases and glycosyltransferases (Moremen et al., 2012). The resulting diversified structures are classified as “hybrid,” which contain both mannose-rich and substituted GlcNAc linkages, and “complex,” wherein GlcNAc-linked moieties have replaced both mannose antennae.

1.5 N-linked Glycosylation in the Central Nervous System

In most mammalian tissue, the vast majority of N-glycans present on surface-localized transmembrane proteins are of the “complex” variety (An et al., 2012; Stanley et al., 2022). In contrast to other tissue types, the neural glycome is distinctive in that many “immature” or high-mannose N-glycans are detected on neuronal cell surfaces (Hanus et al., 2016). The expression profile of glycosidase and glycosyltransferase enzymes in the ER and Golgi, critical in determining the cellular glycome (Moremen et al., 2012), is dramatically altered in the mouse CNS compared to plasma glycoproteins, resulting in divergent glycomes (Williams et al., 2022). Glycosylation patterns differ within the brain as well. This is evident through mass spectrometry analysis of cerebellar vs. cortical glycan populations (Williams et al., 2022) and on the single-protein scale. The protein family Synaptic Cell Adhesion Molecule (SynCAM)1-3 preferentially engage in heterophilic interactions between isoforms expressed on either the pre or postsynapse (Fogel et al., 2007). Glycan modification of these proteins in mice, represented by banding patterns on Western blots, differ by both brain region and age (Fogel et al., 2007; Fogel et al., 2010). These findings demonstrate specific control of glycan maturation between regions of the brain and differential glycosylation altogether in the CNS vs. non-neural tissue.

Beyond differential expression of N-glycan maturation enzymes within the secretory pathway, it has recently become clear that some neuronal transmembrane proteins bypass the secretory pathway altogether. AMPAR subunits GluA1-4 expressed on neuronal surfaces are modified by high-mannose N-glycans and are sensitive to Endoglycosidase H (Endo H), which cleaves N-glycans but is inhibited by fucose modification which occurs in the Golgi (Tucholski et al., 2014; Hanus et al., 2016; Kennedy and Hanus, 2019). By using light-triggered release of proteins from the ER and tracking their subsequent localization, Bourke et al. showed that GluA1 is able to traffic directly from dendritic ER to cell surfaces, bypassing the Golgi. In contrast, NLGN1 is seemingly obligated to localize first to the Golgi, peaking in concentration there within 10 minutes of ER release and arriving at distal cell surfaces significantly later than GluA1 (Bourke et al., 2021). Thus, transmembrane protein trafficking and glycoprotein modification are diversely regulated in the CNS, but the mechanisms which determine a protein's proclivity for canonical or non-canonical secretory processing are unclear.

In the data presented in this dissertation, I investigate the role of N-glycosylation for proper NLGN functioning. In Chapter 2, systematic mutagenesis of predicted N-glycosylation sites throughout the NLGN family reveals a dependence on N-linked glycosylation for the secretory export of NLGNs. Further, a conserved N-glycosylated residue plays a universal role in regulating the surface trafficking of each NLGN isoform. In Chapter 3, I present the characterization of a NLGN4 missense mutation found in a patient with autism. This mutation inhibits N-glycan maturation of NLGN4 protein, and is adjacent to the conserved N-linked glycosylation site mentioned above. The mutant NLGN4 is retained in the secretory pathway and inhibited in its surface localization, reducing overexpression-induced excitatory synaptogenesis NLGN4 at synapses. This work highlights the importance of N-glycans for appropriate synaptic localization of NLGN proteins and implicates ASD-associated mutations as inhibiting N-linked glycosylation.

CHAPTER 2: N-LINKED GLYCOSYLATION CRITICALLY MODULATES SURFACE LOCALIZATION OF NLGN PROTEINS

The research presented in this chapter was performed in collaboration with Orion Benner, Laurie Minamide, Zephyr Lenninger, and Soham Chanda.

2.1 Introduction

NLGNs, as transmembrane proteins, are heavily modified by glycans. Pioneering studies of NLGN1 predicted that O-linked glycans decorate the disordered extracellular stalk domain (Ichtchenko et al., 1995; Comoletti et al., 2003) which was later confirmed through mass-spectrometry (Hoffman et al., 2004). NLGN isoforms are also modified by N-linked glycosylation, shown in one case to regulate recombinant NLGN1's affinity for its binding partner NRXN1β (Comoletti et al., 2003). By mutating each of the four predicted N-glycan sequons in NLGN1's globular domain, the researchers discovered that glycosylation of NLGN1's unique N303 residue specifically governs its interaction with NRXN. It was later revealed that N303 lies within an alternatively spliced peptide sequence, allowing for *in vivo* control of NLGN1's affinity for NRXN by indirectly adjusting N-linked glycosylation (Boucard et al., 2005; Chih et al., 2006; Koehnke et al., 2010). However, the general impact of N-glycosylation for the NLGN family is unclear. NLGN2-4 share two conserved N-linked glycosylation sites with NLGN1, and NLGN2 additionally contains a unique N-glycan site. Whether these glycosylated residues contribute toward fundamental qualities of NLGN proteins including folding stability, surface expression, and subsequent interaction with NRXN has not been described.

N-glycosylation is also closely tied to the trafficking status of NLGNs. Monitoring glycosylation status through application of specific glycosidases is a reliable reporter of whether a glycoprotein has progressed out of the ER and into the Golgi in the canonical secretory pathway. This technique has been utilized to study the trafficking requirements and surface populations of NLGN proteins (Poulopoulos et al., 2012; Hanus et al., 2016; Chmielewska et al.,

2019). Crucially, N-glycan maturation of NLGNs is often impacted by ASD-associated mutations (Zhang et al., 2009; De Jaco et al., 2010; Cast et al., 2021), and although correlated with trafficking defects, the causal relationship between surface expression and glycosylation of NLGN isoforms has not been addressed.

The research presented in this chapter describes the role of N-linked glycosylation for maturation and secretory trafficking of the NLGN protein family. First, I report isoform-specific variation in glycan maturation status of endogenous NLGN expressed throughout the mouse brain. Systematic N-glycan site mutagenesis then reveals a cumulative yet selective impact of a N-glycan sites on NLGN glycoprotein maturation and anterograde secretory trafficking; mutagenic deletion of certain N-glycan sites results in reduced surface availability, while global mutation of N-glycosylated residues dramatically reduces NLGN surface expression, consequentially restricting interaction of NLGNs with presynaptic terminals. Second, through a combination of surface biotinylation and lectin pulldown assays, I reveal that endogenous NLGNs expressed in mouse and human neurons express a uniformly heterogeneous population of N-glycan moieties on the cell surface. This is in contrast to the same proteins expressed ectopically in HEK293 cells, which are primarily modified by “complex” N-glycan moieties. Finally by pharmacologically inhibiting stages of the N-glycan maturation pathway, I further show that N-glycan modification by Golgi-associated mannosidases is unnecessary for NLGN glycoproteins to reach the cell surface. These findings highlight the fundamental importance of N-glycosylation for ER export of NLGNs and demonstrate how alterations in the NLGN glycan profile may weaken the availability of NLGN proteins at neuronal cell surfaces.

2.2 Materials and Methods

Institutional approvals: All cell culture methods as well as lentivirus production procedures were authorized by Colorado State University, Institutional Biosafety Committee (CSU, IBC protocol # 19-059B). All experiments with mice were approved by the Institutional Animal Care and Use Committee (CSU, IACUC protocol # 1482).

Mouse brain dissection: Adult (P60-P75) male and female WT mice of C57BL/6 strain were sacrificed, brains were extracted from decapitated heads, placed in ice-cold Hank's Balanced Salt Solution (HBSS) buffer, and different brain regions were surgically isolated under a dissection microscope (Olympus SZX16) immediately after. The tissues were cut into fine pieces and incubated in RIPA buffer (150 mM NaCl, 5 mM EDTA, 25 mM Tris pH 7.4, 1% Nonidet P-40 substitute, 0.5% sodium deoxycholate) supplemented with Halt protease inhibitor cocktail (PIC; catalog # 78429, Thermo Fisher) for 6-8 hours at 4°C. The lysates were triturated, spun at 4,000 x g for 5 minutes, supernatants with protein extracts were aliquoted, and stored at -20°C prior to experiments.

Primary neuronal cultures: Primary neurons were derived from newly born (P0-P1) pups of C57BL/6 animals. Dissected cortices and hippocampi were digested at 37°C for ~15 minutes inside an incubator, with 10 U/ml papain (catalog # LS003126, Worthington Biochem) in HBSS buffer containing 2 mM Ca^{2+} and 0.5 mM EGTA. The cortices and hippocampi were then washed thoroughly with HBSS buffer, dissociated in N3 media (composition: DMEM/F12 [Thermo Fisher] + N2 [Thermo Fisher] + B27 [Thermo Fisher] + insulin [20 µg/ml, Sigma-Aldrich]), additionally supplemented with 5% fetal bovine serum (FBS, Atlas Biologicals) + 1% penicillin-streptomycin mix (Thermo Fisher), and seeded onto Matrigel (Corning, Sigma-Aldrich) pre-coated glass coverslips placed inside individual wells of 24-well dishes. The day of neuronal plating was considered as 0 day *in vitro* (DIV 0). On DIV 2-3, FBS concentration was reduced to ~2.5% by adding almost equal volume of N3 media without any serum, and included 5-

fluorodeoxyuridine (FdU, 10 µM) to inhibit glial proliferation after reaching 70-80% confluency. Fresh media of 50% volume was added at DIV 10.

Cell lines: The HEK 293T (containing SV40 T-antigen) cells were commercially available from Takara Bio USA (catalog # 632180). The human iPS cells carrying doxycycline-inducible Ngn2 transgene (i.e., the WTC-11 line, (Wang et al., 2017) was a gift from Dr. Michael E. Ward, National Institute of Neurological Disorders and Stroke (NINDS).

Generation of human neurons: WTC-11 cells were maintained in mTeSR™1 / mTeSR™ Plus media (StemCell Technologies) under feeder-free condition. Media was changed every day. When cell density reached 60-70%, they were dissociated with phosphate-buffered saline (PBS) + 0.5 mM EDTA and replated at ~1:6 dilution onto Matrigel -coated wells. During passage, cultures were additionally supplemented with ROCK-inhibitor Y-27632 (2.5 µM, MedChem Express) overnight, but excluded for later media changes. For neural differentiation, these cells were plated at 1:15 dilution, cultured with N3 media (DMEM/F12 [Thermo Fisher] + N2 [Thermo Fisher] + B27 [Thermo Fisher] + insulin [20 µg/ml, Sigma] + 1% penicillin/streptomycin [Thermo Fisher]), and induced by continuous doxycycline (2 µg/ml) exposure. Neurons were harvested 5 days after reprogramming was initiated.

Vector design: Reliable antibodies against NLGN extracellular domains do not exist. Hence, we introduced a hemagglutinin (HA) epitope-tag in NLGN coding sequences (CDS) after their corresponding N-terminal signal peptide (rat NLGN1: 1–45, rat NLGN2: 1–14, mouse NLGN3: 1–34, and human NLGN4X: 1–43 amino-acids) cleavage sites, which does not interfere with their cell-surface trafficking (Chanda et al., 2016; Marro et al., 2019). Alanine-substitutions for individual and all (referred to as ‘Null’) potential N-linked glycosylation sites within the AChE domains of NLGN CDS were performed using site-directed mutagenesis. These constructs were inserted into a vector preceded by cytomegalovirus (CMV) promoter, a Kozak sequence, and followed by a green fluorescent protein (EGFP) cassette driven by internal ribosome entry

site (IRES). The NRXN1β construct without splice-site #4 (NRXN1β^{-S4}) was cloned from rat cDNA preparation and co-expressed with IRES-mOrange reporter.

NLGN overexpression: HEK cells were transfected with NLGN constructs using PEI, media was exchanged at 8 and 24 hours, and cells were analyzed between 48-72 hours by immunocytochemistry and Western blots.

Cell-aggregation assay: Separate HEK cell cultures were transfected with either NRXN1β-mOrange or different NLGN constructs with EGFP reporter. An EGFP-only vector was used as negative control. After 48 hours, cells were washed with PBS and lifted with 1 mM EDTA. They were spun at ~800 x g for 5 minutes, the pellets were triturated and resuspended at a density of 1 x 10^6 cells/ml in DMEM media (Genesee Scientific) supplemented with 20 mM $CaCl_2$. Equal amounts of NRXN- and NLGN -expressing cells were mixed together (100 µl each) at 37°C for 2 hours in a tube rotator. Mixtures were spotted onto glass slides with cut pipette tips and immediately imaged in tile-scan mode using an inverted STELLARIS 5 (Leica Microsystems) laser scanning microscope equipped with a 5x dry objective. Cell aggregates were analyzed using Mander's co-localization coefficient.

Artificial synapse formation: Primary hippocampal neurons containing limited number of astroglia cells were obtained from E16 embryos of timed-pregnant WT C57BL/6J mice, and seeded onto poly-D-lysine (catalog # P0899, Sigma-Aldrich) -coated glass coverslips, at a density of 100-200 cells/mm^2. Neurons were cultured in Neurobasal Plus medium (Thermo Fisher) supplemented with B27, 2% FBS, and 10 µM FdU; the media was half-exchanged (50% fresh + 50% glia-conditioned media) every two days. At DIV 10 of the neuronal cultures, separately maintained HEK cells were transfected with respective NLGN constructs or an EGFP-only negative control. After 48 hours, these HEK cells were lifted with PBS + EDTA, pelleted down, triturated as single cells, and then resuspended in Neurobasal media. Transfected HEK cells were counted using EGFP fluorescence, and distributed at a density of

~3000 cells into each well containing DIV 12 neurons. After 4 days of co-culture, coverslips were fixed with 4% paraformaldehyde (PFA) dissolved in PBS, and stained as described below.

Glycosidase treatment: For glycosidase treatment of endogenous NLGNs, 20 µl lysates from different mouse brain regions or differentiated human neurons were denatured at 70°C (to minimize NLGN aggregation) and treated with either α2-3,6,8,9 Neuraminidase A (sialidase; catalog # P0722, New England Biolabs) or PNGase F (catalog # P0704, New England Biolabs) for 3 hours at 37°C, according to manufacturer specifications. The control samples were treated similarly, but with equal volumes of RIPA buffer instead of glycosidases.

For glycosidase treatments of HA-tagged NLGNs overexpressed in HEK cells, lysates were incubated with mouse anti-HA antibody (1:100; catalog # h3663, Sigma-Aldrich) in a tube rotator overnight at 4°C. The lysates and antibody mix were incubated with protein G-Sepharose beads (catalog # 6511, BioVision) while rotating for 3-4 hours at 4°C. The beads were washed 3 times with RIPA buffer + PIC, aliquoted into 4 equivalent fractions, centrifuged at ~15,000 x g for 4 minutes, and then resuspended into 20 µl RIPA buffer. Aliquots were exposed to either PNGase F, or sialidase, or PNGase F + sialidase + O-glycosidase (catalog # P0733S, New England Biolabs), per manufacturer specifications for 3 hours at 37°C in a tube rotator. To elute deglycosylated NLGNs, the beads were centrifuged, supernatants were removed, and 15 µl SDS loading buffer was added. Samples were boiled for 10 minutes, centrifuged at ~15,000 x g for 4 minutes, and eluates collected for immunoblotting.

Thermal stability assay: Lysates of HEK cells expressing NLGN1-4 WT vs. corresponding glycan-null versions for >= 48 hours were collected in RIPA buffer + PIC, heated for 15 minutes at different temperature gradients in a thermocycler (BioRad T100). The samples were then centrifuged at ~15,000 x g for 5 minutes in order to precipitate aggregated protein fractions, the supernatants were collected and analyzed using Western blots.

Protease sensitivity assay: Transfected HEK cells were lysed and collected in RIPA buffer as described, but without any PIC. Immediately after collection, crude lysates were distributed into individual tubes and treated with varying concentrations of trypsin (catalog # PR-V5280, Fisher Scientific). After 5 minutes, reactions were quenched by adding 10% Sodium dodecyl-sulfate (SDS) loading buffer and analyzed by western-blots.

Data from thermal-stability and protease sensitivity assays were fitted to Boltzmann sigmoidal curves ($y = \frac{1}{1+e^{\frac{V50-x}{Slope}}}$) to compute V50 values for each experimental trial, and compare between WT vs. glycan-null groups.

Glycosyltransferase inhibitor drug treatments: Differentiated WTC-11 neurons were cultured with drugs (Kifunensine [Kf], 5 µM; 1-Deoxymannojirimycin [DMJ], 75 µM; Swainsonine [Sw], 100 µM; or Tunicamycin [Tm] at 0.25 and 0.5 µM) for 48 hours starting at day 4 post differentiation. All drugs were diluted in N3 medium and applied via a partial medium exchange.

Surface biotinylation: Neuronal surface proteins were labeled with biotin using Pierce™ Cell Surface Biotinylation and Isolation Kit (catalog # A44390, Thermo Fisher Scientific) following manufacturer specifications. Briefly, cells were incubated in PBS containing biotin ligase for 10 minutes at RT, then washed with TBS to quench biotin ligation reactions. Cells were lifted and pelleted, and whole-cell lysate was then extracted and incubated with provided NeutrAvidin agarose beads to isolate biotin-labeled proteins. As the NeutrAvidin agarose beads were washed, the initial flow-through was saved and used as internal protein fraction. After beads were washed and biotin-labeled proteins eluted, internal and surface fractions were diluted as necessary to achieve equal respective volumes.

Lectin-based precipitation: Lysate (whole-cell, surface fraction, or internal fraction) was mixed with agarose beads bound with the following lectins: Concanavalin A (ConA; catalog # AL-1003, Vector Labs), Ricinus communis agglutinin I (RCA; catalog # AL-1083, Vector Labs),

or wheat germ agglutinin (WGA; catalog # AL-1023, Vector Labs). Bead-lysate mixes were incubated at 4 °C overnight while rotating end-over-end. Beads were pelleted by light centrifugation and rinsed thrice with ice-cold PBS. To release glycoproteins bound by the lectin-agarose beads, pellets were resuspended in 20-40 µl SDS loading buffer and boiled for 10 minutes. The mixture was vortexed, centrifuged at 16,000x G for 3 min, and eluate collected to run on an SDS-PAGE.

Immunoblotting: Transfected HEK cells were lifted with 1 mM EDTA in PBS, and lysed in RIPA buffer with PIC. Alternatively, samples were collected from various mouse brain regions or iPS cell (WTC-11) -derived human neurons. The protein extracts were mixed with 10% SDS loading buffer, then run on either 5%, 7.5%, or 10% polyacrylamide gel electrophoresis (SDS-PAGE), and transferred to nitrocellulose membrane. The membranes were blocked with 5% bovine serum albumin (BSA) in Tris-buffered saline with 0.1% Tween-20 (TBS-T) while rocking for at least 1 hour at 37°C, and then incubated overnight at 4°C with corresponding primary antibodies diluted in blocking buffer. Primary antibodies included: mouse anti-NLGN1 (1:500; catalog # 129111, Synaptic Systems), or rabbit anti-NLGN2 (1:1000; catalog # 129202, Synaptic Systems), or rabbit anti-NLGN4X (1:1000; catalog # A7986, ABclonal), or mouse anti-HA (1:1000), chicken anti-GFP (1:500; catalog # GFP-1020, Aves Labs), or mouse anti-GAPDH (1:50000; catalog # 60004-1-Ig, Proteintech). Blots were thoroughly washed 5 times with TBS-T over an hour, subsequently incubated with fluorescent-dye conjugated secondary antibodies (1:2000; DyLight 680/800, Invitrogen) diluted in blocking buffer (TBS-T, containing BSA) for 1-2 hours, washed again for 5 times with TBS-T, and then imaged immediately using a LI-COR Odyssey CLx system.

The brightness and contrast of all protein bands were uniformly adjusted using Image Studio Lite (version 5.2) software. Protein contents were estimated by plotting total-intensity profiles for each lane and calculating the peak areas underneath. For glycosidase assays, the

Y-coordinates of individual peaks were recorded, and mobility shifts were normalized to the visible dye-front as well as a 100 kDa ladder (catalog # P007, GoldBio).

Immunostaining: Primary mouse neurons, differentiated human neurons, and HEK cells cultured on coverslips were washed once with PBS and fixed immediately with 4% PFA for 30 minutes at room temperature, followed by an additional PBS wash. Cells were blocked in PBS + 10% cosmic calf serum (CCS, HyClone) for at least 1 hour at 37°C while rocking, incubated with primary antibodies for 2 hours at 37°C or overnight at 4°C, washed 4 times with blocking buffer, and incubated with Alexa Fluor 488/555/647 dye (Invitrogen) -conjugated secondary antibodies for 1-2 hours at 37°C. Coverslips were then washed twice with blocking buffer and twice with PBS, and mounted upside down on glass-slides using Fluoromount-G (Southern Biotech). To detect HA-epitopes on NLGNs localized at the cell surface, cultures were stained under non-permeabilized conditions, i.e., without any Triton X-100. For assays where permeabilization was required, Triton X-100 (0.1%) was subsequently applied to blocking buffer and for all following steps, including washes as well as primary or secondary antibody dilutions.

Primary antibody combinations included: mouse anti-Oct3/4 (1:500-1000; catalog # sc-5279, Santa Cruz Biotechnology), mouse anti-Ki-67 (1:500; catalog # 550609, BD Biosciences), mouse anti-Tuj1 (1:500; catalog # 801202, BioLegend), chicken anti-MAP2 (1:500; catalog # ab5392, Abcam), rabbit anti-Synapsin1/2 (1:1000; catalog # 106002, Synaptic Systems), mouse anti-HA (1:1000; catalog # h3663, Sigma-Aldrich), chicken anti-GFP (1:500; catalog # GFP-1020, Aves Labs), rabbit anti-calnexin (1:500; catalog # PA5-34754, Thermo Fisher), rabbit anti-GM130 (1:300; catalog # A5344, ABclonal), rabbit anti-vGluT1 (1:500; catalog # 135303, Synaptic Systems), rabbit anti-vGAT (1:500; catalog # 131003, Synaptic Systems). When applicable, the cell nuclei were stained with DAPI (1:50000; catalog # D1306, Thermo Fisher) for 5-10 minutes in washing buffer.

Image acquisition and analysis: Images were captured using STELLARIS 5 confocal microscope equipped with Power HyD detectors and LasX software. Series of optical z-sections (~0.5-1 µm thickness) were acquired with 20x (dry, 0.75 na), 40x (oil immersion, 1.3 na), and 63x (oil immersion, 1.4 na) plan-apochromatic objectives.

Images were processed and analyzed using FIJI-ImageJ (NIH) software. Surface trafficking of HA-tagged NLGNs expressed in HEK cells or neurons was monitored by maximum intensity z-projections of HA channels and normalized to corresponding EGFP signals. Subcellular distribution of HA-NLGNs was assessed by measuring signal intensities across line profiles and normalizing them to maximum binned values. In order to quantify synaptic specifications (e.g., puncta density, size, total intensity) formed along neuronal processes, z-projected synaptic signals from regions-of-interest (ROIs) were superimposed and normalized with respect to the length of corresponding EGFP-labeled dendritic segments. For artificial synapse formation assays, the synaptic parameters were similarly normalized by HEK cell surface area. Co-localizations between two markers (e.g., HA-NLGNs with CNX, GM130, vGLUT, vGAT) were assessed by first thresholding individual channels appropriately to eliminate background signals for different experimental batches, and then measuring Mander's coefficients for each optical section within JACoP plugin.

Data Presentation: For all experiments, all average values indicate means ± SEM (standard-deviation [SD] of a parameter divided by square-root of number of samples), and are presented along with number of independent observations, e.g., number of animals (immunoblots: mouse brain samples) or cultures (immunoblots: HEK cells and human neurons) examined, or field-of-views analyzed / number of experimental batches (immuno-staining: HEK cells and mouse primary neurons). For near-normally distributed datasets, statistical evaluations between conditions were conducted using unpaired (paired for batch-wise comparisons), two-tailed, Student's t-test (*** $P < 0.005$; ** $P < 0.01$; * $P < 0.05$; ns = not significant, $P > 0.05$);

nonparametric Mann-Whitney U-test was used otherwise. Single- or two-factor ANOVA was performed for groupwise assessments, as mentioned.

2.3 Results

2.3.1 Regulation of Endogenous NLGN Glycan Maturation

While NLGNs have long been known to be subject to modification by glycosylation (Ichtchenko et al., 1995; Comoletti et al., 2003), the landscape of endogenous NLGN glycosylation throughout the brain has yet to be examined. Toward this end, whole-protein lysate was extracted from six broadly defined regions of adult mouse brain. NLGNs, whether ectopically expressed or endogenous, stereotypically display multiple bands of differing mass on Western blots, believed to represent populations of differentially modified glycoprotein (Zhang et al., 2009; Poulopoulos et al., 2012). Here, lysate immunoblotted for NLGN1 indeed revealed two major bands of differing mass, one close to the predicted molecular weight (MW) of unmodified NLGN1 (~94 KD) and one more massive band well above 100 KD, representing heavily glycosylated mature protein.

To identify glycan modification of endogenous NLGNs, brain region lysates were incubated with specific glycosidases and run on Western blots alongside untreated lysate from the same region to assess gel mobility changes indicative of glycan cleavage. PNGaseF is an endoglycosidase capable of cleaving all mammalian N-glycans from the Asn sidechain (Tarentino et al., 1985). Treatment with PNGaseF reduced the mass of both major NLGN1 protein bands regardless of the brain region the lysate was collected from (Fig. 1.1A-B). Incubation of lysate with sialidase, an exoglycosidase that cleaves terminal sialic acid residues from glycan chains, only induced a mass shift for higher-MW NLGN1 protein bands (Fig. 1.1C-D). Since N-glycans are initially added to nascent peptide chains in the ER, but modification by sialic acid occurs in the Golgi (Bhide and Colley, 2017), this indicates the more massive NLGN1 band has been processed in the Golgi and represents diversified NLGN1 glycoprotein. Conversely, the lower-mass NLGN1 band is unlikely to have been processed along the secretory pathway and is representative of immature glycoprotein.

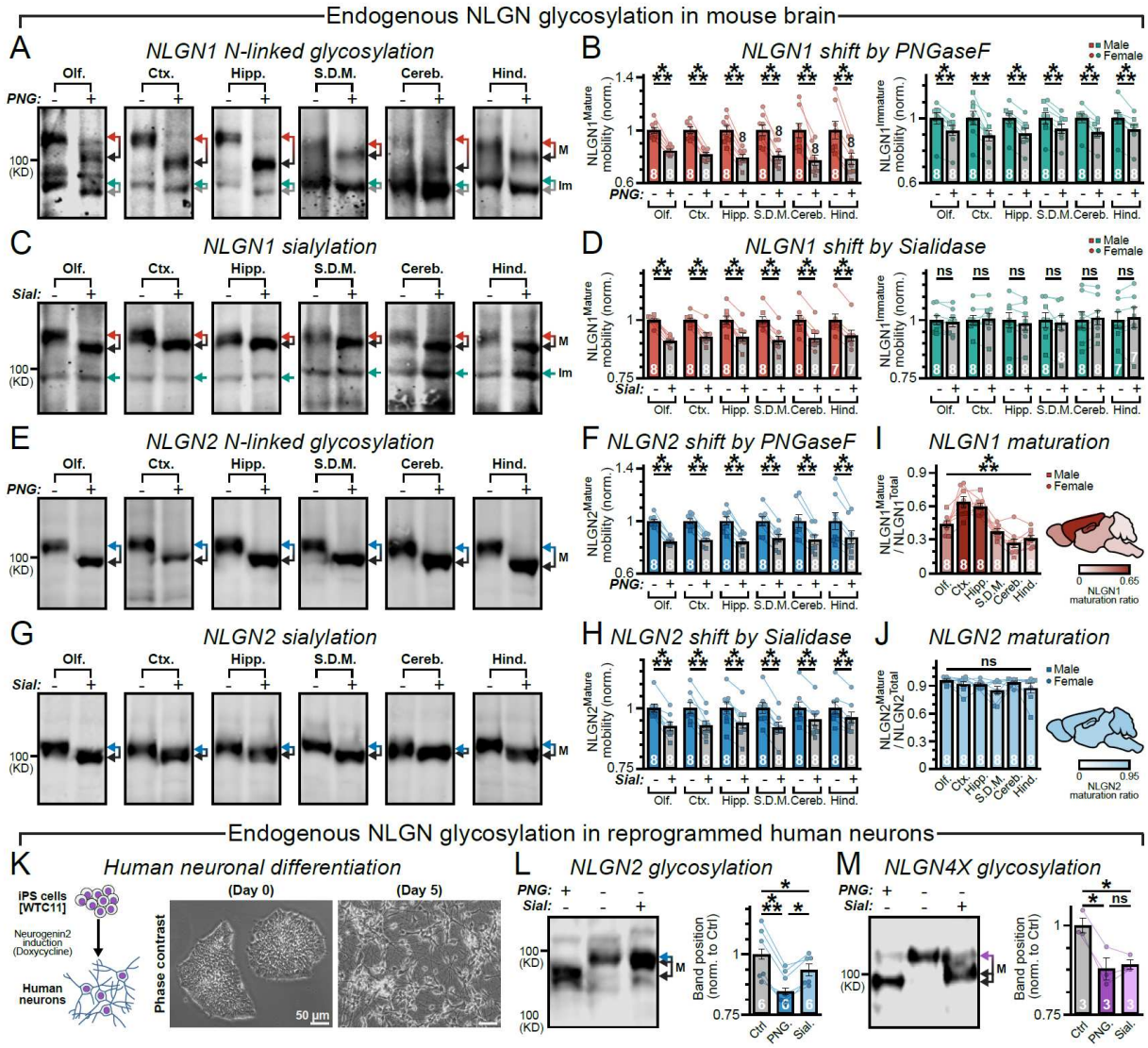

Figure 1.1: **Endogenous NLGNs are post-translationally modified by N-linked glycosylation.** (Generated in collaboration with Soham Chanda)

A. Representative immunoblots of endogenous NLGN1 extracted from mouse olfactory bulb (Olf.), cerebral cortex (Ctx.), hippocampus + dentate gyrus (Hippo.), striatum + thalamus + midbrain (S.T.M.), cerebellum (Cereb.), and hindbrain (Hind.), before and after ("-" and "+", respectively) incubated with PNGase F (PNG) enzyme. Connected arrowheads indicate PNGase F -mediated mobility shifts of NLGN1, for both maturely (labeled as "M", red to black) vs. immaturely (labeled as "Im", green to grey) glycosylated products.

B. Shifts in MW by PNGase F treatment (connected lines) normalized to untreated controls for mature (left panel) vs. immature (right panel) versions of endogenous NLGN1. Samples were analyzed from both male (squares) and female (circles) animals, but averaged together since both genders exhibited a similar trend.

C-D. Same as **A** and **B**, except all samples were treated with Sialidase (SIAL), which only affected the MW of maturely (red arrowheads) but not immaturely (green arrowheads) glycosylated forms of endogenous NLGN1.

(Fig. 1.1 cont.)

E-H. Same as **A-D**, except western-blots of maturely glycosylated endogenous NLGN2, when subjected to PNGase F (**E-F**) or Sialidase (**G-H**) treatment. Note the limited levels of immature NLGN2 products (**E**, **G**).

I-J. Normalized summary plots (bar-graphs, left) and cartoon representations (heat maps, right) illustrate maturely glycosylated fractions of endogenous NLGN1 (**I**) vs. NLGN2 (**J**), at different mouse brain regions.

K. Schematic diagram (left) and example images of culture morphologies (right) of an iPS cell line (WTC-11, day 0) rapidly reprogrammed into human neurons (day 5) by doxycycline-induced Ngn2 expression.

L-M. Sample immunoblots (left) and normalized band-shifts (right) of endogenous NLGN2 (**L**) and NLGN4X (**M**) extracted from differentiated human neurons and treated with glycosidases, i.e. PNGase F and Sialidase.

Bar-graphs represent means ± SEM, with numbers indicating total number of animals (**A-J**, male + female) or independent batches of cultures (**L-M**) analyzed. Individual data-points are plotted as color-matched symbols (see Source Data). Statistical significance was weighed using two-tailed, paired, Student's t-test (panels **A-H**, and **L-M**), or one-way ANOVA (**I-J**), with *** $P < 0.005$; ** $P < 0.01$; * $P < 0.05$; ns = not significant ($P > 0.05$).

The same blots were also probed with NLGN2 antibody raised in a different host species. Unlike NLGN1, endogenous NLGN2 protein was predominantly detected as one band, with an apparent MW of just over 100 KD (Fig. 1.1 E, G). This band was sensitive to both PNGaseF and sialidase regardless of the brain region of origin, indicating modification of most NLGN2 by N-linked glycosylation and sialic acid residues throughout the mouse brain (Fig. 1.1 F, H). Less massive, sialidase-resistant NLGN2 bands were barely detectable in mouse brain lysate, regardless of sex; mature NLGN2 glycoprotein made up ~90% of the protein detected in each brain region (Fig. 1.1J). In contrast, the ratios of mature/immature NLGN1 differed significantly across analyzed brain regions. Mature, more massive NLGN1 was abundant in the cortex and hippocampus, while immature NLGN1 dominated in the cerebellum and hindbrain, again regardless of the sex of the mouse analyzed (Fig. 1.1I). These results reveal a sex-independent but isoform- and region-dependent regulation of endogenous NLGN glycan maturation in adult mouse brains.

We next wondered whether endogenously expressed human NLGN proteins are similarly modified by N-glycans and sialic acid. In order to assess glycan modification of human-expressed NLGN proteins, we turned to the WTC-11 line of human induced pluripotent stem cells (iPSCs), which express the transcription factor (TF) neurogenin-2 (Ngn2) upon treatment with doxycycline (Zhang et al., 2013; Wang et al., 2017). After just five days of differentiation, these cells adopt a clear neuronal morphology (Fig. 1.1K). By treating whole-cell lysate collected from differentiated WTC-11 neurons with PNGaseF or sialidase before immunoblotting with NLGN2 antibody, we confirmed that NLGN2 is expressed and modified by both N-glycans and sialic acid in this cell line (Fig. 1.1L). Humans also express NLGN4X, evolutionarily divergent from mouse-expressed NLGN4-*like* (Bolliger et al., 2008; Maxeiner et al., 2020). Glycosidase treatment of WTC-11 neuron lysate followed by probing for NLGN4X on Western blots again confirmed expression and modification of NLGN4X protein with N-linked

glycosylation and further maturation through the addition of sialic acid (Fig. 1.1M). Thus, it is evident that quickly following neuronal differentiation, newly synthesized NLGNs are glycosylated and processed through the Golgi in human neurons.

2.3.2 Contribution of N-glycan Sites to NLGN Glycoprotein Maturation and Stability

The ECD of the NLGN protein family contains a globular acetylcholinesterase (AChE)-like conformation, wherein each isoform contains two to four N-linked glycosylation sequons found across five unique or conserved residues, which we have termed Sites I-V (Fig. 1.2A). Having observed variable diversification of NLGN glycoproteins throughout the mouse brain, and given that a functional contribution of only one N-glycan site has been thoroughly characterized (NLGN1-N303; Comoletti et al., 2003; Boucard et al., 2005), we questioned whether any particular N-glycosylated residue might disproportionately contribute to NLGN protein maturation. HA-tagged NLGN variants were generated wherein asparagine residues predicted to be glycosylated were mutated to alanine either individually (i.e. single-site mutants) or all together (N-glycan-Null or simply Null mutants, Fig. 1.2A). These constructs were transfected into HEK293 cells preceding a co-transcribed fluorescent reporter (IRES-EGFP), and whole-protein lysate was extracted after 2-3 days of expression (Fig. 1.2B). Lysates were analyzed on Western blots for the ratio of mature (i.e. more massive) glycoprotein to total protein. Here, the observed impact of single-site mutations on NLGN maturation varied by protein isoform and mutated residue. For NLGN1, each single-site mutant caused a ~20% decrease in mature protein ratio, implying redundant contributions of these N-glycan sites toward glycoprotein processing (Fig. 1.2C). In contrast, NLGN2 single-site mutations differed in their impacts on protein maturation. NLGN2-N98A (Site I) mutant was ~90% in the immature form, while NLGN2-N136A (Site II) and N511A (Site V) mutants were each roughly 50% in the mature protein form (Fig. 1.2D). Although, of note, N136A and N511A mutants exhibited different banding patterns on the immunoblot, suggesting divergent contributions toward

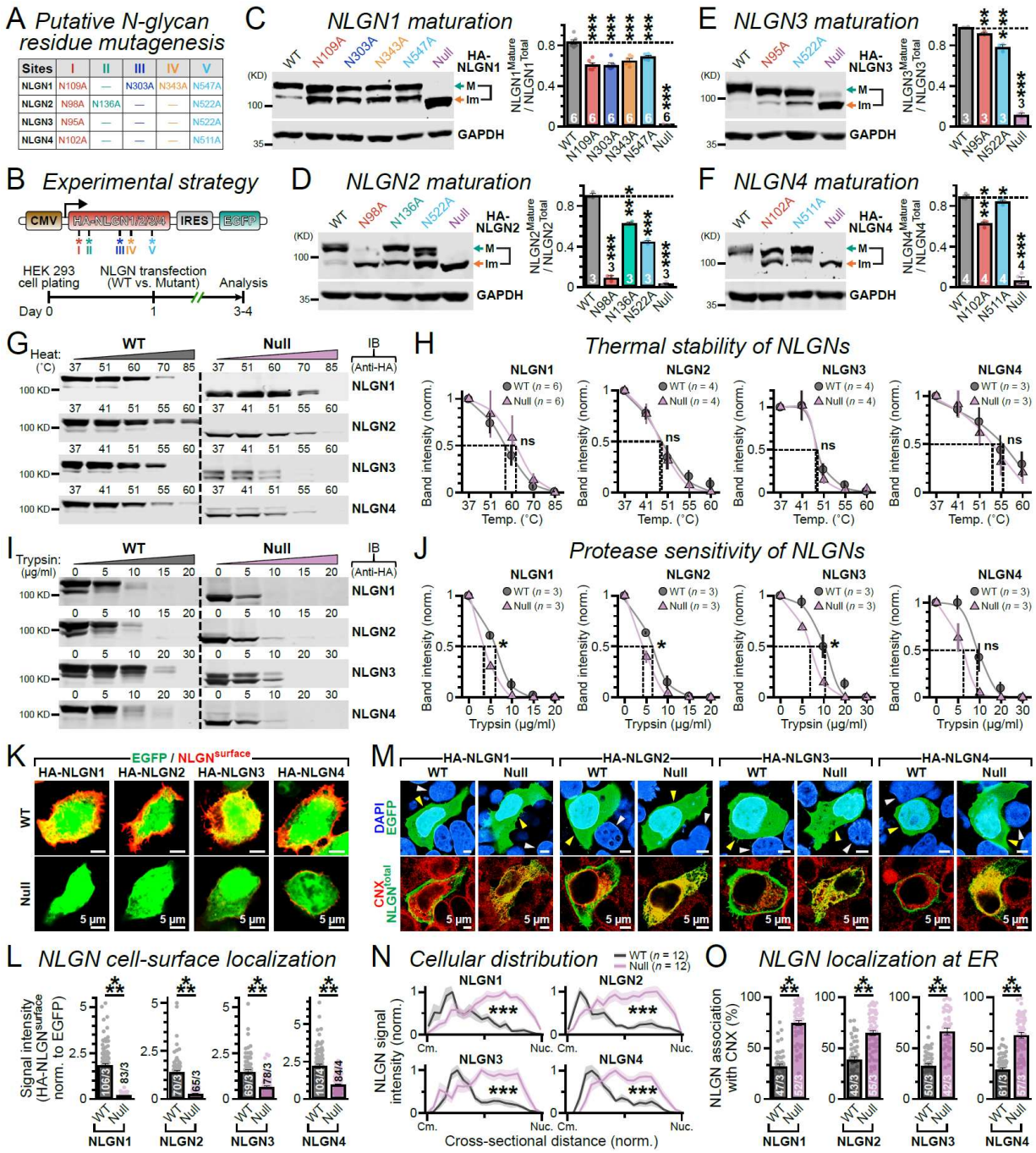

Figure 1.2: **Loss of glycosylation prevents NLGN's maturation and surface transport.** (Generated in collaboration with Orion Benner, Zephyr Lenninger)

A. Table enlists all Asparagine residues at equivalent positions (unique or conserved sites I-V) that constitute consensus sequences for N-linked glycosylation within the AChE-like domains of NLGN1-4. These residues were Alanine-substituted, either individually (i.e., single site mutants) or all together (i.e., glycan-null mutants), to generate the glycosylation-deficient versions for all NLGN isoforms (for details, see Materials & Methods).

(Fig. 1.2 cont.)

B. A cartoon representation of expression vector design (top) and schematic diagram of experimental timeline (bottom) for analyzing HA-tagged NLGN WT vs. glycan mutant versions (asterisks, not to scale) in HEK cells.

C-F. Example immunoblots (left) of maturely (labeled as “M”, green arrows) vs. immaturely (labeled as “Im”, orange arrows) glycosylated products, and average fractions of mature NLGNs (right, normalized to total = mature + immature), for WT vs. glycan site mutations: NLGN1 (**C**), NLGN2 (**D**), NLGN3 (**E**), and NLGN4 (**F**).

G-H. Representative western-blots (**G**) and normalized band intensities (**H**) of HA-tagged NLGN1-4 WT vs. their corresponding glycan-null versions (as labeled), when subjected to increased heat exposure. Data in **H** are fitted (color-coded solid lines) with Boltzmann sigmoid function (see Materials & Methods), and half-decay temperatures (i.e., V50 values) for residual protein levels are indicated (black dotted lines).

I-J. Same as **G-H**, except NLGNs were digested with Trypsin, and half-decay concentrations were indicated.

K-L. Confocal images (≈ 0.5 µm optical section, **K**) of HEK cells immunostained for HA-tagged NLGN1-4 (left to right) WT vs. corresponding glycan-null mutants, under non-permeabilized condition (without Triton X-100), and surface NLGN signals per cell normalized by their respective intracellular EGFP intensities (**L**).

M. Example images of HEK cells immunolabeled for total protein levels (i.e., surface + intracellular) of HA-tagged NLGN1-4 WT vs. their glycan-null variants under a permeabilized condition (with Triton X-100), co-expressed EGFP signals, and co-stainings for ER marker Calnexin (CNX) and nuclear DAPI, as indicated.

N. Subcellular localization of NLGN1-4 WT (grey) vs. glycan-deleted (purple) versions, as distributed between cell membrane (Cm.) and nucleus periphery (Nuc.) in transfected HEK cells (see **M**); the relative distance was sorted into 20 bins per cell radius, and signals were normalized to their maximum intensity positions.

O. Mander’s coefficients for NLGN1-4 (left to right) co-localizing with ER-marker CNX, in HEK cells (see **M**).

All quantifications reflect means ± SEM, and numbers of independent experimental batches (for immunoblots) or cells imaged (for immunostaining) / individual trials are reported as insets. All data-points (see Source Data) are included as color-matched circles. Statistical significances between conditions were evaluated using two-tailed, unpaired, Student’s t-test (panels **C-J**, and **O**), or two-sample, Mann-Whitney U-test (panel **L**), or two-way ANOVA test (panel **N**), with *** $P < 0.005$; ** $P < 0.01$; * $P < 0.05$; ns = not significant ($P > 0.05$)

N-glycan processing. For NLGN3 and NLGN4, which both contain only conserved N-glycan Sites I and V, single-site mutations had minimal effects on mature protein abundance (Fig. 1.2E-F). However, in the case of each NLGN isoform, N-glycan-Null mutants demonstrated the lowest overall glycoprotein maturation, with defects ranging from ~90% (NLGN3 and NLGN4, Fig. 1.2E-F) to almost complete reduction of mature glycoprotein (NLGN1, Fig. 1.2C).

NLGNs are also modified by O-linked glycans, which decorate the extracellular stalk domain linking the AChE-like and transmembrane domains. We hypothesized that since N-glycan-Null mutagenesis reduced each NLGN protein's mass to roughly that of the unmodified amino acid chain (~90-96 KD; Fig. 1.2C-F), O-linked glycosylation would also be impaired as a result of N-glycan elimination. To test for this, whole-protein lysate extracted from NLGN-WT or -N-glycan-Null transfected HEK cells was treated with glycosidases. PNGaseF and sialidase were again utilized to probe for N-linked glycosylation (which should be absent from Null variants) and sialic acid, which modifies both N- and O-linked glycan chains (Van den Steen et al., 1998; Stanley, 2011). Additionally, we employed an O-glycosidase cocktail. Due to the vast heterogeneity of O-linked glycans, a universal O-glycosidase analogous to PNGaseF does not exist (Wandall et al., 2021). So, to reduce protein mass as much as possible and improve enzyme efficiency, O-glycosidase was supplemented with sialidase and PNGaseF. As observed with endogenous mouse NLGNs, the application of both PNGaseF and sialidase reduced the apparent mass of WT NLGN variants (Fig. 1.3A). A combination of PNGaseF, sialidase, and O-glycosidase increased the gel mobility of WT variants to nearly that of untreated Null variants. However, it did not entirely reduce NLGN protein mass. This is likely due to the limited activity of O-glycosidase or potentially the presence of other PTMs (e.g. mono-ubiquitination or palmitoylation). Unlike NLGN WT variants, no glycosidase treatment significantly increased the mobility shift of Null variant NLGNs, regardless of isoform (Fig. 1.3 B-E). Therefore, the deletion

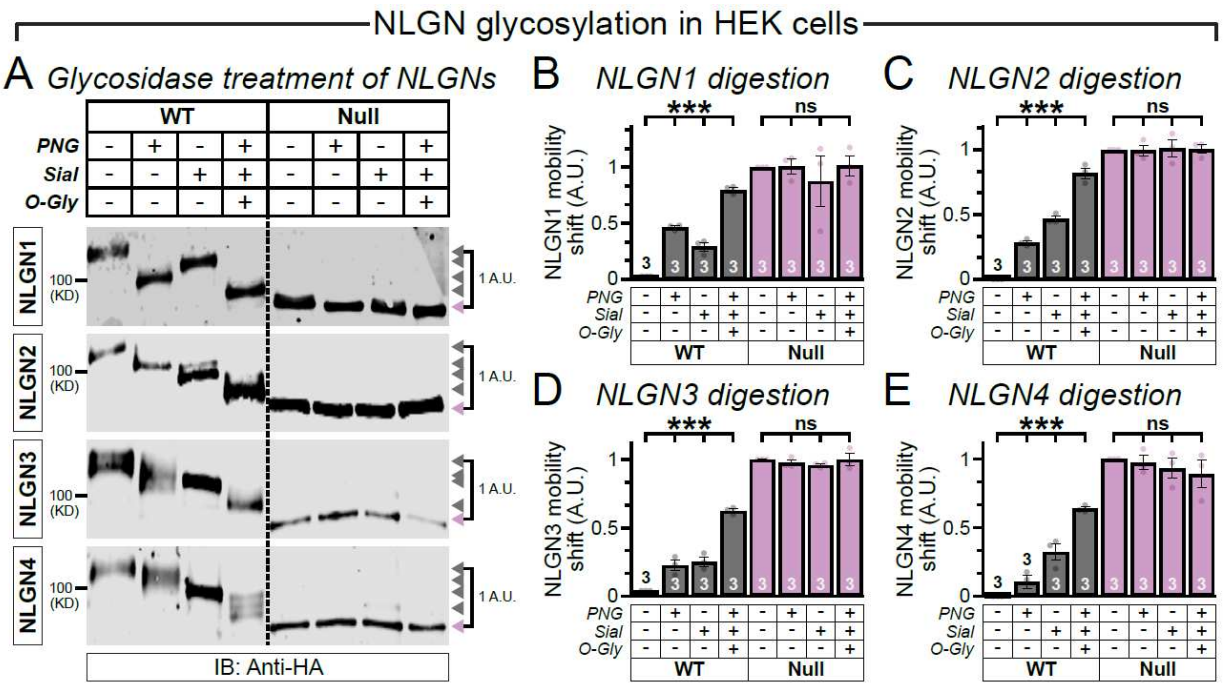

Figure 1.3: **WT NLGNs but not the glycan-null variants undergo extensive glycosylation.**

HEK 293T cells were transfected with HA-tagged WT NLGNs (NLGN1-4) vs. their corresponding null variants; protein extracts were incubated with PNGase F (PNG), sialidase (Sial), or O-glycosidase (O-Gly), as indicated ('+' treated, '-' untreated), and the mobility shifts of individual NLGN bands were probed with anti-HA antibody.

A. Representative immunoblots of NLGN WT (left) vs. null (right) variants, separated by a vertical dotted line. Changes in NLGNs' molecular weights after glycosidase treatments were normalized (1 A.U. = Arbitrary Unit) by the relative distance between each untreated WT (grey arrowheads) vs. null (purple arrowheads) versions.

B-E. Migrations of NLGN1 (**B**), NLGN2 (**C**), NLGN3 (**D**), and NLGN4 (**E**) bands, after glycosidase digestions.

All quantifications represent means ± SEM; color-coded filled circles on the bar-graphs indicate data-points from independent experimental batches ($n = 3$ for all conditions, see Source Data). Statistical comparisons between multiple groups were performed by one-way ANOVA, *** $P < 0.005$; ns = not significant ($P > 0.05$).

of N-glycosylated residues also impairs NLGN modification by other PTMs, including O-linked glycosylation and sialic acid addition.

N-linked glycosylation is crucial for protein quality control carried out in the ER. The folding chaperones CNX and CALR bind the terminal glucose residues of immature glycan chains, which upon proper protein folding, are trimmed to promote export from the ER (Mitra et al., 2006). Considering this, we wondered if N-glycan-Null NLGN proteins would exhibit reduced conformational stability. First, we employed a thermal shift assay to determine whether a lack of N-glycans would alter the temperature at which NLGN proteins denature and aggregate. Lysate was collected from HEK cells expressing WT or Null variants of NLGN isoforms, heated along a temperature gradient, then centrifuged to pellet aggregated proteins. Equal volumes of supernatant were then collected and probed for soluble HA-tagged NLGNs on Western blots. Here, we observed no effect of N-linked glycosylation loss on the temperature stability of NLGN proteins (Fig. 1.2G-H). Protein stability can also be a determining factor in protease sensitivity, as perturbations along the backbone of misfolded peptides will increase accessibility for proteases (Zheng et al., 2011; Samelson et al., 2016; Niwa et al., 2019). So, NLGN variant-transfected HEK cells were again lysed – however, this time in the absence of protease inhibitors. Quickly after collection, lysates were incubated for five minutes with increasing concentrations of trypsin before quenching with a protease inhibitor cocktail and SDS. The absence of N-glycans did impact the average trypsin concentration required to degrade half of the full-size protein (Fig. 1.2I-J). However, increased trypsin sensitivity likely results from the lack of steric hindrance provided by N- and O-glycan chains on the Null protein variants (Liu et al., 2008; Zheng et al., 2011; Friligou et al., 2021). Therefore, it is unlikely that the absence of N-linked glycosylation per se strongly impacts protein folding or temperature stability of NLGN proteins.

2.3.3 N-linked Glycosylation Promotes NLGN Export from the ER

N-linked glycosylation is an essential regulator of protein transport through the secretory pathway and localization to cell membranes (Melikian et al., 1996; Rosnoblet et al., 2013; Park et al., 2020). Additionally, several ASD- and ID-associated NLGN mutations impact both glycoprotein maturation and surface expression (Zhang et al., 2009; Nguyen et al., 2020; Cast et al., 2021). So, in order to investigate the contribution of N-linked toward NLGN surface expression, HEK cells were seeded onto glass coverslips and transfected with HA-tagged NLGN-WT or -Null constructs, then fixed with PFA after two days of expression. Under non-permeabilized conditions, cells were stained with HA antibody to mark surface-localized NLGN. Normalizing to the co-transcribed EGFP reporter, we observed a dramatic decrease in NLGN cell surface expression upon N-glycan-Null mutagenesis (Fig. 1.2K-L). Considering the possibility that decreased surface expression could be due to protein degradation, we confirmed via Western blot that introduction of the Null mutation does not reduce overall NLGN-to-EGFP reporter protein ratios compared to the NLGN-WT variants (Fig. 1.4A-D). Therefore, it is evident that N-linked glycosylation promotes the surface localization of NLGN proteins.

A lack of N-glycan-Null variants at the surface but no corresponding decrease in total protein expression strongly implies that the mutant proteins are retained in the secretory pathway. When transfected HEK cells were immunostained for HA under permeabilized conditions, we observed markedly different intracellular distributions of NLGN-WT and -Null variants (Fig. 1.2M). While each NLGN isoform's WT variant was concentrated toward the cell membrane, Null variants were more uniformly distributed throughout the interior of the cell (Fig. 1.2N). We also co-stained these cells for established markers of the secretory pathway, CNX for the ER, and GM130 for the Golgi apparatus. The average colocalization of each NLGN isoform with the ER increase ~2-fold upon mutation of N-glycosylated residues (Fig. 1.2M, O), which paralleled an increase in colocalization with the Golgi for all isoforms but NLGN3 (Fig. 1.4E-H).

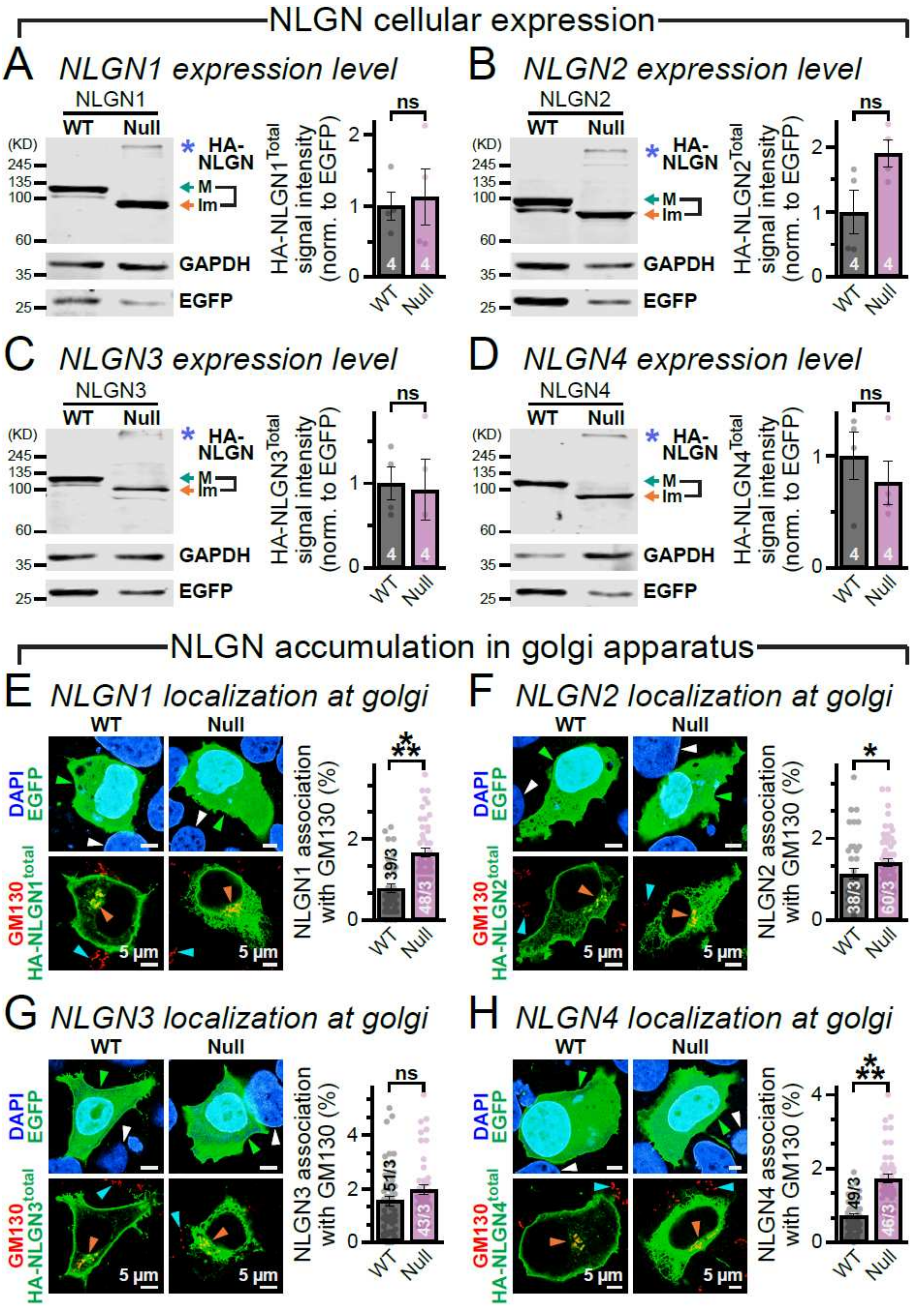

Figure 1.4: **Lack of glycosylation impairs NLGNs' surface export via secretory pathway.**

HEK cells expressed HA-tagged WT vs. glycosylation-deficient NLGNs, followed by an IRES-EGFP cassette.

A-D. Western-blot samples (left) and summary plots (right) of overexpressed protein levels for WT vs. glycan-null versions of NLGN1 (**A**), NLGN2 (**B**), NLGN3 (**C**), and NLGN4 (**D**), when normalized to their corresponding EGFP signals. Arrowheads are maturely (M) vs. immaturely (Im) glycosylated NLGNs; asterisks = aggregated products frequently observed for all glycosylation-deficient NLGNs; GAPDH was used as a loading control.

(Fig. 1.4 cont.)

E-H. Cells were permeabilized using Triton X-100, immunolabeled for both surface + intracellular HA-epitopes (i.e. total NLGNs), a golgi-complex marker GM130, and nuclear DAPI stain. Sample images (left) and average percentages (Mander's co-efficient, right) of HA-tagged NLGN1 (**E**), NLGN2 (**F**), NLGN3 (**G**), and NLGN4 (**H**), WT vs. glycan-null mutants associated with GM130. Orange vs. cyan arrowheads point at golgi apparatus co-localized with HA-NLGNs of transfected cells (green arrows) or from untransfected neighbors (white arrows).

Average values indicate means ± SEM, with individual data-points as color-matched filled circles. Numbers on bar-graphs denote total batches tested or field-of-views analyzed / independent biological replicates. Statistical significance was measured using either two-tailed, unpaired, Student's t-test (panels **A-D**), or two-sided, Mann-Whitney U-test (panels **E-H**), with *** $P < 0.005$; * $P < 0.05$; ns = not significant, $P > 0.05$ (see Source Data).

Altogether, the results here suggest that mutagenic removal of NLGN N-linked glycosylation does not dramatically impact protein expression or stability but rather impairs the proteins' export from the ER and subsequent expression of the protein on the cell surface.

2.3.4 N-glycan-Null Mutation Reduces NLGN Proteins' Presynaptic Recruitment Through Surface Expression Defects

It stands to reason that reducing the availability of NLGN proteins at the cell surface through N-glycan site mutation would also reduce their ability to interact with presynaptic terminals. However, it has been shown before that the absence of N-glycans enhances NLGN1-NRXN binding (Comoletti et al., 2003). We, therefore, wondered whether there would be any impairment or augmentation of N-glycan-Null mutants' NRXN affinity when considering protein trafficking defects. To that end, we performed a cell aggregation assay to isolate the interaction between NRXN and NLGN variants. Individual cultures of HEK cells were transfected with NLGN constructs, either WT or Null variants, preceding an EGFP reporter or EGFP alone as a control. A separate culture was transfected with NRXN1β lacking the splice site 4 insert (SS4-) preceding an mOrange fluorescent reporter (Fig. 1.5A). After two days of expression, cells were lifted using 1 mM EDTA in PBS, then pelleted and resuspended in DMEM + 20 mM $CaCl_2$ at ~1 x 10^6 fluorescent cells per ml. Equal volumes of NRXN- and EGFP-expressing cell suspensions were then mixed end-over-end for two hours at 37°C, then spotted onto glass slides to image fluorescently labeled cell aggregates formed through NLGN-NRXN interactions (Fig. 1.5B).

As anticipated, cells expressing NLGN-WT variants formed clear aggregates with red, NRXN1β $^{SS4-}$-expressing cells, while EGFP-only controls did not. All N-glycan-Null variants formed fewer aggregates than their respective WT but still more than EGFP controls (Fig. 1.5C-F). The NLGN1-Null mutant, which exhibits the greatest decrease in surface expression vs. its WT counterpart (Fig. 1.2L), was the most dramatically reduced in its interaction with NRXN vs.

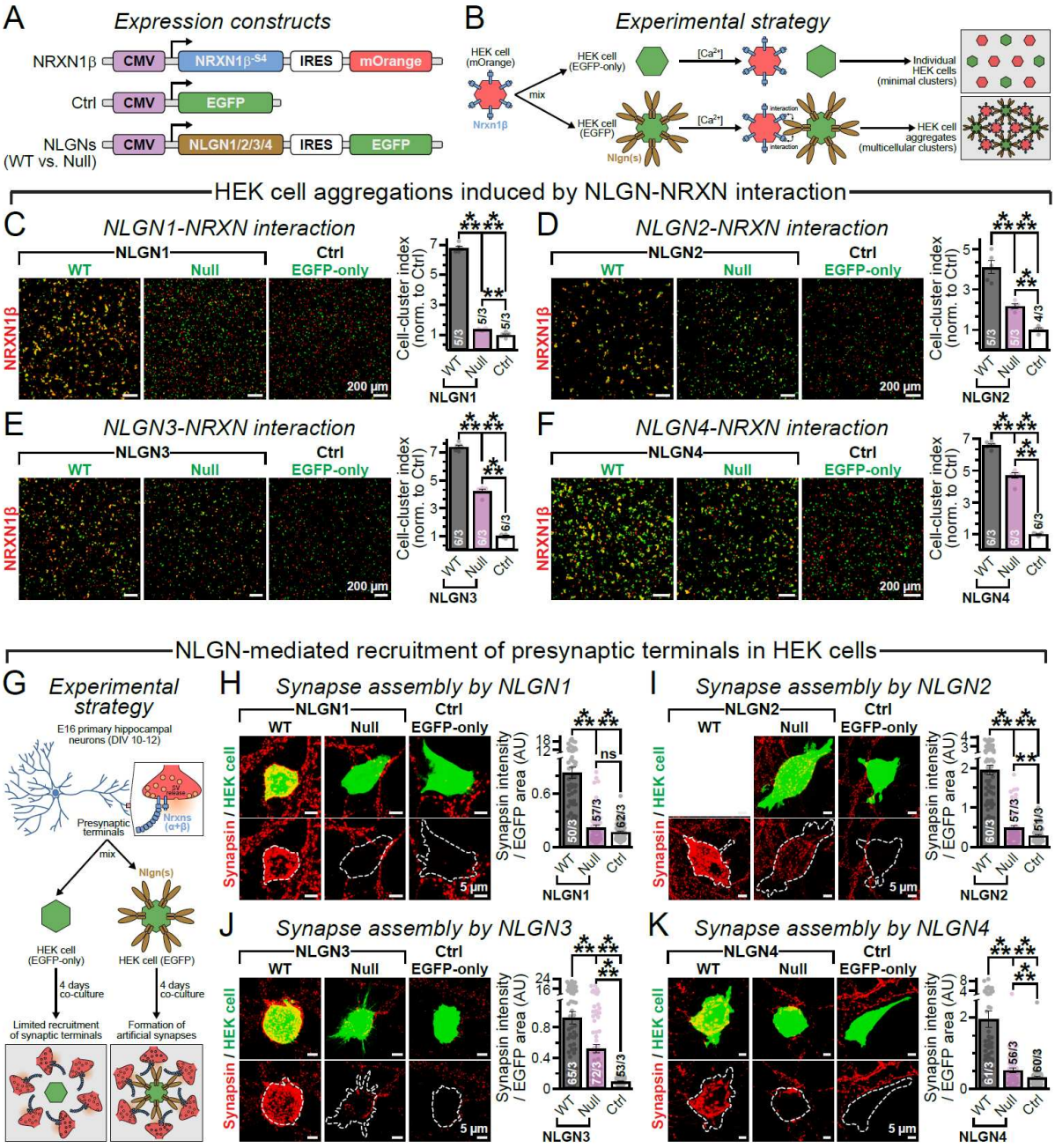

Figure 1.5: **Lack of glycosylation impairs NLGNs' function as a trans-synaptic CAM.** (Generated in collaboration with Laurie Minamide)

A-B. Design of expression constructs (**A**) and schematic diagram of experimental strategy (**B**) to probe NLGN-NRXN interactions at the cell surface using HEK cell -aggregation assay (for details, see Materials & Methods).

C-F. Example images (left) and Mander's co-localization coefficients (average bar-graphs, right) of HEK 293T cells expressing NRXN1β (mOrange-labeled) mixed with HEK cells expressing either WT vs. glycosylation-null versions of NLGNs [NLGN1 (**C**), NLGN2 (**D**), NLGN3 (**E**), and NLGN4 (**F**)], or a control vector (EGFP-labeled).

(Fig. 1.5 cont.)

G. HEK 293T cells were transfected with WT vs. glycosylation-deficient NLGNs, or a control EGFP-only vector, and subsequently co-cultured with primary hippocampal neurons derived from day 16 embryos (E16); NLGNs' ability to recruit presynaptic terminals was monitored after 4 days (see Materials & Methods for details).

H. Representative images (left) of EGFP-positive HEK cells co-expressing NLGN1 variants (top panels) and surrounded by Synapsin-immunolabeled presynaptic specifications from adjacent primary neurons (coinciding within dotted outlines, bottom panels); Synapsin signal intensities (right) from different conditions, as indicated.

I-K. Same as **H**, except for WT vs. glycosylation-deficient mutants of NLGN2 (**I**), NLGN3 (**J**), and NLGN4 (**K**).

Summary plots are provided as means ± SEM, with total number of samples analyzed / independent batches, Individual data-points are provided as color-matched open circles (see Source Data). Statistical assessments across conditions were performed using two-tailed, unpaired, Student's t-test (panels **C-F**), or two-sided, non-parametric, Mann-Whitney U-test (panels **H-K**), with *** $P < 0.005$; ** $P < 0.01$; ns = not significant ($P > 0.05$).

NLGN1-WT but still formed significantly greater aggregates than the negative control (Fig. 1.5C), altogether implying no major alteration in Null variants' ability to interact with NRXN.

To assess whether N-glycan-Null mutation further impacted NLGN proteins' recruitment and interaction with presynapses, we turned to the artificial synapse formation assay, a well-established protocol involving co-culture of SCAM-expressing heterologous cells with a neuronal culture, inducing recruitment of neuronal presynaptic terminals (Scheiffele et al., 2000; Ko et al., 2009). Changes in presynapse recruitment observed in N-glycan-Null mutants compared to WT variants is thus indicative of impairment or augmentation of presynaptic interaction through surface expression defects or reduced steric hindrance, respectively. HEK cells expressing WT or N-glycan-Null constructs were co-cultured with embryonic day 16 (E16) primary mouse neurons for 4 days. Cells were then fixed and immunostained for the presynaptic marker synapsin to assess the recruitment of presynaptic terminals by each NLGN variant (Fig. 1.5G). Here, while NLGN1-WT-expressing cells efficiently recruited presynaptic terminals, those expressing NLGN1-Null recruited no more synapsin-positive puncta than EGFP control (Fig. 1.5H). Despite moderate aggregation formation for NLGN2, 3, and 4 N-glycan-Null variants in Fig. 1.5D-F, in neuronal co-culture, these mutants were greatly impaired in their recruitment of presynapses (Fig. 1.5I-K). These results indicate that, as a whole, N-linked glycosylation plays a decisive role in NLGN proteins' ability to recruit presynapses by mediating surface trafficking and subsequent availability for NRXN interaction.

2.3.5 Conserved N-glycan Site I Universally Reduces NLGN Surface Expression and Interaction with Presynaptic Terminals

Removal of all N-linked glycosylation sites in NLGN AChE-like domains through alanine substitution (i.e. Null mutation) dramatically impaired the anterograde secretory trafficking of each NLGN isoform, diminishing the protein's ability to form transsynaptic interactions. Since NLGN proteins contain multiple unique and conserved N-glycan sequons (Fig. 1.2A), we

wondered whether any individual N-linked glycosylation site contributed more than others toward NLGN isoforms' forward trafficking. HEK cells seeded onto coverslips were transfected with WT or single-site mutant NLGN constructs, then fixed and immunostained for surface HA-NLGN expression. Here, mutation of individual N-glycan sites conferred slightly varying effects on surface expression depending on the NLGN isoform. Each NLGN1 single-site mutant exhibited a moderate impairment in surface expression compared to WT (Fig. 1.6A), akin to the redundant influence of each site toward glycoprotein maturation (Fig. 1.2C). For the other NLGNs, despite each N-glycosylated residue contributing somewhat to protein maturation (Fig. 1.2D-F), not every site appears critical for protein trafficking. NLGN2-N136A (Site II, unique) was not impaired in its surface expression vs. WT (Fig. 1.6B). Mutation of the conserved Site V, interestingly, only impacted protein trafficking for NLGN1 and NLGN2 (Fig. 1.6A-B); NLGN3-N522A and NLGN4-N511A were not reduced in their respective localization to the surface (Fig. 1.6C-D). In contrast, mutation of the other conserved N-glycan site, Site I, reduced surface expression for each NLGN isoform, suggesting a universally important role for this particular N-glycan site.

To test whether individual N-glycan sites contribute toward NLGN presynaptic recruitment, we performed another artificial synapse assay, co-culturing NLGN-WT or -single-mutant-transfected HEK cells with E16 primary mouse neurons for 4 days. Staining these co-cultures for synapsin revealed that not every variant associated with decreased surface expression caused a reduction in presynapse recruitment. NLGN1 residue N303 is known to reduce NLGN1-NRXN interaction through steric hindrance (Comoletti et al., 2003). Accordingly, the NLGN1-N303A mutant, while reduced in its overall surface expression (Fig. 1.6A), recruited presynapses as well as its WT counterpart (Fig. 1.6E). NLGN1 and NLGN2 Site V mutants (N547A and N522A, respectively) did not significantly reduce synapsin recruitment (Fig. 1.6F-G), despite an apparent reduction in surface localization. However, this result may be due to

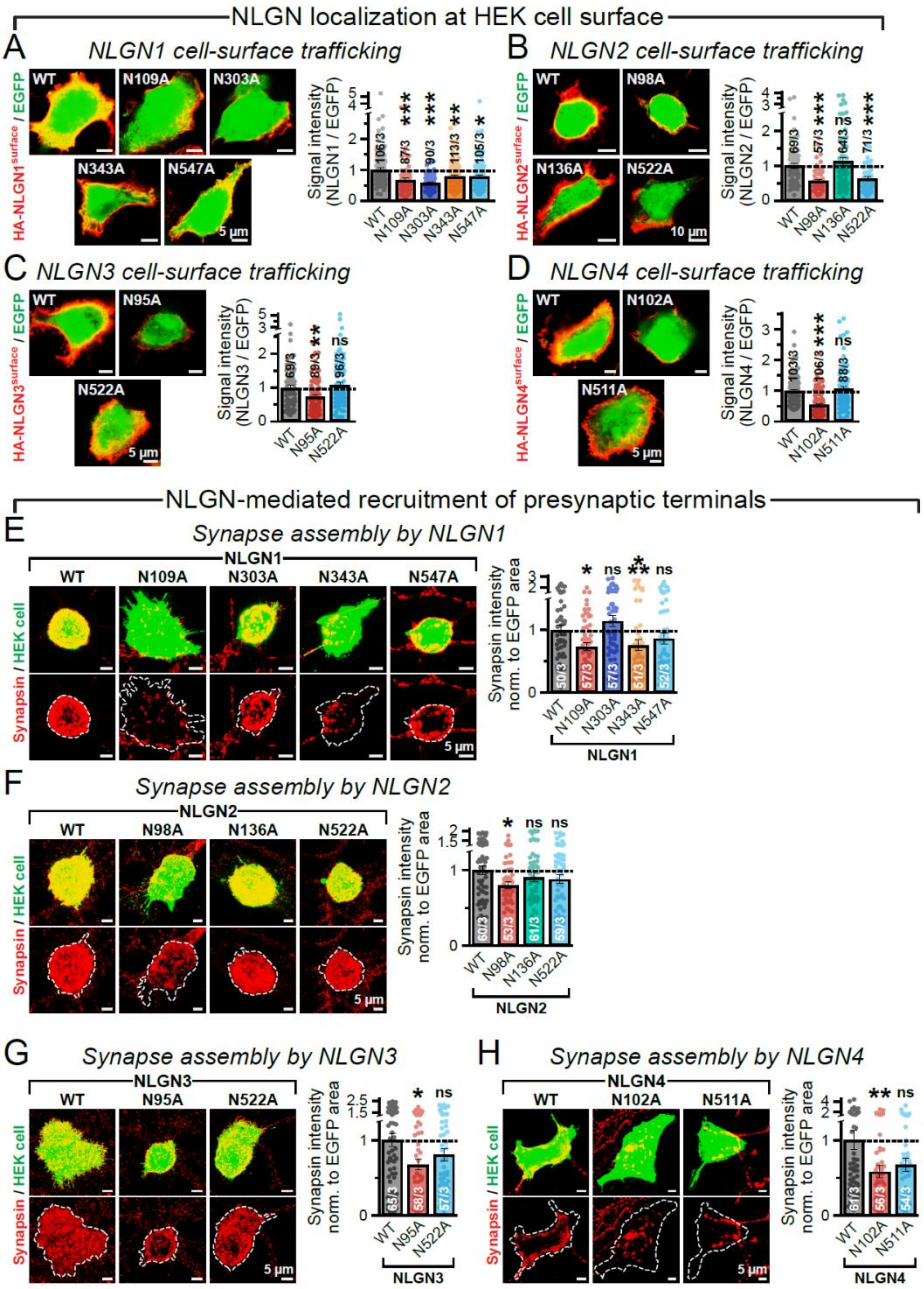

Figure 1.6: **Glycan mutations impair NLGN-mediated assembly of presynaptic terminals.** (Generated in collaboration with Orion Benner, Laurie Minamide)

HEK cells expressed HA-tagged NLGN WT vs. single-site glycan mutants, followed by IRES-EGFP constructs. Cells were also co-cultured with primary neurons (see Fig. 3G), and tested for their ability to recruit synapses.

A-D. Cells were immunostained for surface HA-epitopes under non-permeabilized condition. Example images (left, ≈ 0.5 µm optical thickness) and surface NLGN signals normalized to soluble EGFP levels (right) of HEK cells expressing HA-tagged NLGN1 (**A**), NLGN2 (**B**), NLGN3 (**C**), and NLGN4 (**D**), WT vs. single-site mutants.

(Fig. 1.6 cont.)

E. Representative images (left) of EGFP-labeled HEK cells co-expressing NLGN1 variants (top panels), and surrounded by Synapsin-positive presynaptic specifications from adjacent primary neurons (coinciding within dotted outlines, bottom panels); average Synapsin intensities (right) from different conditions, as indicated.

F-H. Same as **E**, except for WT vs. single-site glycan mutants of NLGN2 (**F**), NLGN3 (**G**), and NLGN4 (**H**).

All numerical data are means ± SEM, with total number of cells analyzed / number of independent trials, and individual data-points (color-matched open circles, see Source Data). Statistical significance was calculated by two-sample, Mann-Whitney U-test, with *** $P < 0.005$; ** $P < 0.01$; * $P < 0.05$; ns = not significant, $P > 0.05$.

surface expression recovery over a longer culture time. However, Site I mutation invariably decreased each NLGN isoform's ability to interact with presynapses (Fig. 1.6E-H). The consistent loss-of-function phenotypes resulting from mutating the conserved N-glycan Site I suggest a distinct role of this N-glycan site for NLGN protein forward trafficking and subsequent interaction with presynaptic proteins.

2.3.6 Endogenous NLGNs are Heterogeneously Glycosylated on Neuronal Cell Surfaces

Canonically, the majority of N-glycans found on secreted and cell membrane proteins are either "complex" or "hybrid" form (Bieberich, 2014; Stanley et al., 2022). Recent evidence, however, points toward unconventional N-glycan maturation and processing in neurons (Hanus et al., 2016; Williams et al., 2022). Therefore, we aimed to characterize the glycan profiles of endogenous NLGN glycoprotein on neuronal cell membranes by probing for the three major forms of N-linked glycans — high-mannose, "hybrid," or "complex." Because in mouse brain high-mass NLGN bands were sensitive to sialidase, indicating trafficking through the Golgi (Fig. 1.1), we hypothesized that the N-glycans modifying NLGN protein localized to cell surfaces would be mostly "complex" or "hybrid" form, as these structures arise in the Golgi (Stanley, 2011). To examine the glycan modifications of surface-localized NLGNs, we combined surface biotinylation and lectin pull-down assays (Fig. 1.7A-B). Primary neurons were cultured from either the cortex or hippocampus of newborn mice, and after 14 days, cell surfaces were treated with biotin ligase before cells were pelleted and lysed. Lysate was incubated with neutravidin beads to separate biotin-conjugated surface proteins from the internal protein population. Then, both surface and internal fractions were partitioned and incubated with lectin-conjugated agarose beads: Concanavalin-A (ConA) to bind high-mannose glycans (Li et al., 2020; Oinam et al., 2022), Ricinus communis agglutinin (RCA) to bind "hybrid" glycans through high affinity for Gal-GlcNAc moieties (Wu et al., 2006), or wheat germ agglutinin (WGA) to bind "complex"

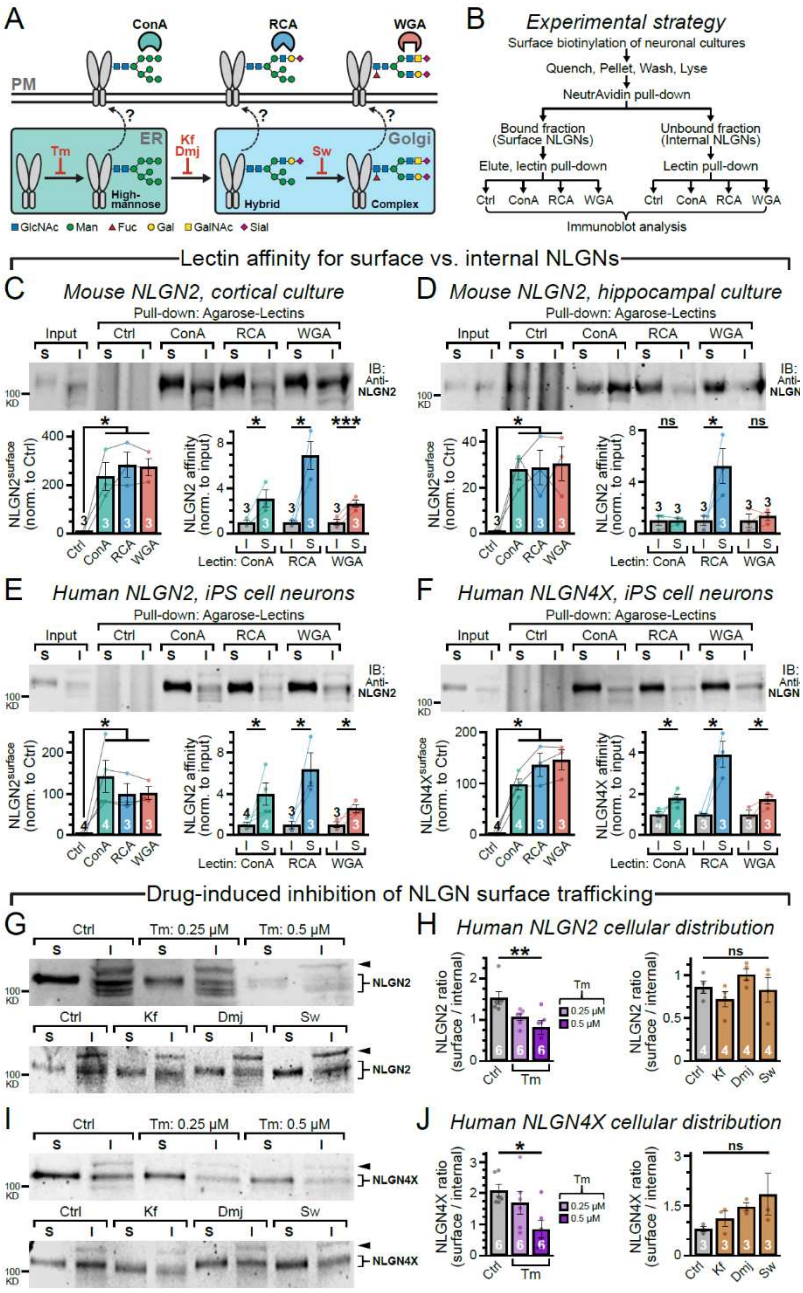

Figure 1.7: **Glycosyltransferase inhibition reduces NLGN surface localization.** (Generated in collaboration with Soham Chanda)

A. Left: Graphic illustrating experimental questions and design. Tunicamycin (Tm) inhibits initial transfer of N-glycans to glycoproteins, kifunensine (Kf) and 1- deoxymannojirimycin (DMJ) inhibit type I mannosidases required for hybrid and complex glycan formation, and swainsonine (Sw) inhibits type II mannosidases, required for complex N-glycan formation. Right: Lectins used for pulldown experiments. ConA preferentially binds alpha-anomeric mannose. RCA preferentially binds Galβ1–4GlcNAc glycan motifs. WGA preferentially binds terminal sialic acid and GlcNAc residues.

(Fig. 1.7 cont.)

B. Experimental timeline for human iPSC-derived neurons. Drug application and lectin pulldown were only performed as required for experiments.

C-F. Western blots of endogenous NLGNs expressed in mouse primary and human iPSC-derived neuronal cultures after surface biotinylation and lectin pulldown. Surface (S) and internal (I) fractions were incubated with lectin-conjugated agarose beads to determine approximate glycan residue enrichment. Blots were analyzed for both relative surface enrichment vs. control (bottom left) and relative lectin affinity for surface vs internal NLGN populations (bottom right).

G. Tm, but not Kf, DMJ or Sw, inhibits NLGN2 surface expression. Western blots demonstrate relative surface (S) vs. internal (I) populations of endogenous NLGN2 and after 48 h treatment with Tm, both 0.25 and 0.5 µM (top), Kf, DMJ, and Sw (bottom). Asterisks indicate non-specific antibody binding.

H. Quantification of **G**.

I. Same as G, except Western blots were probed for endogenous NLGN4X

J. Quantification of **I**.

Summary plots are provided as mean ± SEM, with total number of samples analyzed displayed as inset numbers. Individual data-points are provided as color-matched open circles (see Source Data). Statistical assessments across conditions were performed using one-tailed paired (**C-F** bottom left) or two-tailed paired (**C-F** bottom right) Student's t-test, or one-way ANOVA (**H**, **J**) with *** $P < 0.005$; ** $P < 0.01$; ns = not significant ($P > 0.05$).

lectins containing terminal sialylgalactose moieties (Gallagher et al., 1985). After lectin pull-down, eluted proteins were run on Western blots and probed for NLGN1 or NLGN2.

Surprisingly, for both hippocampal and cortical cultured neurons, ConA-bound beads interacted with surface-localized NLGN2 to the same extent as RCA- and WGA- bound beads (Fig. 1.7C-D), and the same was observed for NLGN1 collected from cortical neuron culture (Fig. 1.8A). This result suggests that high-mannose N-glycans, canonically associated with ER-localized glycoprotein, are present on the surface populations of NLGN1 and NLGN2. Importantly, ConA did pull down internal NLGN2, which included faint lower-mass protein bands absent from the surface population (Fig. 1.7C-D), which according to others and our study represents ER-associated, immaturely glycosylated NLGN protein (Zhang et al., 2009; Poulopoulos et al., 2012; Cast et al., 2021). WGA-bound beads pulled down surface but also internal NLGN2, indicating “complex” sialylgalactose moieties present on glycans of both populations. While expected for surface proteins, “complex” glycan moieties identified on internal NLGN2 glycoprotein may represent NLGN2 in the process of anterograde transport, or recycled NLGN2 trafficked to endosomes by Sorting Nexin 27 (Halff et al., 2019). RCA consistently pulled down surface NLGN2 with greater efficiency than internal, especially evident in hippocampal culture (Fig. 1.7D), demonstrating that “hybrid” glycan structures are especially associated with surface-localized NLGN2 expressed in mice.

To investigate the glycan modifications of human surface-expressed NLGNs, we differentiated WTC-11 neurons for 4-5 days, long enough to express and glycosylate endogenous NLGN2 and NLGN4X glycoprotein (Fig. 1.1K-M). Surface biotinylation followed by lectin pull-down of surface and internal populations revealed that, like in mouse neurons, both NLGN2 and NLGN4X expressed on the surface of human neurons are positive for high-mannose N-glycan structures (Fig. 1.7E-F). In fact, all three lectins tested consistently pulled

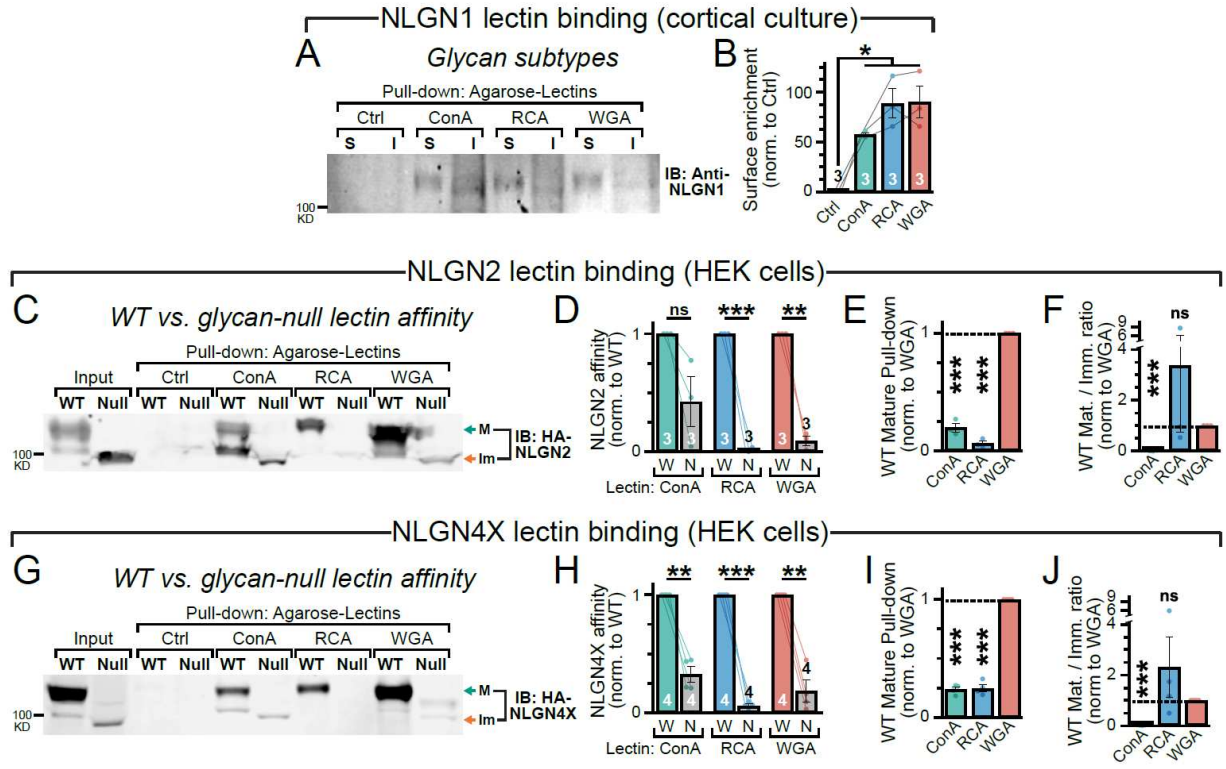

Figure 1.8: **Surface-localized NLGN1 is positive for multiple glycan types.** (Generated in collaboration with Soham Chanda)

A. Western blot shows endogenous NLGN1 expressed in mouse primary cortical neurons after surface biotinylation followed by lectin pulldown.

B. Blots in **A.** were analyzed for surface enrichment and relative lectin affinity of NLGN1 vs. control.

C. Western blot shows NLGN2-WT vs. -Null expressed in HEK cells and pulled down with lectin-conjugated beads or bare sepharose as control.

D. Quantification of lectin affinity for NLGN2-WT vs. Null.

E. Quantification of Mature NLGN2-WT pulldown efficiency relative to input.

F. Quantification of Mature / Immature protein ratio of NLGN2-WT pulled down by each lectin.

G. Western blot shows NLGN4X-WT vs. -Null expressed in HEK cells and pulled down with lectin-conjugated beads or bare sepharose as control.

H. Quantification of lectin affinity for NLGN4X-WT vs. Null.

I. Quantification of Mature NLGN4X-WT pulldown efficiency relative to input.

J. Quantification of Mature / Immature protein ratio of NLGN4X-WT pulled down by each lectin.

Summary plots are provided as mean ± SEM, with total number of samples analyzed displayed as inset numbers. Individual data-points are provided as color-matched open circles (see Source Data). Statistical assessments were performed using one-tailed paired Student's t-test with *** $P < 0.005$; ** $P < 0.01$; ns = not significant ($P > 0.05$).

down surface-expressed NLGN2 and NLGN4X, indicating a heterogeneous N-glycan population decorating these proteins.

Finally, to compare neuronal and heterologous cell glycan processing, we performed lectin pull-down assays with ectopic NLGN2/4-WT vs. Null expressed in HEK cells (Fig. 1.8C, G). As expected, all three lectins bound WT variants with greater affinity than they did Null (Fig. 1.8D, H). Focusing on the WT variants, although maturely glycosylated bands were pulled down by each lectin, WGA-recognized glycoprotein was significantly enriched compared to ConA- and RCA-recognized (Fig. 1.8E, I), indicating a greater ratio of sialylgalactose-modified glycoprotein than high-mannose- or Gal-GlcNAc-modified. Further, the fraction of mature vs. immature protein recognized by ConA was decreased for both NLGN2- and NLGN4-WT, while RCA- or WGA-recognized protein was predominantly mature (Fig. 1.8F, J). Increased detection of immature bands by ConA is indicative of a more conventional glycan maturation pattern for NLGNs expressed in HEK cells, and contrasts the relatively equal populations of glycan moieties on endogenously-expressed NLGNs present on neuronal cell surfaces (Fig. 1.7C-F).

2.3.7 High-Mannose N-glycans are Sufficient for Endogenous NLGN Surface Expression

Alanine substitution of N-linked glycosylation sites revealed the importance of these PTMs for NLGN surface export, as without N-glycans NLGN proteins are largely retained in the ER. However, N-linked glycans undergo multiple stages of diversification through a combination of glycosidase and glycosyltransferase reactions (Stanley, 2011; Bieberich, 2014), and mutating N-linked glycosylation sites indirectly eliminates these maturation steps as well. We therefore sought to investigate whether downstream glycan maturation steps play a role in promoting surface export of NLGNs, or if initial transfer of the N-glycan structure in the ER is the most critical step in this process. To this end, we employed four drugs (Fig. 1.7A). Tunicamycin (Tm) disrupts high-mannose N-glycan biosynthesis (Banerjee et al., 2011), inhibiting N-linked glycosylation from the outset and is highly toxic to cells. Kifunensine (Kf) and

deoxymannojirimycin (DMJ) inhibit Type I Golgi mannosidases required to form “hybrid” and “complex” structures, and Swainsonine (Sw) inhibits Type II Golgi mannosidases required for “complex” N-glycan formation (Tulsiani et al., 1982; Herscovics, 1999).

We assessed the impact that Tm, Kf, DMJ, and Sw had on human NLGN surface expression by surface-biotinylating WTC-11 neurons after 48 h of individual drug treatment and comparing ratios of surface / internal NLGN to control cells treated with DMSO. Here, neither Kf, DMJ, nor Sw reduced the ratio of surface protein for either NLGN2 or NLGN4X (Fig. 1.7G-J). Treatment with low doses of tunicamycin, however, reduced surface levels NLGN2 and NLGN4X while having less of an impact on the internal populations of these proteins. Therefore, while later stages of N-glycan maturation appear not to be required for NLGN surface localization, inhibition of initial N-glycan transfer through pharmacological or mutagenic approaches (i.e. alanine substitution, see Fig. 1.2) reduces the ability of NLGNs to reach the cell surface.

2.4 Discussion

My work here has shown that initial modification by N-glycosylation, but not N-glycan maturation within the Golgi, promotes NLGN export through the secretory pathway and expression on neuronal cell surfaces. We observed *in vivo* differences in NLGN1 glycoprotein maturation throughout the brain, while simultaneously NLGN2 maturation ratios remained consistent (Fig. 1.1). Further, comprehensive mutagenesis of N-glycosylated residues dramatically reduced the ER export and surface localization of NLGN protein (Fig. 1.2M-O).

Within the ER, N-linked glycosylation is an important factor in the CNX chaperone folding cycle (Moremen et al., 2012; Ferris et al., 2014). While N-glycosylation promotes some transmembrane proteins' structural stability and proper folding (Melikian et al., 1996; Mitra et al., 2006; Glozman et al., 2009), we observed no major impact on the stability or total expression of NLGN proteins after loss of N-linked glycosylation (Figs. 1.2G-J, 1.4A-D). NLGN-Null variants demonstrated a minor but significant increase in sensitivity to protease digestion (Fig. 1.2I-J), although this could result from either a slight reduction in overall stability or decreased steric hindrance due to N-glycan loss (Liu et al., 2008; Zheng et al., 2011; Friligou et al., 2021). N-glycan-Null variants retained the ability to interact with NRXN and presynaptic terminals, although, possibly due to strong impairments in surface trafficking, these interactions were severely diminished (Fig. 1.5).

Titration of Tm at low concentrations reduced surface levels of endogenous NLGN2 and NLGN4X in human neurons (Fig. 1.7G-J). Conversely, inhibiting Golgi mannosidase types I and II, critical for N-glycan maturation and diversification, failed to reduce NLGN surface levels (Fig. 1.7G-J). This, alongside alanine substitution of N-glycosylated residues, suggests that the initial transfer of N-glycan chains is critical in advancing NLGN proteins to the cell surface.

2.4.1 Addition of the High-Mannose N-glycan Structure in the ER Regulates NLGN Secretory Trafficking

Suppression of each NLGN isoform's N-glycosylation through alanine substitution led to protein retention in the ER of HEK cells (Figs. 1.2). Consequently, when HEK cells transfected with Null variants were co-cultured with primary mouse neurons, presynaptic recruitment by each isoform decreased (Figs. 1.5H-K, 1.6E-H), demonstrating the potential for N-glycan transfer to indirectly affect NLGN proteins' transsynaptic interactions by regulating surface expression. Glycosylation of certain N-glycan sequons, but not others, is critical for ER export of neuronal transmembrane proteins including AMPAR subunits GluA1 and GluA2, and NMDAR subunit GluN1 (Lichnerova et al., 2015; Takeuchi et al., 2015; Kandel et al., 2018; Morise et al., 2020). We observed similar site-specific impacts of N-glycosylation on NLGN secretory export. The conserved N-glycan Site I especially promotes surface expression and subsequent engagement of presynapses by each NLGN isoform (Fig. 1.6). For NLGN3 and NLGN4, only Site I and N-glycan-Null mutation reduced protein surface localization (Figs. 1.2K-L, 1.6C-D), indicating critical regulation of NLGN secretory transport by N-linked glycosylation of Site I for these particular isoforms.

In agreement with N-glycosylated residue mutagenesis, the fraction of endogenous NLGN2 and NLGN4X expressed on neuron cell membranes was reduced upon inhibiting high-mannose N-glycan biosynthesis via exposure to Tm (Fig. 1.7G-J). Interestingly, pharmacological inhibition of Golgi mannosidases with Kf, Dmj, and Sw had no impact on endogenous NLGN2 or NLGN4X surface expression (Fig. 1.7G-J), matching reported effects of these drugs on AMPAR maturation and surface expression (Hanus et al., 2016). The analogous effects of Tm treatment and mutation of N-glycosylated residues highlight the importance of high-mannose N-glycan transfer in the ER for NLGN forward trafficking and suggest a minimal

requirement for Golgi-mediated glycan maturation for surface expression of NLGN glycoproteins.

2.4.2 Differential Golgi-mediated N-glycan Processing of Neuronal NLGN Glycoproteins

Canonical processing of glycoproteins follows a well-characterized model. Almost all transmembrane and secreted proteins are N-glycosylated and trafficked through the Golgi apparatus, where N-glycans are diversified into structures with few exposed mannose residues (Herscovics, 1999; Stanley, 2011). We detected RCA- and WGA-recognized NLGN glycoprotein on cell surfaces of mouse hippocampal, cortical, and human iPSC-derived cultured neurons (Figs. 1.7C-F, 1.8A). This indicates the presence of GlcNAc-Gal and sialylgalactose glycan moieties, respectively associated with “hybrid” and “complex” structures, on these glycoproteins. Curiously, ConA-conjugated beads, which characteristically bind mannose residues, also pulled down surface-localized endogenous NLGNs to the same extent as RCA- and WGA-conjugated beads (Fig. 1.7C-F). In HEK cells, however, WGA-beads had greater affinity than ConA- or RCA-beads for mature NLGN bands (Fig. 1.8E, I), more closely matching the canonical profile of surface-expressed glycoproteins.

Evidence is mounting for unconventional secretory trafficking and processing in neurons. Some surface-localized neuronal proteins, including AMPAR subunits GluA1-4, have been reported to express high-mannose glycan moieties (Tucholski et al., 2014), and a fraction of surface GluA1 lacks a core fucose residue, a hallmark of Golgi-matured glycoprotein (Hanus et al., 2016). Accordingly, recent work has shown that some, but not all, GluA1 exported from the ER bypasses the Golgi apparatus (Bourke et al., 2021), resulting in a diverse population of GluA1 glycoprotein on neuronal cell surfaces, modified by mannose-rich glycans recognized by ConA but not completely devoid of GlcNAc or fucose residues (Tucholski et al., 2014). In contrast, NLGN1 is consistently trafficked to soma-localized Golgi before surface localization (Bourke et al., 2021). Endogenous NLGN1 on neuron surfaces is entirely core-fucosylated,

indicating again that the entire population of this protein passes through the Golgi (Hanus et al., 2016).

Quantitative analysis of ConA interaction with numerous glycan structures has shown that ConA preferentially binds glycans with one or more monoantennary terminal mannose residues (Li et al., 2020; Oinam et al., 2022). ConA affinity for mannose-enriched glycans decreases with increased branch diversification through GlcNAc and Gal addition, but is unimpacted by core fucosylation. The interaction of endogenous NLGNs with ConA, RCA, and WGA (Figs. 1.7C-F, 1.8A-B) indicates the presence of glycan structures consisting of core-fucosylated, minimally diversified, and mannose-exposed N-glycan chains on surface NLGNs. Importantly, mass-spectrometry analysis revealed that N-glycan structures fitting this description are in fact enriched in the neural glycome (Williams et al., 2022), and ConA reliably binds to these structures (Li et al., 2020; Oinam et al., 2022). Thus, ConA interaction alongside interaction of RCA and WGA with surface NLGN populations could suggest differential N-glycan maturation by neuronal Golgi glycosidases and glycosyltransferases as NLGN proteins are trafficked through the secretory pathway. Although surface-localized NLGNs are fucosylated (Hanus et al., 2016) and are clearly among the population of neuronal proteins that follow Golgi-directed secretory processing (Bourke et al., 2021), our data would suggest that their subsequent export to the surface is not dependent on exhaustive N-glycan modification (Fig. 1.7G-J). However, a crucial requirement for NLGN proteins to reach the cell surface seems to be the initial transfer of N-glycan structures in the ER.

2.4.3 Regulation of Endogenous Glycosylation May Influence NLGN Surface Expression

The maturation ratio of NLGN glycoprotein, determined by sialidase sensitivity (Fig. 1.1C, G), varies throughout the adult mouse brain in an isoform-dependent fashion; a greater percentage of total NLGN1 was modified by sialic acid in the cortex and hippocampus than in the cerebellum and hindbrain (Fig. 1.1I). NLGN2, on the other hand, was expressed almost

entirely in a sialidase-sensitive form (Fig. 1.1J). Considering the importance of N-glycan site occupancy (Fig. 1.2) and the availability of high-mannose glycan structures (Fig. 1.7) for promoting NLGN maturation, what might be the consequence of this altered maturation pattern for NLGN1? WGA-recognized glycan moieties on surface-expressed NLGNs (Figs. 1.7C-F, 1.8A) support recent studies showing that NLGN glycoproteins follow the canonical secretory pathway in neurons (Hanus et al., 2016; Bourke et al., 2021). Thus, although glycan maturation may not directly regulate NLGN surface export (Fig. 1.7G-J), the maturation profile of NLGN glycoprotein in neurons presumably represents their trafficking status. A decrease in the fraction of sialidase-sensitive NLGN1 in the cerebellum and hindbrain could suggest that NLGN1 may be poorly trafficked in these regions, and glycoprotein maturation possibly impaired via protein retention in the ER.

Substrate-specific glycan regulation, such as what we observed for endogenous NLGN1, is frequently reported. Instances of hypoglycosylation are most evident in patients with congenital disorders of glycosylation and in oligosaccharyltransferase (OST) subunit knockdown and knockout studies (Jaeken and Matthijs, 2007; Shrimal et al., 2013; Chang et al., 2018; NIH, 2023), but are also observed in healthy protein samples; not all predicted N-glycan sites are reportedly modified (Petrescu et al., 2004; Hülsmeier et al., 2007; Zhu et al., 2014; Hülsmeier et al., 2016). Additionally, brain region-specific regulation of N-glycosylation has been observed on both a glycome and single-protein scale, and is an ongoing realm of study (Fogel et al., 2007; Fogel et al., 2010; Toghi Eshghi et al., 2014; Gizaw et al., 2015; Klarić and Lauc, 2022; Williams et al., 2022). Not only is the neural glycome significantly simplified compared to the glycomes of other tissues, but the expression of both ER- and Golgi-associated glycosidase and glycosyltransferase genes varies between different regions of the brain as well (Klarić and Lauc, 2022; Williams et al., 2022). These findings explain protein-specific regulation of glycosylation

patterns, observed frequently for the SynCAM family of synaptic cell adhesion molecules (Fogel et al., 2007; Fogel et al., 2010) and NLGN1 (Fig. 1.1).

The research presented in this chapter suggests that as NLGNs are transported through the secretory pathway, initial N-glycosylation of the protein is most critical for proper maturation and secretory trafficking of NLGN protein (Figs. 1.2, 1.7). We also detected elevated levels of mannose-rich glycan moieties on endogenous NLGN expressed in neurons vs. those expressed ectopically in HEK cells (Figs. 1.7, 1.8). Cellular glycan profiles largely depend on glycosyltransferase expression in the Golgi (Moremen et al., 2012; Stanley et al., 2022), and differential expression of Golgi-associated glycan maturation enzymes was recently reported between neuronal and non-neuronal tissue (Williams et al., 2022). Further, we detected isoform-specific differences in glycan maturation of NLGN1 between regions of the adult mouse brain, with increased levels of sialidase insensitive and presumably ER-localized NLGN1 in the cerebellum and hindbrain (Fig. 1.1). While perhaps cerebellum- and hindbrain-expressed NLGN1 is hypoglycosylated (Fig. 1.2, 1.6), the exact mechanism resulting in decreased glycan maturation remains unclear. Further investigation into N-glycan site occupancy would be required to determine whether hypoglycosylation is a method by which the surface expression of endogenous NLGNs is regulated.

CHAPTER 3: R101Q MUTATION IMPAIRS NLGN4 GLYCOSYLATION AND REDUCES SURFACE LOCALIZATION IN HUMAN NEURONS

The research presented in this chapter was performed in collaboration with Daniel Boesch, Alisa Shaw, and Soham Chanda.

3.1 Introduction

Autism spectrum disorder (ASD) is a multifaceted developmental disorder defined by impaired non-verbal communication and social interaction, restricted and repetitive behaviors, and hyper/hypo-reactivity to sensory input (DSM-V, 2013). ASD is often comorbid with intellectual disability, epilepsy, and psychiatric diagnoses, including ADHD, anxiety, and depression (Spence and Schneider, 2009; Romero et al., 2016). Approximately four males are diagnosed for every one female (Maenner et al., 2023), and the disorder is ~80% heritable, most often attributed to *de novo* mutations (Beaudet, 2007; Sebat et al., 2007; Taylor et al., 2014). Common genes mutated in patients with ASD are those governing synaptic properties, including synapsin, which regulates NT vesicle release, SHANK, a family of postsynaptic scaffolding proteins, NRXNs, and NLGNs (Giovedí et al., 2014; Monteiro and Feng, 2017; Stessman et al., 2017; Guang et al., 2018). Mutations in these genes are theorized to alter the E/I balance in the CNS, and it was confirmed through functional EEG recordings that children with ASD indeed exhibit elevated E/I ratios compared to age-matched neurotypical children (Bruining et al., 2020).

NLGN gene variants were among the first to be directly linked to an ASD diagnosis. The isoform most frequently associated with ASD is NLGN4 (also called NLGN4X), located on the X-chromosome (Jamain et al., 2003; Laumonnier et al., 2004; Chocholska et al., 2006; Lawson-Yuen et al., 2008; Pampanos et al., 2009; Zhang et al., 2009). While not every polymorphism in this gene results in an autistic phenotype (Xu et al., 2017), over 50 NLGN4 variants have been identified that are strongly implicated in ASD (SFARI, 2021a). These mutations include

chromosomal deletion (Chocholska et al., 2006), truncations (Laumonnier et al., 2004), and both inherited and *de novo* missense mutations that confer effects ranging from impaired folding and loss-of-function (Zhang et al., 2009) to increased receptor affinity (Yan et al., 2005; Marro et al., 2019), and some with yet unknown molecular consequences (Xu et al., 2014; Nguyen et al., 2020). This chapter focuses on the characterization of molecular and consequential cellular impacts of the missense variant NLGN4-R101Q.

The R101Q variant was discovered in a child diagnosed as severely autistic, exhibiting delayed verbal communication development and impairments in executive functioning. Neuropsychological tests performed by the proband's clinician included Social Responsiveness Scale (Constantino, 2005, 2012) test, Aberrant Behavior Checklist (Aman, 1994), Vineland Adaptive Behavior Scale (Sparrow et al., 2016), and Childhood Autism Rating Scale (Schopler and Van Bourgondien, 2010), each reliably placing the proband within the range of severe autism. Whole-exome sequencing revealed a missense mutation within the proband's X-linked NLGN4 gene. While many reported ASD-associated mutations are *de novo*, this mutation, c.302G>A, p.Arg101Gln (R101Q), is inherited from the proband's mother, who displays no signs of developmental disability. In this chapter, I characterize the molecular features of NLGN4-R101Q, the conservation of those effects when equivalent RQ mutations are introduced in NLGN1-3, and finally the synaptic morphological consequences of the NLGN4-R101Q variant expressed in human neurons.

3.2 Materials and Methods

Adapted from Cast et al. 2021.

Structural Prediction of NLGN4: The amino-acid sequence of human NLGN4 was uploaded to Phyre2 web-portal and fit against the previously resolved rat NLGN1 crystal structure with 100% confidence. The resulting PDB file was modeled and colored using Chimera (University of California San Francisco). A 40% transparency was applied to the surface model in order to visualize its secondary structures. The alpha-helix bundle involved in NLGN4-dimerization and the residues creating NRXN1-contact sites were respectively highlighted with purple and green (reported by Leone et al., 2010). The location of R101Q mutation and adjacent N-linked glycosylation site (N102) were colored-coded blue and red, respectively.

General Experimental Design: All experiments were carried out with the approval of Colorado State University Institutional Biosafety Committee (IBC, protocol 19-059B). Experiments (except the western blots and induced neurogenesis) were conducted in 'blinded' fashion; i.e., the experimenters were unaware of the sample types being analyzed.

Vector Design: Reliable antibodies for NLGN4 do not exist. Therefore, we introduced a hemagglutinin (HA) or FLAG epitope-tag in wild-type (WT) human NLGN4X coding sequence (CDS) after its N-terminal signal peptide (1-41 amino acids) cleavage site, which does not interfere with NLGN4's surface trafficking (Chanda et al., 2016; Marro et al., 2019). The R101Q and N102A mutations were introduced in HA-NLGN4X CDS using site-directed mutagenesis. Similar strategies were implemented for generating HA-tagged rat NLGN1/2 and mouse NLGN3 expression cassettes carrying R101Q-equivalent mutations. These constructs were then inserted into a vector preceded by cytomegalovirus (CMV) promoter, a Kozak sequence, and followed by an Internal Ribosome Entry Site (IRES)-driven fluorescent protein, either enhanced

green fluorescent protein (eGFP) or mOrange. The HA-tagged rat NRXN1β without splice-site #4 (NRXN1β^{-SS4}) was cloned and expressed using a similar approach.

NLGN Immunoblotting: HEK293 cells were transfected with respective vectors using polyethylenimine (PEI), and allowed to express the constructs for 48 hours with media exchanges at 8 and 24 hours. Cells were collected by scraping and lysed in RIPA buffer (150 mM NaCl, 5 mM EDTA, 25 mM Tris pH 7.4, 1% Nonidet P-40 substitute, 0.5% Sodium Deoxycholate) supplemented with Halt™ protease inhibitor cocktail (PIC, Thermo Scientific, Cat# 78429). Lysates were mixed with 2.5-5% sodium dodecyl sulphate (SDS) loading buffer, run on a 7.5% poly-acrylamide gel (PAGE), and transferred to a nitrocellulose membrane. Membranes were blocked with 1-3% bovine serum albumin (BSA) in Tris-buffered saline and then immunostained overnight at 4°C with mouse anti-HA (1:1000; Sigma-Aldrich, Cat# h3663) or rabbit anti-HA (1:3000; Proteintech, Cat# 51064-2-AP) antibodies. Membranes were stained with fluorescent secondary antibodies and imaged using a LI-COR Odyssey CLx imaging system. Mouse anti-GAPDH primary antibodies ([1:60000; Proteintech, Cat# 60004-1-Ig] or [1:10000; Sigma-Aldrich, Cat# MAB374]) were used as well-loading control, whereas a mouse anti-GFP antibody (1:1000; ABClonal, Cat# AE012) was used as transfection control for quantifying relative protein expressions (NLGNs / EGFP intensity). Normalized ratios of mature vs. immature NLGNs were calculated as corresponding fractions of total (mature + immature) NLGN1/2/3/4 levels.

Cell-Aggregation Assay: Human embryonic kidney (HEK293) cells (60-70% confluent) were separately transfected with either EGFP-only control or NLGN4(WT/R101Q)-IRES-EGFP, and NRXN1β-IRES-mOrange constructs. After 48 hours, cells were washed once with PBS and dissociated with EDTA (1 mM in PBS). Cells were triturated and resuspended at a concentration of $1x10^6$ cells/ml in DMEM media (Genesee Scientific) supplemented with 10 mM $CaCl_2$. NRXN-expressing cells (300 µl) were mixed with appropriate combinations of control vs. NLGN4 WT

vs. R101Q mutant -expressing cells (300 µl) in a tube-rotator for 2 hours at room temperature. Cell mixtures were imaged using a Keyence BZ-X710 microscope and analyzed using Mander's coefficient of co-localization.

Immunoprecipitation: To monitor NLGN4 homodimerization, lysates from HEK293 cells expressing both HA- and FLAG-tagged NLGN4 constructs (WT/R101Q) were collected in RIPA buffer and incubated with mouse anti-HA antibody (1:250; Sigma-Aldrich, Cat# h3663) or non-specific mouse Immunoglobulin G (IgG) antibody as an isotype control (1:250; Sigma-Aldrich, Cat# PP100) in a tube-rotator overnight at 4°C. For heterodimerization analysis, lysates were collected in 1% NP-40 buffer and similarly incubated with anti-HA antibody. The lysate and antibody mix were incubated with protein G-sepharose beads (BioVision, Cat# 6511-1) while rotating for 4 hours at 4°C. These mixes were then washed 3 times with RIPA buffer supplemented with PIC. Next, the beads were resuspended in 25 µl SDS loading buffer and placed in boiling water for 20 minutes. The mixture was vortexed, spun (13,000 rpm for 5 minutes), and the eluate was collected to run on an SDS-PAGE. The gels were transferred to a nitrocellulose membrane and blotted with mouse anti-HA (1:1000; Sigma-Aldrich, Cat# h3663) and rabbit anti-FLAG (1:2000; Sigma-Aldrich, Cat# F7425) antibodies.

Glycosidase Treatment: For deglycosylation experiments, HA-tagged NLGN4 WT vs. R101Q mutant proteins were immunoprecipitated using anti-HA antibody and protein G-sepharose beads, as described above. The beads were then spun down at 13000 rpm for 2 minutes, resuspended in 20 µl RIPA + PIC, and treated with either Endoglycosidase H (Endo H, New England Biolabs, Cat# P0702S) or PNGase F (New England Biolabs, Cat# P0704S) per manufacturer specifications for 1 hour at 37°C in a tube-rotator. Nonidet P-40 substitute was omitted from PNGase F treatments due to its presence in RIPA buffer. These deglycosylated products were collected by centrifugation, the supernatants were removed, and 15 µl SDS

loading buffer was added. Tubes were boiled for 10 minutes, spun again to remove any aggregates, and the eluates were collected for western-blot analysis.

Lentivirus Production: For neuronal expression, the EGFP-only control or NLGN4(WT/R101Q)-IRES-EGFP cassettes were cloned into a lentiviral vector under human Synapsin (hSyn1) promoter, followed by a Woodchuck regulatory element (WRE), and flanked by 5' and 3' long terminal repeats (LTR). Similar policy was adopted to generate lentiviruses for NLGN4(WT/R101Q)-IRES-mOrange and SEP-GluA1 (AMPA receptor [AMPAR] subunit GluA1 fused to super ecliptic pHluorin [SEP, a pH-sensitive variant of EGFP]) constructs. The viral vectors used for Neurogenin-2 (Ngn2) -induced neuronal reprogramming of embryonic stem (ES) cells included Ngn2-T2A-Puromycin^{Resistance} and rtTA (driven by Tet-on and Ubiquitin promoters, respectively).

Three helper plasmids (pRSV-REV, pMDLg/pRRE, and VSV-G; 7 µg each) and corresponding expression vectors (20 µg) were co-transfected with PEI into 70-80% confluent HEK293T (containing SV40 T-antigen to facilitate virus production) cells plated on 10 cm dishes. At 8-9 hours post-transfection, the culture medium was exchanged completely, and the supernatant containing viral particles was collected after 36 hours and 60 hours. The supernatant was then pooled and spun at 1200 rpm for 6 minutes to remove any HEK cell debris. The supernatant was then spun at 30,000 rpm for 2 hours at 4°C (Beckman L8-70M ultracentrifuge equipped with SW41Ti rotor). The viral pellet was resuspended overnight in ~100 µl DMEM media, subsequently aliquoted, and frozen at -80°C before use.

Generation of Human Neurons: Human ES (male H1-line, WiCell WA01) cells were maintained under feeder-free conditions in mTeSR plus media (StemCell Technologies). Media was changed every day. When cell density reached ~70%, they were dissociated with PBS-EDTA (0.5 mM) and plated at 1:6 dilution onto Matrigel (BD Biosciences) -coated wells. During

passaging, the cultures were additionally supplemented with ROCK-inhibitor Y-27632 (2.5 µM, MedChemExpress) overnight.

Differentiation of human ES cells into neural stem cell (NSC) monolayer was achieved by dual SMAD inhibition (Chambers et al., 2009) with minor modifications as described previously (Chanda et al., 2019). In brief, Oct3/4-positive H1-ES cells were treated with LDN193189 (100 nM, StemCell Technologies) and SB431542 (10 µM, StemCell Technologies) for 6 days to induce them into Nestin-positive NSCs. The NSCs were then passaged and expanded by 1:6 split, and subsequently treated with Cytarabine (Ara-C, 2 µM) to prevent further proliferation. During this period, the NSCs spontaneously differentiated into Dcx-positive neurons. The cells were finally dissociated with accutase (Innovative Cell Technologies) and replated with primary mouse glia (passage 1-2, derived from C57BL/6 strain) on Matrigel-coated coverslips at 1:50 ratio. These cells were cultured in N3 media (DMEM/F12 [Thermo Fisher], N2 [Thermo Fisher], and B27 [Thermo Fisher], supplemented with insulin [20 µg/ml, Sigma] and penicillin/streptomycin [Thermo Fisher]).

Transcription factor (TF) -mediated direct neuronal reprogramming was achieved as described before (Zhang et al., 2013; Chanda et al., 2019). In brief, the H1-ES cells were co-infected with lentiviruses expressing rtTA and Ngn2-t2A-Puromycin^{Resistance}, induced with doxycycline (2 µg/ml), selected using puromycin (1 µg/ml), and cultured together with mouse glia in N3 media. The NSC-derived or Ngn2-induced human neurons were additionally infected with control or NLGN4(WT/R101Q) -expressing lentiviruses, as needed.

Immunostaining: After 48 hours of transfection, the HEK293 cells were washed once with PBS and immediately fixed with 4% paraformaldehyde (PFA) for 20-30 minutes at room temperature, followed by an additional wash with PBS. Human neurons expressing NLGN constructs were similarly fixed with 4% PFA. Cells were blocked in 10% cosmic calf serum (CCS) for 1 hour at 37°C, incubated with primary antibodies for 1-2 hours at 37°C, washed 4

times with blocking buffer, followed by incubation with fluorophore-conjugated secondary antibodies for 1 hour at 37°C. Cells were then washed 4 times with PBS and mounted on glass slides using Fluoromount-G (Southern Biotech). For immunostaining experiments where permeabilization was required, 0.1% triton X-100 was added to the blocking buffer and for all subsequent steps including washes or antibody dilution. Cells were also nuclear-stained with DAPI (1:50000; Thermo Fisher, Cat# D1306) for 10 minutes when applicable. Images were acquired using an inverted microscope (Olympus, IX83) equipped with LaserStack units (Intelligent Imaging Innovations, 3iL33) and spinning disk confocal scanner (Yokogawa, CSU22), or a STELLARIS 5 (Leica Microsystems) laser scanning microscope. A series of z-projections were obtained with 0.5-1 µm optical thickness using either a 20x dry objective or 40-63x oil-immersion objectives.

Primary antibodies for immunolabeling included mouse anti-HA (1:1000; Sigma-Aldrich, Cat# h3663), rabbit anti-Calnexin (1:500; Thermo Fisher, Cat# PA5-34754), rabbit anti-GM130 (1:300; ABClonal, Cat# A5344), chicken anti-GFP (1:500; Aves Labs, Cat# GFP-1020), mouse anti-Oct3/4 (1:200, Santa Cruz Biotechnology, Cat# sc-5279), mouse anti-Nestin (1:500; R&D Systems, Cat# MAB1259), goat anti-Dcx (1:500; Santa Cruz Biotechnology, mixture of Cat# sc-8066 and 8067), mouse anti-Tuj1 (1:1000, BioLegend, Cat# 801202), chicken anti-MAP2 (1:400; Abcam, Cat# ab5392), mouse anti-MAP2 (1:500; Sigma-Aldrich, Cat# M1406), rabbit anti-Synapsin1/2 (1:500; Synaptic Systems, Cat# 106002), rabbit anti-vGAT (1:200; Synaptic Systems, Cat# 131003), rabbit anti-vGLUT1/2 (1:500; Yenzym, mixture of Cat# YZ6089, 6093, 6102), and Alexa Fluor 488/555/647-conjugated secondary antibodies (Invitrogen). A mouse anti-GFP antibody (1:500; ABClonal, Cat# AE012) was used to further amplify surface SEP-GluA1 signals under non-permeabilized condition.

Image Analysis: All images were analyzed using FIJI-ImageJ (NIH, USA) software. Images of HA-NLGN surface localization in HEK293 cells were converted into maximum-

intensity projections (2-3 optical slices) and the mean signal-intensity per cell was normalized to corresponding fluorescent reporter-protein intensity. Images of NLGN4 co-localization at ER and Golgi were appropriately thresholded and analyzed using Mander's coefficient within JACoP plugin. To quantify synaptic puncta along neuronal processes, images were obtained with maximum-intensity projection, channels containing neurite arbors were converted into ROIs to specify analysis areas for synaptic markers. The ROI masks were then skeletonized, and total pixel length of these skeletons was measured for normalization.

Quantitative RT-PCR: Ngn2-induced human neurons from control, NLGN4 WT, and NLGN4 R101Q conditions were washed with ice-cold PBS, and collected in 500 µl TRIzol™ reagent. 250 µl chloroform was added to the cell lysate, vortexed vigorously, centrifuged at 12000 x g for 15 minutes, aqueous phase collected, and RNA precipitated by adding 250 µl isopropanol and centrifuging at 12000 x g for 10 minutes. The RNA pellets were washed with 70% ethanol, air-dried, and dissolved in nano-pure water.

Complementary DNA (cDNA) was generated from 200-400 ng total RNA using SuperScript™ III First-Strand Synthesis SuperMix (Invitrogen, Cat# 11752-050) following the manufacturer's protocol. Quantitative PCR (qPCR) was performed on a CFX-96 (Bio-Rad) machine using SYBR Green master mix (Gold Biotechnology, Cat# M-915). Two independent primer sets were designed that spanned two NLGN4 exons [Set 1: forward, 5'-GAAGCCCGTCATGGTCTATATC-3'; reverse, 5'-AGTATTCCCAGACGGTAGTTAATG-3'. Set 2: forward, 5'-ACCTGGATGAGAGATCCTTACT-3'; reverse, 5'-CGTGGGCACGTAGATGTTTA-3']. A human GAPDH primer set [forward, 5'-TTGAGGTCAATGAAGGGGTC-3'; reverse, 5'-GAAGGTGAAGGTCGGAGTCA-3'] was used as an internal control to normalize the NLGN4 expression levels per sample.

Data Presentation: For batch-wise comparisons (i.e. immunoblots and qPCR), the total number of experimental replicates are indicated with corresponding average values. For all

other experiments (i.e. electrophysiology and imaging), the average values are presented with X/Y, where ‘X’ represents the total number of neurons recorded (electrophysiology) or field-of-views analyzed (imaging) from ‘Y’ number of independent batches. All average data indicate means ± SEM (standard-deviation [SD] of parameter tested divided by square-root of number of samples). In most cases, statistical comparisons between conditions were made using unpaired (paired for batch-wise comparisons), two-tailed, Student’s t-test (*** $P < 0.005$; ** $P < 0.01$; * $P < 0.05$; ns = not significant, $P > 0.05$). In some cases, one-way ANOVA (for group assessments) or Kolmogorov-Smirnov (KS, for cumulative distribution) tests were performed, as mentioned in the figure legends.

3.3 Results

3.3.1 Molecular Characteristics of NLGN4-R101Q Variant

The R101Q mutation is located within the globular acetylcholinesterase-like domain of NLGN4, directly adjacent to a consensus sequon for N-linked glycosylation (Site I, see Chapter 2) and upstream of a Cys-loop (Fig. 2.1A). Many ASD-associated missense mutations have been described in this region (Nguyen et al., 2020), including R87W (Zhang et al., 2009), G94R (Xu et al., 2014), and G99S (Yan et al., 2005). In the tertiary NLGN4 structure, the R101Q mutation is opposite NLGN4's dimerization domain and the NRXN contact surface (Fig. 2.1B).

First, we aimed to determine whether NLGN4-R101Q protein expression is comparable to WT. HEK293 cells were transfected with HA-tagged NLGN4-WT or R101Q, each followed by a co-transcribed fluorescent reporter (Fig. 2.2A). These cells were lysed after two days of expression and whole-cell lysate analyzed on Western blot. Like other NLGN proteins, we observed bands of two distinct masses for NLGN4-WT, a lower mass form representative of immature glycoprotein, and a more intense, higher mass form thought to be indicative of surface localized and mature NLGN glycoprotein (Poulopoulos et al., 2012), see Figs. 1.2, 1.7. While introduction of the R101Q mutation resulted in only a minor decrease in total NLGN4 protein level vs. the EGFP reporter, we noticed an additional impact of the mutation on the ratio of mature/total protein levels. Over 90% of NLGN4-WT was present in mature form, decreasing to ~60% mature for NLGN4-R101Q with a corresponding increase in immature protein levels (Fig. 2.2B-C). Several other ASD- and ID-associated NLGN4 mutations impact cell surface expression of the protein (Zhang et al., 2009; Nguyen et al., 2020), so to probe for any such effect brought on by the R101Q variant, HEK cells were seeded onto glass coverslips, transfected with HA-NLGN4-WT or -R101Q constructs (Fig. 2.2A) and fixed after two days of expression. Immunostaining for surface-localized HA under non-permeabilized conditions and normalizing to co-transcribed mOrange, we observed ~40% less NLGN4-R101Q on the surface

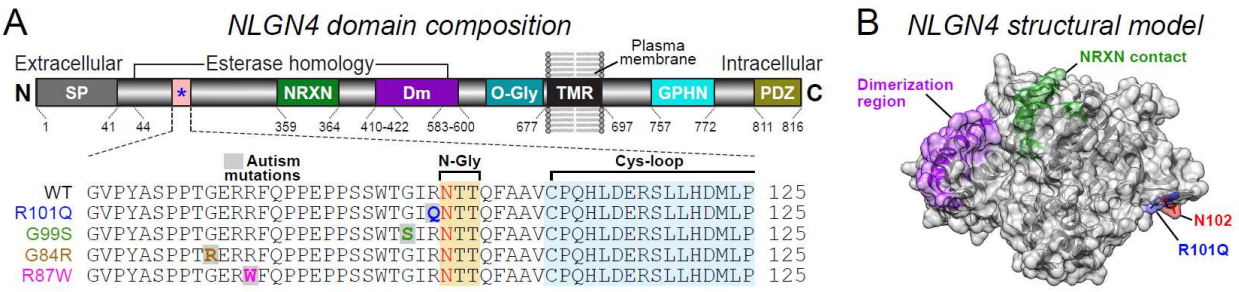

Figure 2.1: **Description of NLGN4 missense mutation in an autistic patient.**

A. Annotated map of NLGN4 with domain composition and corresponding amino-acid numbers (top, not to scale): signal peptide (SP, grey), NRXN-binding domain (NRXN, green), dimerization residues (Dm, purple), O-glycosylation site (O-Gly, teal), transmembrane region (TMR, black), Gephyrin-binding domain (GPHN, cyan), and PDZ-binding sequence (PDZ, gold). The R101Q mutation is located within the esterase homology domain of NLGN4 (bottom, magnified view), neighboring a consensus site for N-linked glycosylation (N-Gly, yellow) and proximal to a Cysteine-loop structure (Cys-loop, blue). The R101Q variant is also adjacent to previously-reported ASD mutations, e.g. G99S, G84R, and R87W.

B. Model of NLGN4 extracellular domain indicating spatial orientation of the R101Q mutation (blue), proximal to N-glycosylation (red) residue, and distal from dimerization (purple) and NRXN-contacting (green) regions.

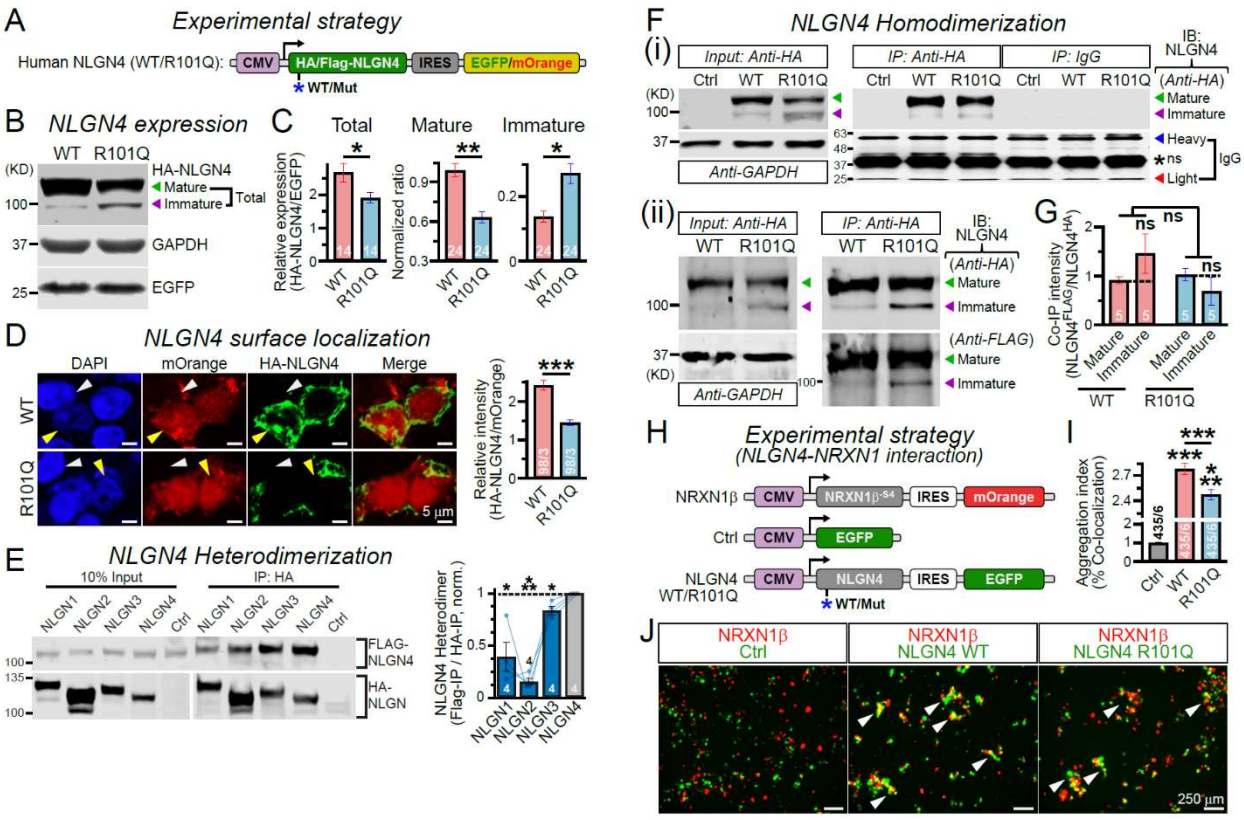

Figure 2.2: **R101Q mutation prevents maturation and surface localization of NLGN4.**
(Generated in collaboration with Michael Ghebrial, Alisa Shaw)

A. Design of NLGN4 (WT/R101Q) expression vectors (for details, see Materials and Methods).

B. Representative immunoblot of HA-tagged NLGN4 (top) collected from HEK293 cells expressing NLGN4 WT or R101Q variant; arrowheads indicate mature (green) vs. immature (purple) NLGN4 products. GAPDH was used as a loading control (middle), and EGFP was used as transfection control (bottom).

C. Bar-graphs summarize relative expression of total (mature + immature, left), mature (middle) or immature (right) products in WT vs. R101Q conditions when normalized to corresponding EGFP levels.

D. Sample images (left) of HEK293 cells transfected with NLGN4 WT (top) and R101Q (bottom) constructs co-expressing mOrange (red), immunolabeled with HA-antibody under non-permeabilized condition (green), and counterstained for DAPI (blue). Yellow vs. white arrowheads point at transfected vs. non-transfected cells, respectively. Summary-graph (right) of HA-NLGN4 surface expression normalized to mOrange signal intensity.

E. Left: Co-immunoprecipitation of HA-NLGN1/2/3/4, or negative control, co-transfected with FLAG-NLGN4-WT. The same lanes were immunolabeled with mouse anti-HA vs. rabbit anti-FLAG antibodies. Right: Quantification of FLAG-NLGN4 signal vs. respective HA-NLGN1/2/3/4 signal.

F. Immunoprecipitation experiment **(i)** from HEK293 cells in untransfected control (Ctrl) or those expressing HA-tagged NLGN4 (WT vs. R101Q) constructs: sample immunoblots (IBs) with anti-

(Fig. 2.2 cont.)

HA antibody for 10% input (left, with GAPDH as a loading control), or when immunoprecipitated (IP) with anti-HA antibody vs. IgG control (right); arrowheads point at mature (green) vs. immature (purple) NLGN4 products, IgG heavy (blue) or light (red) chains, and asterisk indicates a nonspecific (ns) 'sticky' band. To assess NLGN4 dimerization **(ii)**, both HA- and FLAG-tagged versions of NLGN4 were co-expressed in HEK cells, immunoprecipitated with anti-HA antibody (right) and the same lanes were immunolabeled with mouse anti-HA vs. rabbit anti-FLAG antibodies.

G. Summary graph indicates relative intensity of immunoprecipitated FLAG-NLGN4 compared to HA-NLGN4, for mature vs. immature products in WT vs. R101Q conditions.

H. Experimental strategy for probing NLGN4-NRXN interaction (for details, see Materials and Methods).

I-J. Average bar-graphs (**H**) and example images (**I**) of aggregates (white arrowheads) formed by HEK cells expressing NRXN with mOrange reporter, and either control vector or NLGN4 (WT/R101Q) with EGFP reporter. Quantification of cell-aggregates were performed using Mander's coefficient of co-localization, and normalized to control condition.

All numerical data are presented as means ± SEM, with total number of batches analyzed (for western-blots) or field-of-views analyzed / independent batches (for imaging). Statistical significance was evaluated by two-tailed, unpaired (paired for batch-wise comparisons, **C** and **F**), Student's t-test, or one-way ANOVA (across all conditions, in **F**), with *** $P < 0.005$; ** $P < 0.01$; * $P < 0.05$; ns = not significant, $P > 0.05$.

of transfected HEK cells compared to WT (Fig. 2.2D), indicating a surface expression defect correlating with the observed impairment of protein maturation.

NLGN proteins constitutively form dimers, which is likely required for ER export (Poulopoulos et al., 2012). Thus, a dimerization defect could potentially cause the reduced surface expression observed for NLGN4-R101Q. We first sought to characterize the heterodimerization preferences of NLGN4. FLAG-tagged NLGN4-WT was co-transfected into HEK cells alongside HA-tagged NLGN1/2/3/4-WT. Lysates were collected after 48 h of expression and immunoprecipitated with anti-HA antibody before analysis on Western blot. By quantifying the relative intensity of FLAG-NLGN4 vs. immunoprecipitated HA-NLGN for each dimer pair, we found that NLGN4 preferentially homodimerizes while substantially heterodimerizing with NLGN3 and minimally heterodimerizing with NLGN1 or NLGN2 (Fig. 2.2E). Considering this, we tested whether R101Q mutation impacts NLGN4 homodimerization. Here, it is evident that the R101Q mutation had no impact on protein dimerization; the relative intensities of FLAG and HA signal were not significantly different between WT and R101Q conditions for both mature and immature bands (Fig. 2.2Fii-G).

Next, we performed a cell-aggregation assay to test whether R101Q mutation impacted another key quality of NLGN proteins, interaction with NRXN. HEK cells were transfected with NRXN1β lacking splice site 4 (SS4-) followed by an IRES-mOrange reporter, while separate cultures of HEK cells were transfected with NLGN4-WT-IRES-EGFP, NLGN4-R101Q-IRES-EGFP, or EGFP control (Fig. 2.2H). After two days of expression, cells were lifted with 1mM EDTA in PBS, fluorescent cells counted, and then equimolar ratios of mOrange- and EGFP-expressing cells were mixed in DMEM supplemented with 10 mM $CaCl_2$ to facilitate NLGN-NRXN interaction. After two hours of rotation, cells were spotted onto glass slides and imaged. As expected, NRXN1β $^{SS4-}$-expressing mOrange cells interacted minimally with EGFP-only control cells, while incubation of NLGN4-WT with NRXN1β $^{SS4-}$-expressing cells induced the

formation of cellular aggregates (Fig. 2.2I-J). Addition of the R101Q mutation to the NLGN4-expressing cells caused a minor but significant decrease in colocalization of EGFP and mOrange cells, which was still well above the observed interaction with EGFP controls (Fig. 2.2I-J). We thus conclude that NLGN4-R101Q is likely not impaired in its interaction with NRXN, and the observed decrease in cell aggregation is instead due to the decrease in surface expression of the mutant protein.

3.3.2 NLGN4-R101Q is Specifically Impaired in Glycan Maturation and Secretory Transport

As mentioned, the R101Q mutation identified in the proband is directly adjacent to a sequon for N-linked glycosylation. This sequon corresponds to the conserved Site I (see Chapter 2, Fig. 1.2A), which for all other NLGN protein isoforms promotes glycoprotein maturation and surface localization. X-ray crystallography has previously confirmed a glycan chain modifying this asparagine residue on the WT protein (Fabrichny et al., 2007). Since N-linked glycosylation is added co-translationally to nascent peptide chains entering the ER, we questioned whether the R101Q mutation could interfere with glycan occupancy at this site. We introduced an alanine substitution at NLGN4 residue N102 to fully inhibit glycosylation (Fig. 2.3A) and analyzed the maturation profile via Western blot. Much like the R101Q variant, the ratio of mature/immature protein decreased upon the introduction of N102A mutation (Fig. 2.3B), suggesting that NLGN4-R101Q may be impaired in its glycan maturation. To investigate this possibility, we treated NLGN4-WT and -R101Q protein extracted from transfected HEK cell lysate with endoglycosidases: EndoH and PNGaseF. EndoH cleaves N-glycan chains between the two GlcNAc residues of the N-glycan core but is inhibited by the addition of fucose to the primary GlcNAc residue, which occurs in the Golgi apparatus (Stanley, 2011). EndoH sensitivity is thus a reliable indicator of ER-associated immature glycans. PNGaseF cleaves all mammalian N-glycans from the amino acid chain regardless of further modifications. Incubating WT and R101Q variants with PNGaseF increased the mobility shift of both mature and

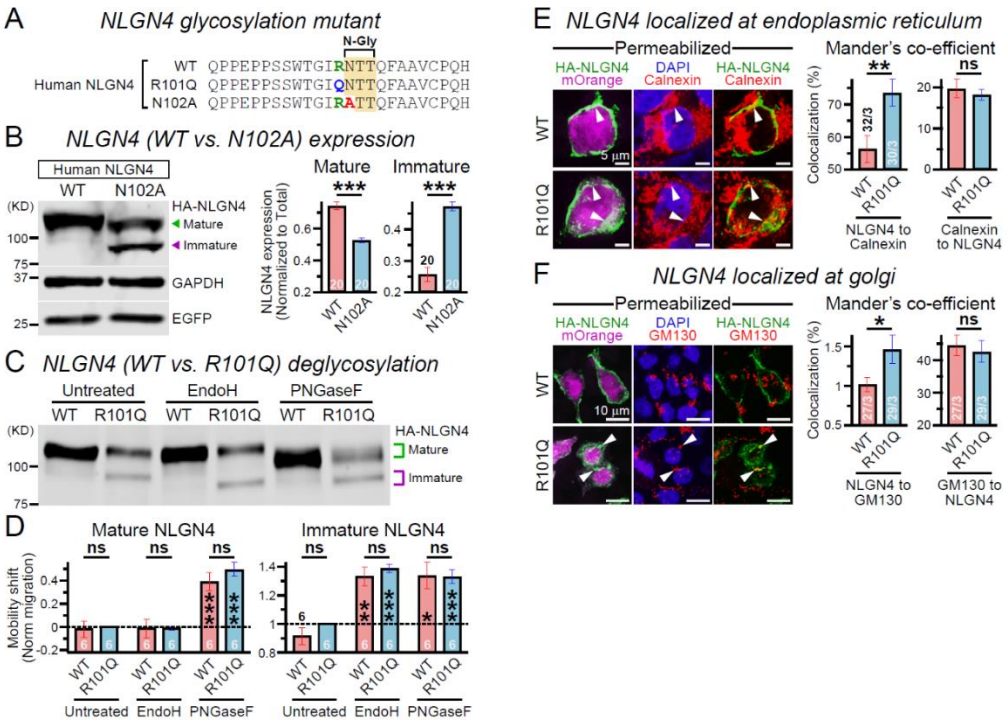

Figure 2.3: **R101Q mutation blocks NLGN4 glycosylation and retains it at intracellular compartments.** (Generated in collaboration with Daniel Boesch)

A. Alanine-substitution of NLGN4 N102 residue to prevent N-linked glycosylation (N-Gly).

B. Western-blot (left) illustrating mature (green arrowhead) vs. immature (purple arrowhead) HA-NLGN4 products harvested from HEK293 cells expressing NLGN4 WT vs. N102A mutant, with EGFP as a transfection control and GAPDH as a loading control. Summary-graphs (right) of total, mature and immature NLGN4 normalized to EGFP signal. **C-D.** Example immunoblot (**C**) for NLGN4 WT and R101Q variant, before (untreated) and after enzymatic deglycosylation with glycosidases, i.e. Endo H and PNGase F. Bar-graphs (**D**) represent relative positions of mature (left) and immature (right) NLGN4 products. To compare across multiple experimental batches with slightly variable mobility shifts, the position of all bands was normalized (dotted lines) to corresponding distance between the mature and immature bands in untreated R101Q condition.

E. Representative images (left) of HEK293 cells expressing NLGN4 WT (top) or R101Q mutant (bottom), as visualized by an IRES-driven mOrange reporter, and stained with DAPI, HA-antibody, and Calnexin-antibody (respective channels) under permeabilized conditions. Arrowheads point at intracellular HA-NLGN4 co-localized with soluble mOrange and ER-marker Calnexin. Summary graphs (right) quantify the correlation between HA-NLGN4 and Calnexin signals, measured via Mander's coefficients.

F. Same as **E**, except the cells were counterstained with GM130 antibody.

The values on bar-graphs represent means ± SEM for number of experimental batches (immunoblots), or field-of-views analyzed (imaging) / number of independent batches. Statistical significance was weighed by two-tailed, paired (for immunoblots) or unpaired (for imaging), Student's t-test, with *** $P < 0.005$; ** $P < 0.01$; * $P < 0.05$; ns = not significant, $P > 0.05$.

immature bands, evident through Western blot (Fig. 2.3C, right). EndoH, however, caused only the immature protein band to decrease in mass on Western blots (Fig. 2.3C-D), indicating that the low-mass NLGN4 protein, which increases in abundance upon introduction of the R101Q mutation, is immaturely glycosylated.

N-linked glycosylation is an important regulator of transmembrane protein trafficking through the secretory pathway (Melikian et al., 1996; Rosnoblet et al., 2013; Park et al., 2020). We have so far observed that the NLGN4-R101Q variant is impaired in its surface localization (Fig. 2.2D) and Golgi apparatus-associated N-glycan maturation (Fig. 2.3D) while its total protein expression is only somewhat reduced (Fig. 2.2C). Therefore, we hypothesized that NLGN4-R101Q would be retained along the secretory pathway. HEK cells seeded onto glass coverslips were transfected with HA-NLGN4-WT or -R101Q, preceding co-transcribed IRES-mOrange. These cells were permeabilized with Triton-X-100 and immunostained with HA antibody and antibodies against markers of the ER (CNX) or the Golgi (GM130). Colocalization analysis revealed that the R101Q variant was more often colocalized with both the ER and the Golgi than the WT variant (Fig. 2.3E-F). Together, these results suggest that the R101Q mutation impairs both glycan maturation and secretory export of NLGN4 protein, culminating in a decrease in protein surface localization.

3.3.3 The Effects of RQ Mutation are Conserved in Other NLGN Isoforms

Both the R101 residue and adjacent N-linked glycosylation sequon found in NLGN4 are conserved in other members of the NLGN family, except for mouse NLGN4-*like* (Fig. 2.4A and see Chapter 2). Therefore, we wondered whether the effects of NLGN4-R101Q would be conserved in other NLGN isoforms. Equivalent RQ mutations were made in HA-tagged NLGN1, 2, and 3, which were then transfected into HEK cells alongside WT counterparts. When whole-protein extract from these cells was analyzed on Western blots, decreases in mature protein ratio similar to that of NLGN4-R101Q were observed for each mutated isoform (Fig. 2.4C-E),

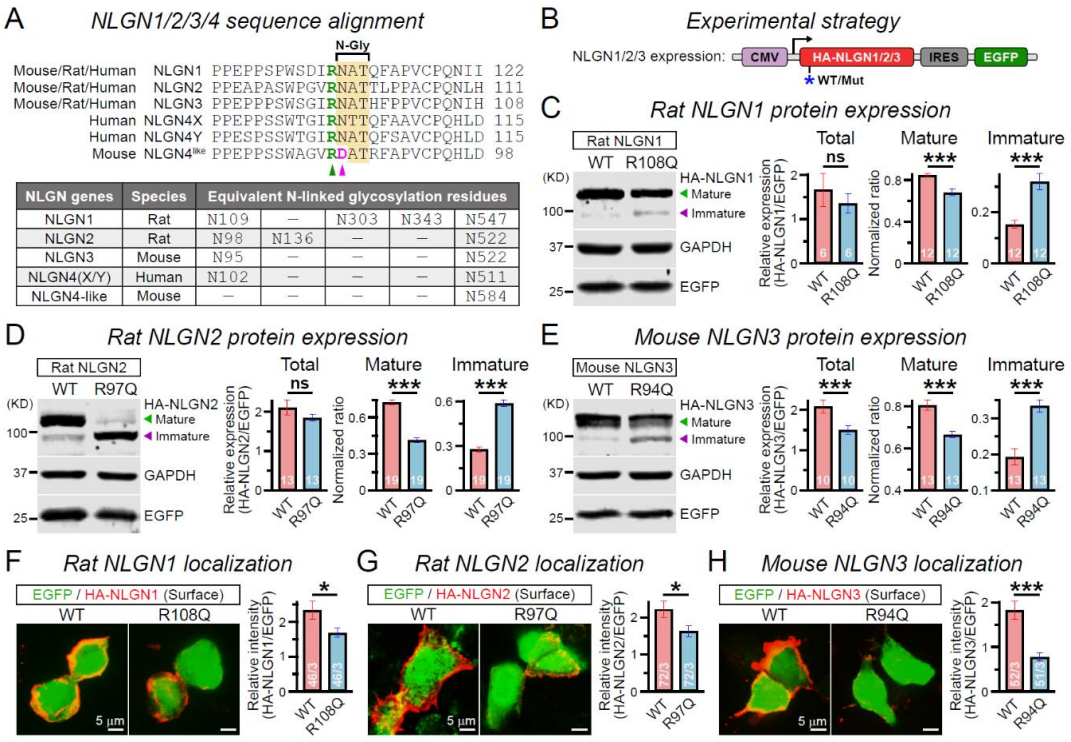

Figure 2.4: **R101Q-equivalent mutations similarly affect maturation and surface trafficking of all NLGNs.** (Generated in collaboration with Daniel Boesch)

A. Sequence alignment (top) of mouse/rat/human versions of NLGN1/2/3/4X/4Y indicate a conserved arginine residue (green arrowhead) followed by an asparagine glycosylation site (N-Gly) in all NLGNs, except in mouse NLGN4 that contains an aspartate residue instead (pink arrowhead). No NLGN4 homolog was identified in rat. The table (bottom) lists all comparable N-linked glycosylation sites of NLGN1/2/3/4 from different species.

B. Strategy for expressing HA-tagged NLGN1/2/3 with or without the R101Q-equivalent mutations (for details, see Materials and Methods).

C. Representative immunoblot (left) and normalized ratios (right) of HA-tagged mature (green arrowhead) vs. immature (purple arrowhead) NLGN1 products extracted from HEK293 cells expressing rat NLGN1 WT or R108Q mutant proteins. EGFP and GAPDH were respectively used as transfection control and loading control.

D-E. Same as **C**, except for rat NLGN2 containing R97Q mutation (**D**), and mouse NLGN3 containing R94Q mutation (**E**).

F-H. Sample images (left) represent immunostaining of HA-tagged NLGNs under non-permeabilized conditions in HEK293 cells co-expressing IRES-driven EGFP, and summary-graphs (right) of HA-NLGN signal intensity relative to EGFP, for rat NLGN1 WT vs. R108Q mutant (**F**), rat NLGN2 WT vs. R97Q mutant (**G**), and mouse NLGN3 WT vs. R94Q mutant (**H**).

All summary data are presented as means ± SEM, with total number of independent replicates (**C-E**) or field-of-views (**F-H**) / number of experimental batches. Statistical significance was assessed by two-tailed, paired (**C-E**) or unpaired (**F-H**), Student's t-test, with *** $P < 0.005$; * $P < 0.05$.

while a decrease in total protein expression was only observed for NLGN3-R94Q (Fig. 2.4E). Interestingly, we observed a unique banding pattern for each RQ variant protein (See Fig. 2.4C vs. D vs. E). Seeing that the effects of RQ mutation on protein maturation were present in NLGN1/2/3, we hypothesized that surface expression defects would be as well.

As with NLGN4, we transfected coverslip-seeded HEK cells with WT or RQ variants of HA-NLGN1/2/3, staining for surface localized HA epitope under non-permeabilized conditions. When normalized to EGFP expression, we noticed a significant decrease in surface localized NLGN protein upon the introduction of RQ mutation for each isoform. Of note, the most profound effect on surface expression was observed for NLGN3-R94Q. NLGN3, like NLGN4, contains only two N-linked glycosylation sites, while NLGN1 and NLGN2 contain these two sites and also two or one unique glycosylation sites, respectively (Fig. 2.4A). If, as we hypothesize, the effects of RQ mutation are indeed mediated through impaired glycan addition or maturation at the directly adjacent Asn, this could suggest a compensatory effect of other N-glycan sites for the secretory trafficking of NLGN proteins, discussed in Chapter 2.

3.3.4 R101Q Mutation Exclusively Impairs Glutamatergic Synaptogenic Effects of Overexpressed NLGN4

NLGN proteins are critical regulators of synaptic maturation, interacting with the presynapse via NRXN binding and postsynaptically regulating neurotransmitter receptors (Comoletti et al., 2003; Budreck and Scheiffele, 2007; Giannone et al., 2013; Elegheert et al., 2017). While genetic knockout of NLGNs in mice does not reduce the formation of synapses (Varoqueaux et al., 2006; Chanda et al., 2017), NLGN overexpression is well known to induce presynaptic morphologies (Scheiffele et al., 2000; Ko et al., 2009; Letellier et al., 2018). Most of these studies have utilized the reliable model system of primary mouse neuron culture, which is appropriate for examining the well-conserved NLGN1, 2, and 3. However, the role of human NLGN4 protein has only been minimally characterized and remains somewhat controversial,

especially in the context of human neurons (Bemben et al., 2015; Marro et al., 2019). So, to assess the impact of the NLGN4-R101Q variant on human synapse morphology, we turned to a well-established method of neuronal differentiation from hESCs: SMAD pathway inhibition (Chambers et al., 2009). Small molecules that inhibit activin receptor-like kinase (ALK) receptors on the surface of hESCs were added to the culture medium, and after 7 days hESCs differentiated into neural stem cells (NSCs; Fig. 2.5A, C). Following the subsequent addition of AraC to select for post-mitotic cells, NSCs spontaneously differentiated into neurons of a variety of subtypes. 30 days post differentiation, we added lentivirus encoding HA-NLGN4-WT/R101Q preceding an IRES-GFP, all driven by the human synapsin-1 (hSyn1) promoter, or hSyn1-EGFP alone as a negative control (Fig. 2.5B). Then, 60 days after initiating differentiation, we fixed cells for immunofluorescent staining.

First, NLGN4-WT and -R101Q-infected cultures were immunostained for Tuj1 and synapsin to determine whether the introduction of R101Q mutation impacted neuronal viability or synapse formation. While there was no difference in the number of cell bodies per field or total volume of Tuj1-positive neurites per cell body (Fig. 2.5D), we did observe a significant decrease (~50%) in overall synapsin intensity for R101Q variant-infected culture vs. WT, normalized to total Tuj1 (Fig. 2.5D). Scrutinizing the morphology of synapsin puncta, we observed that the density of synapsin-positive presynapses decreased from >4 to ~2 μm^{-1} while puncta area on maximum-projection images decreased from ~0.6 to ~0.45 μm^2 (Fig. 2.5E).

Synapsin is expressed at both glutamatergic and GABAergic presynapses, and so the observed decreases in size and density of synapsin could indicate changes in either excitatory or inhibitory synapse morphology. So, we next immunostained control, NLGN4-WT or NLGN4-R101Q cultures for either vesicular GABA transporter (vGAT) or vesicular glutamate transporter (vGLUT) to respectively mark GABAergic or glutamatergic presynapses, each co-immunostained for the dendritic marker MAP2**.** Overexpression of both NLGN4-WT and-R101Q

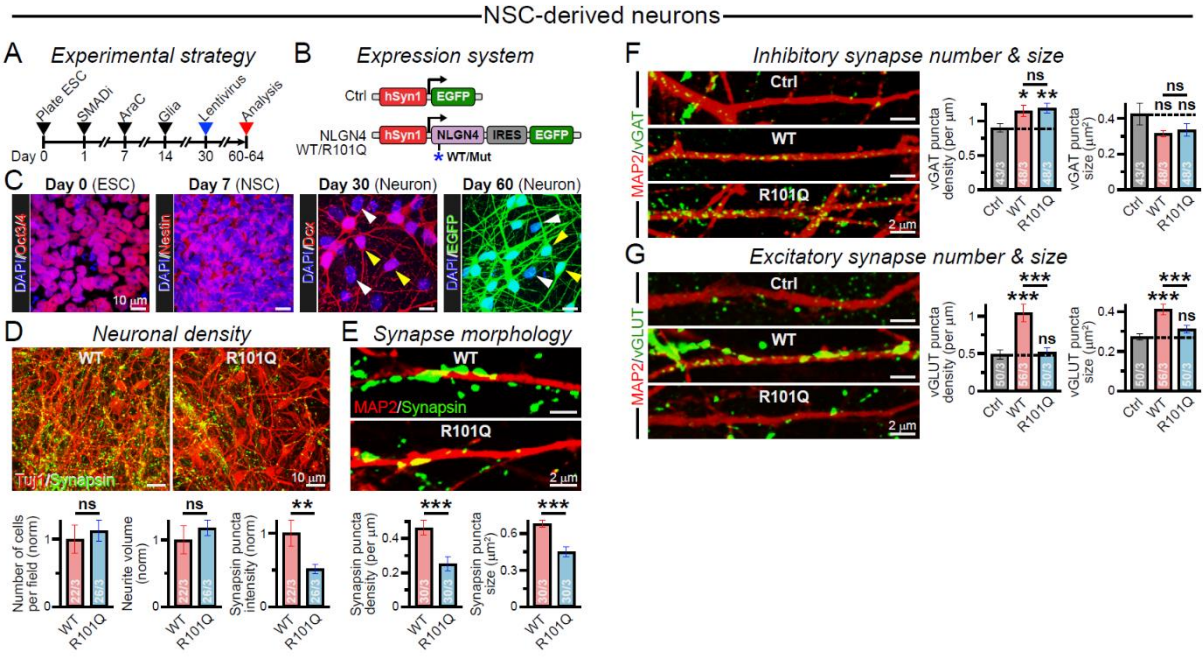

Figure 2.5: **R101Q mutation inhibits NLGN4-induced excitatory synapse formation in NSC-derived human neurons.** (Generated in collaboration with Soham Chanda)

A. NSCs were induced from H1-ES cells by dual-SMAD inhibition. The NSC-derived neurons were co-cultured with glia, infected with lentivirus expressing transgenes, and analyzed at indicated time-points (arrowheads).

B. Design of lentiviral vectors expressing NLGN4 WT or R101Q variant under hSyn1 promoter followed by an IRES-EGFP construct. An EGFP-only vector was used as infection control (Ctrl).

C. Images illustrate cellular identities, when immunolabeled for ES cell marker (Oct3/4), NSC marker (Nestin), or neuronal marker (Dcx), at different stages of the differentiation protocol. DAPI was used for nuclear stain. At day 60, elaborate neuronal morphology was confirmed by EGFP signal. Arrowheads point at neurons (yellow) and glial cells (white) in the culture.

D. Sample images (top) depict NSC-derived neurons expressing NLGN4 WT vs. R101Q variant, when immunostained for cytoskeletal marker Tuj1 and synaptic marker Synapsin. Bar-graphs (below) represent normalized counts of cell bodies per field-of-view (left), total neurite volume (middle), and integrated signal intensity of Synapsin (right), for WT vs. R101Q conditions.

E. Representative images (top) of MAP2-positive dendritic segments counterstained for Synapsin, and summary graphs (bottom) of the density and size of Synapsin puncta, as quantified from cells expressing NLGN4 WT vs. R101Q mutant.

F. Example images (left) of MAP2-positive dendritic branches from cells in control, NLGN4 WT and R101Q mutant conditions, as counterstained for an inhibitory synapse marker vGAT. Summary graphs (right) of the density and size of vGAT puncta.

G. Same as **F**, except the neurons were immunolabeled for vGLUT, an excitatory synapse marker.

(Fig. 2.5 cont.)

Averages indicate mean ± SEM, with total number of field-of-views analyzed / number of batches. Statistical significance was tested by two-tailed, unpaired, Student's t-test, with *** $P < 0.005$; ** $P < 0.01$; * $P < 0.05$; ns = not significant, $P > 0.05$.

in these cultures slightly increased the density of vGAT puncta while minorly but non-significantly reducing the average size of these puncta to approximately the same degree (Fig. 2.5F). Therefore, changes in synapsin intensity cannot be due to any difference in GABAergic synapse morphology between NLGN4-WT or -R101Q-infected cultures. Instead, vGLUT immunostaining revealed that the greatest difference between these NLGN4 variants was their respective consequences for glutamatergic synapses. Compared to control, NLGN4-WT overexpression doubled vGLUT puncta density from ~0.5 to ~1 μm^{-1}. The size of vGLUT puncta likewise increased from <0.3 to ~0.4 μm^2. Contrarily, overexpression of the R101Q variant resulted in no significant change in vGLUT puncta density or size compared to control (Fig. 2.5G). Thus, human NLGN4 affects glutamatergic synapse morphology to a greater extent than GABAergic in human neurons, and this effect is dramatically reduced for the R101Q variant.

3.3.5 R101Q Mutation Reduces NLGN4-Mediated Synaptogenesis in Ngn2-induced Neurons

In order to strictly address the effects of NLGN4-R101Q at excitatory synapses, we utilized a different protocol to generate human neurons. hESCs were directly differentiated into a monoculture of glutamatergic neurons through ectopic expression of the transcription factor neurogenin-2 (Ngn2), and simultaneously infected with control or NLGN4-WT/R101Q lentivirus (Fig. 2.6A). To first establish whether NLGN4-WT or -R101Q overexpression altered neuronal morphology in this cell type, we analyzed the density of neurons, soma size, primary neurite numbers, and average neurite length, finding no significant difference between NLGN4-WT/R101Q-overexpressing cultures and control (Fig. 2.6B-C). To first validate that Ngn2-neurons infected with NLGN4 constructs expressed similar quantities of mRNA we utilized RT-qPCR. NLGN4 mRNA levels in cells expressing either the WT or R101Q variant were equivalent, each roughly ten-fold higher than endogenous NLGN4 mRNA detected in control cells (Fig. 2.6D).

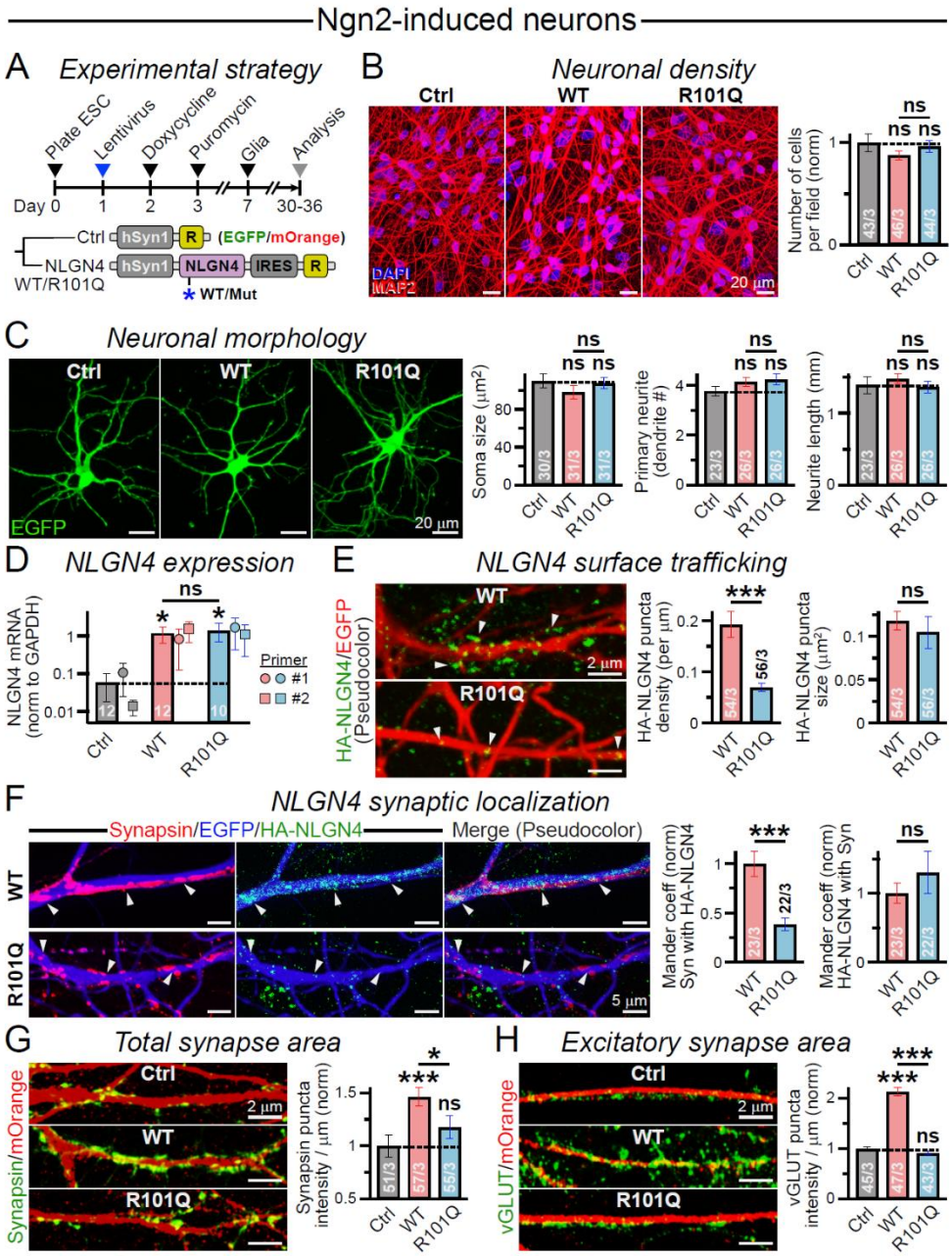

Figure 2.6: **R101Q mutation impairs NLGN4's surface localization and inhibits NLGN4-mediated synaptogenesis in Ngn2-induced neurons.** (Generated in collaboration with Soham Chanda)

A. Neurogenesis was induced in H1-ES cells by ectopic expression of Ngn2 using high-titre lentivirus, cells were selected using puromycin, and co-cultured with mouse glia for an extended period (timeline, top). In addition, cells were also sparsely infected with lower-titre lentiviruses expressing either a control vector or HA-tagged NLGN4 WT vs. R101Q variant under hSyn1 promoter (abbreviated construct maps, bottom), each followed by an IRES-EGFP or IRES-mOrange reporter (R).

(Fig. 2.6 cont.)

B. Representative images (left) depict Ngn2-induced neurons co-infected with lentivirus expressing a control vector, or NLGN4 WT vs. R101Q variant, when immunostained for dendritic marker MAP2; bar-graph (right) represents normalized counts of cell bodies per field-of-view.

C. Representative images (left) of Ngn2-induced human neurons expressing either a control vector or NLGN4 WT vs. R101Q variant, as their morphological parameters were assessed using an EGFP reporter. Summary graphs (right) of soma size, primary dendrite number, and average neurite length per cell.

D. NLGN4 mRNA levels were estimated by qRT-PCR and normalized to those of GAPDH (internal control) for Ngn2-induced neurons expressing either a control vector, or NLGN4 WT vs. R101Q mutant constructs. The average bar-graphs combine values from two independent primer sets (set #1 [circles; n = 6 Ctrl, 6 WT, and 5 for R101Q] and set #2 [squares; n = 6 Ctrl, 6 WT, and 5 for R101Q]).

E. Sample images (left) of EGFP-expressing dendritic segments (pseudo-colored for better visibility) from NLGN4 WT (top) vs. R101Q (bottom) conditions, when immunostained with anti-HA antibody (arrowheads) under non-permeabilized state. Summary graphs (right) of surface HA-NLGN4 puncta density and size.

F. Representative images (left) of EGFP-labeled dendritic segments from WT (top) vs. R101Q (bottom) conditions, when incubated with anti-HA antibody under non-permeabilized state, then permeabilized and co-immunostained with Synapsin antibody. The channel-colors were artificially reassigned to provide better visibility for synaptic signals; arrowheads point at synaptic puncta. Summary graphs (right) indicate synaptic distribution of NLGN4, characterized using normalized Mander's co-localization coefficients between HA-NLGN4 and Synapsin signals.

G-H. Dendritic sections of mOrange-expressing human neurons from control, NLGN4 WT, and NLGN4 R101Q conditions immunostained with either Synapsin (**E**, left) or vGLUT (**F**, left) antibody, and integrated intensity of Synapsin (**E**, right) or vGLUT (**F**, right) puncta normalized with respect to the dendrite length.

Average bar-graphs represent means ± SEM, with number of frames analyzed / number of experiments, or only the number of independent batches (for **B**). Statistical significance was assessed by two-tailed, unpaired (one-tailed and paired for **B**), Student's t-test, with *** $P < 0.005$; * $P < 0.05$; ns = not significant, $P > 0.05$.

Having verified equivalent mRNA expression, we next fixed and immunostained NLGN4-infected cultures with HA antibody under non-permeabilized conditions to detect surface-localized HA-NLGN4. Having observed both decreased surface expression in HEK cells and weakened glutamatergic synaptogenesis in hESC-differentiated neurons, we expected to detect less NLGN4-R101Q on cell surface than WT. Indeed, surface-localized NLGN4-R101Q diminished compared to the WT variant, with puncta density dropping from ~0.2 to ~0.05 μm^{-1} upon introduction of the mutation. However, the average size of HA-NLGN4-WT vs. -R101Q puncta remained unchanged (Fig. 2.6E). Co-staining these cultures for synapsin, we found that the fraction of synapsin puncta colocalized with HA-NLGN4 was decreased by over half for the R101Q mutant vs. WT, as expected with the NLGN4-R101Q variant's surface expression defects. However, the fraction of surface HA-NLGN4 that colocalized with synapsin was not reduced by R101Q mutation (Fig. 2.6F). These results indicate that in human neurons, the surface expression of NLGN4-R101Q is reduced dramatically compared to WT. However, when considering the relative expression of NLGN4 protein at the cell surface, what NLGN4-R101Q that does make it to the plasma membrane is not impaired in its own recruitment to synapses as evidenced by equivalent puncta sizes and relative colocalization with synapsin.

Finally, we aimed to characterize the respective impacts on pre- and post-synaptic morphologies by NLGN4-WT and NLGN4-R101Q in these cells. We immunostained control, NLGN4-WT or -R101Q-infected cultures for synapsin and vGLUT. Overexpression of NLGN4-WT, but not -R101Q, robustly increased both synapsin and vGLUT intensity compared to control (Fig. 2.6G-H), as observed in NSC-derived neurons. Altogether, these data demonstrate that NLGN4-R101Q is a loss-of-function variant. Due to increased retention in the ER and a correlating defect in glycan maturation, the R101Q variant is poorly trafficked to cell surfaces compared to WT and exerts a dramatically reduced influence on excitatory synaptic morphologies.

3.4 Discussion

Numerous mutations associated with ID and ASD have been identified in the NLGN4X gene. Among these are copy number variations, chromosomal deletion, and nonsense mutations (Jamain et al., 2003; Laumonnier et al., 2004; Chocholska et al., 2006; Lawson-Yuen et al., 2008; Zhang et al., 2009), clearly indicating that a lack of NLGN4 protein is causative for these conditions. However, many mutations identified among patients with autism include missense mutations, with ambiguous effects on the molecular characteristics of NLGN4 protein (Yan et al., 2005; Xu et al., 2014; Nguyen et al., 2020). The work presented in this chapter characterized the impacts of one such missense mutation, p.Arg101Gln. The R101Q mutation causes impaired N-glycan maturation of NLGN4, evidenced by an increase in the EndoH-sensitive fraction and a corresponding decrease in mature, EndoH-resistant protein (Fig. 2.3C-D). Further, the NLGN4-R101Q variant is retained in the secretory pathway (Fig. 2.3E-F), failing to express on the surface of both heterologous cells and neurons to the extent of NLGN4-WT (Figs. 2.2D, 2.6E). The primary characteristics of NLGN4-R101Q appear to be consistent with WT, however. We observed no significant impact of the mutation on NLGN4 homodimerization (Fig. 2.2E), and NRXN interaction also remains largely unchanged save for decreases expected due to trafficking defects (Fig. 2.2H-J). This molecular phenotype is distinct from another well-characterized ASD-association point mutant, NLGN4-R87W, which is misfolded and tagged for degradation by the ER-associated degradation pathway (Zhang et al., 2009). NLGN4-R101Q protein expression is only slightly reduced compared to WT (Fig. 2.2C), which does not account for the >60% loss of NLGN4-R101Q at cell surfaces vs. WT (Figs. 2.2D, 2.6E).

3.4.1 NLGN4-R101Q Synaptogenic Properties are Impaired Through Reduced Surface Expression

In human neurons, the R101Q variant fails to produce the synaptic effects of the WT protein. We observed that overexpression of NLGN4-WT induced glutamatergic synaptogenesis

in two different neuron culture types, matching the reported synaptic preference of endogenous NLGN4 in humans (Marro et al., 2019). NLGN4-R101Q surface expression is impaired in neurons (Fig. 2.6E), and as such, we observe decreased excitatory synaptogenesis in Ngn2-induced and NSC-derived human neurons expressing the R101Q mutant vs. WT (Figs. 2.5G, 2.6H). These data support the conclusion that NLGN4, like NLGN1, primarily affects human glutamatergic synapses, in contrast to the evolutionarily divergent mouse NLGN4-*like*, which is mainly associated with inhibitory glycinergic or GABAergic synapses (Hoon et al., 2011; Unichenko et al., 2018). This highlights the importance of a human neuronal system when characterizing NLGN4-related mechanisms, especially for potential knock-in or knock-out studies.

While NLGN4, like NLGN1, localizes to glutamatergic postsynapses, recent data suggests they may impart different molecular and functional effects. Earlier studies found that overexpression of NLGN4 in a human neuronal context increases the density of excitatory synapse markers (Marro et al., 2019), which we corroborate here (Fig. 2.5G, 2.6H), and which matches the synaptic morphological phenotype of NLGN1 overexpression (Letellier et al., 2018; Letellier et al., 2020). However, unlike NLGN1, Marro et. al. found that NLGN4 overexpression reduced the frequency of miniature excitatory postsynaptic currents (mEPSC) from ~4 to ~2 Hz. Evoked AMPAR amplitude was similarly decreased. While our data and those of Marro et. al. were collected in a WT background, in a NLGN1-3 knock-down background, NLGN4 overexpression increases mESPC frequency from 0 to ~2 Hz (Bemben et al., 2015; Nguyen et al., 2020). Therefore, it is likely that while NLGN1 and NLGN4 both induce presynaptic formation when overexpressed, NLGN4 recruitment of AMPARs is weaker than that of NLGN1, and the two may potentially compete for positioning at excitatory postsynapses. In the context of the R101Q mutation, the results presented in this dissertation would suggest that NLGN4-

R101Q attenuation of AMPAR recruitment would be impaired as a result of reduced surface localization, and indeed we found this to be the case (Cast et al., 2021).

3.4.2 RQ Mutations Reduce NLGN Glycoprotein Maturation of Each Isoform

Regardless of the potential interplay between NLGN isoforms at synapses, the NLGN4-R101Q mutation induces a loss-of-function phenotype through a mechanism conserved in other NLGN isoforms. The NLGN4 R101 residue is directly adjacent to an N-linked glycosylation sequon, N102. This glycosylation site, as well as the upstream Arg residue, is conserved in NLGN1-3 (Fig. 2.4A). Equivalent RQ mutations introduced in NLGN1-3 altered protein characteristics similarly to NLGN4-R101Q, i.e. reducing surface expression and glycoprotein maturation (Fig. 2.4B-H). This would indicate a common quality of NLGN1-4 that the RQ mutation disrupts. Chapter 2 of this dissertation described how N-glycosylation Site I (i.e. NLGN4-N102), adjacent to the conserved Arg residue, regulates secretory export and subsequent presynaptic recruitment for each NLGN isoform.

Given the conserved sequences of NLGN1-4 near N-glycan Site I and the striking similarities between RQ mutation and N-glycan Site I alanine substitution (compare Figs. 1.2D and 2.4D, NLGN2-R97Q and NLGN2-N98A), these mutations likely converge on a mechanism resulting in both reduced glycoprotein maturation and ER export of NLGN protein. Due to the co-translational nature of N-linked glycan modification by the ER oligosaccharyltransferase (OST) complex, the efficiency of polysaccharide transfer by both STT3A and STT3B is known to be influenced by upstream amino acid residues (Gavel and von Heijne, 1990; Wormald et al., 2002; Ben-Dor et al., 2004; Petrescu et al., 2004; Murray et al., 2015; Hülsmeier et al., 2016; Huang et al., 2017). Therefore, it is not unlikely that upstream ASD-associated mutations such as R101Q could reduce glycan occupancy of N102.

CHAPTER 4: CONCLUSIONS AND FUTURE DIRECTIONS

The incorporation of synaptic cell-adhesion molecules (SCAMs) into electrochemical synapses acts to regulate the molecular composition and coordination of the pre- and postsynapse, which are both crucial for maintaining proper synaptic signaling (Meyer et al., 2004; Batool et al., 2019; Südhof, 2021). In this dissertation, I have shown how N-linked glycosylation of the NLGN family of SCAMs regulates the proteins' surface expression by influencing their export from the ER. While mutagenic deletion of certain individual N-glycosylated residues impacted NLGN surface expression (Fig. 1.6A-D), complete inhibition of N-linked glycosylation sites greatly reduced NLGNs' surface expression (Figs. 1.2K-L, 1.7). This implies a cumulative effect of N-glycosylation in enhancing the secretory export of these proteins. Of the two conserved N-glycan sites in the NLGN family, only the mutation of one (i.e., Site I) consistently reduced all major NLGN isoforms' surface export and recruitment of presynapses (Fig. 1.6). Thus, while not a master regulator of NLGN export, N-glycan Site I holds universal importance in promoting the surface export of NLGN proteins.

An ASD-associated NLGN4 variant, NLGN4-R101Q, exhibits strikingly similar characteristics to the NLGN4 Site I mutant, namely reduced surface localization and a reduction in higher-mass EndoH-insensitive population of NLGN4 protein (Fig. 2.2). The mutated R101 residue is directly adjacent to NLGN4's N-glycan Site I, at residue N102, and just as Site I is conserved in all human NLGN isoforms, so is this Arg residue. Analogous RQ mutations made in NLGN1, NLGN2, and NLGN3 expressed in HEK cells confer defects in glycoprotein maturation and surface expression similar to the isoforms' respective Site I mutations (Fig. 2.4). In a neuronal context, overexpression of NLGN4-R101Q fails to induce excitatory synaptogenesis as observed for overexpression of NLGN4-WT due to drastically reduced surface levels (Fig. 2.5F-G). However, the percentage of surface-expressed NLGN4-R101Q that

is colocalized with presynapses is no different than that of the WT variant (Fig. 2.6F). This again indicates that the major phenotype of this variant is decreased surface localization, and not relative assignment to synapses when the protein is successfully trafficked to the cell surface. Experiments in Chapter 2 of this dissertation strongly suggest that the initial addition of N-glycans, inhibited by both tunicamycin (Tm) treatment and alanine-substitution of glycosylated residues (Figs. 1.2, 1.7), is a critical determinant of NLGN surface expression. Given the similar characteristics of NLGN4-N102A and NLGN4-R101Q, and of NLGN1-3 Site I and RQ mutants, I hypothesize that RQ mutation of NLGNs impairs initial N-linked glycosylation of Site I, which consequentially reduces the proteins' surface expression.

4.1 Occupancy of N-glycan Site I in NLGN4-R101Q

Although technically independent of the N-linked glycosylation consensus sequon, it is plausible that the R101 residue of NLGN4 could influence the glycan occupancy of N102. The partially non-overlapping substrate specificities of the mutually exclusive catalytic subunits of the OST complex, STT3A and STT3B, indicate that N-glycan site occupancy is dependent on more than simply the presence of the consensus sequon (Shrimal et al., 2013; Shrimal et al., 2015; Cherepanova and Gilmore, 2016; Cherepanova et al., 2019). Generally, an upstream aromatic residue often augments N-glycosylation efficiency of a particular site, although the strength of this effect appears to depend on the initial efficiency of the sequon (Ben-Dor et al., 2004; Huang et al., 2017). Structural analyses have also revealed roles for accessory proteins in mediating glycan transfer in a sequence-dependent manner. Tusc3, an accessory subunit of STT3B-OST complexes, forms a transient disulfide bond with Cys residues of the peptide substrate up or downstream of the N-glycosylation site (Schulz et al., 2009; Mohorko et al., 2014). This facilitates STT3B-mediated glycosylation by sequestering and partially relaxing the structure of the nascent peptide. However, while it is possible that RQ mutation could impact glycan transfer efficiency by altering OST interaction with the peptide substrate, without data linking RQ

mutation to a lack of N-glycan occupancy, our current findings only confirm a correlative relationship between such mutations and glycoprotein maturation and surface expression. Should RQ mutant NLGNs also exhibit decreased Site I occupancy, then this would likely be the mechanism by which the surface expression of RQ mutants is impaired, opening possible avenues for therapeutic care of patients with such mutations.

The simplest test for glycan site occupancy of NLGN mutants is enzymatic cleavage followed by protein sequencing via mass spectrometry (Hülsmeier et al., 2007; Hülsmeier et al., 2016). When the glycosidase PNGaseF cleaves N-linked glycans from the amino acid chain, the nitrogen atom of the Asn residue is removed as well, converting the residue to an Asp. Thus, to probe glycan site occupancy, lysate from differentiated human neurons expressing NLGN4-WT, -R101Q, or -N102A could be treated with PNGaseF, then NLGN peptides could be purified via an HA tag and sequenced. The respective ratios of Asp- to Asn-containing fragmented peptides would reveal the relative glycan occupancy of any predicted N-glycosylated site throughout the protein. This technique could be used to probe whether R101Q mutation inhibits N-linked glycosylation of Sites I or V, and whether the absence of a glycan at Site I (i.e., N102A mutation) affects the glycan occupancy of Site V. This procedure could also be expanded to include a surface biotinylation step. If it is the case that R101Q mutation of NLGN4 reduces glycosylation of N102, perhaps the population of NLGN4 that does localize properly to cell surfaces is predominantly glycosylated at this residue, while NLGN4 retained intracellularly is not.

An additional set of experiments to analyze the influence of R101Q mutation for NLGN4 N-glycan occupancy could be knockdown of the two catalytic subunits of the OST complex, STT3A and STT3B. These have partially non-overlapping substrate specificity; STT3A preferentially glycosylates nascent peptides as they are translocated into the ER, while STT3B is thought to mostly glycosylate peptides post-translationally as they are undergoing the folding

process (Cherepanova and Gilmore, 2016; Cherepanova et al., 2019). If RQ mutation does indeed reduce the ability of STT3A and/or STT3B to glycosylate NLGN4 as a substrate, then I would predict that the elimination of one or both of these subunits would minimally impact NLGN4-R101Q surface expression. In other words, should NLGN4 be preferentially glycosylated at N102 by either catalytic subunit, then expression of NLGN4-R101Q or -N102A in STT3A/B knockdown cells would have a redundant effect on overall NLGN4 surface expression. In this case, we would also expect that NLGN4-WT expressed in a STT3A/B knockdown context would be reduced in surface expression and glycoprotein maturation, similarly to the N102A variant. Alternatively, STT3A and B could overlap in glycosyltransferase activity for NLGN4 residue N102. Should this be the case, NLGN4-WT would likely be efficiently trafficked to cell surfaces in the context of individual STT3A or STT3B knockdown, but be retained in the ER when both subunits are knocked down.

4.2 Deciphering the Varied Maturation of NLGN1 in Mouse Brain

While the intricacies of the neuronal secretory pathway are not yet fully understood, it has become clear that some transmembrane proteins are able to bypass the Golgi, trafficking directly from the ER to the cell membrane (Hanus et al., 2016; Bowen et al., 2017). Among these unconventionally trafficked proteins are AMPAR subunits GluA1 and GluA2 (Tucholski et al., 2014; Hanus et al., 2016; Kennedy and Hanus, 2019). NLGN1, on the other hand, is likely obligated to traffic through the Golgi apparatus before localizing to the plasma membrane in cultured mouse hippocampal neurons (Bourke et al., 2021). In this dissertation, glycosidase analysis of NLGN1 expressed throughout the mouse brain revealed differential populations of sialic acid-modified NLGN1 in the cortex and hippocampus vs. the cerebellum and hindbrain (Fig. 1.1). Considering that the literature suggests NLGN1 follows the canonical secretory pathway in neurons, I hypothesize that reduced modification by sialic acid in the cerebellum and hindbrain of adult mice corresponds to reduced surface expression of NLGN1 in these regions.

Quantification of endogenous NLGN1 surface trafficking *in vivo* would not be a trivial task. While antibodies against NLGN1 exist (See Fig. 1.1), they are relatively weak and somewhat nonspecific. Thus, immunofluorescent staining of mouse brain slices for endogenous NLGN1 and comparing surface vs. total signal intensities, while perhaps the most straightforward route of analysis, is largely unfeasible. Utilizing a mouse line with an epitope tag knocked into the NLGN1 locus, however, could effectively be used for an experiment of this sort. An alternative and more straightforward method to probe for endogenous surface levels of NLGN1 could be comparative surface biotinylation of organotypic cultured mouse brain slices (Gabriel et al., 2014; Heise et al., 2018). Similar to experiments in Fig. 1.7, surface biotinylation and internal vs. surface protein population separation could be performed with cultured slices of mouse cortex, hippocampus, or cerebellum. Following elution and population separation, analysis of surface vs. internal levels of NLGN1 via quantitative Western blot would reveal whether surface localization of NLGN1 in these regions corresponds to maturation levels observed in Fig. 1.1. This experiment could be expanded further by the use of glycosidases to probe for glycan modifications of surface and internal NLGN1. EndoH, in particular, would reveal whether NLGN1 is required to traffic through the Golgi before reaching the cell surface throughout multiple brain regions, as observed in cultured mouse neurons (Hanus et al., 2016; Bowen et al., 2017).

4.3 Influence of N-glycosylation Toward NLGN-NRXN Molecular Interaction

One question that remains is the degree to which N-linked glycosylation directly affects the binding of NRXN with NLGN2, 3, or 4. Earlier studies have conclusively shown that for NLGN1, it is predominantly the glycosylation of residue N303 that reduces its interaction with NRXN1β through steric hindrance (Comoletti et al., 2003; Boucard et al., 2005; Chih et al., 2006). We confirmed this in our experiments: despite NLGN1-N303A trafficking to HEK cell surfaces at 50% of the intensity of WT, artificial synapse formation assays showed that HEK

cells expressing NLGN1-WT or -N303A recruit presynapses to the same degree (Fig. 1.6). The major downside to both the artificial synapse and cell aggregation assays is that interaction of NLGN isoforms with NRXN in these experiments depends on the surface availability of the NLGN protein. While we observed decreases in synapse recruitment and aggregate formation with complete mutagenic deletion of N-glycan sites, trafficking defects supersede any changes in molecular interaction.

The most straightforward assay to probe for any changes in NLGN-NRXN interaction conferred by N-glycan site deletion would be similar to the already performed artificial synapse recruitment assay, but with the additional counterstain for HA-tagged NLGNs. Normalizing the degree of presynaptic recruitment to surface levels of NLGN would provide a more direct assessment of the ability of that NLGN variant to interact with presynaptic NRXNs. HEK cells expressing the NLGN constructs could be co-cultured with a variety of neuronal subtypes, including reprogrammed human neurons or primary mouse hippocampal neurons. Beyond this alteration to the artificial synapse assay, more biochemical approaches would be required to evaluate changes in NLGN-NRXN interaction affinity as a result of glycan site deletion.

Early studies utilized recombinant NLGN1 and NRXN1β extracellular domains (ECDs) expressed and purified from HEK cells in surface plasmon resonance (SPR) analysis (Comoletti et al., 2003). While SPR would yield the most accurate measure of NLGN-NRXN affinities, an alternative approach could be a quantitative pull-down assay. HA-tagged NLGN ECDs could be bound at varying concentrations to anti-HA beads, then incubated with free NRXN ECD and pelleted (Pollard, 2010). Quantification of the free NRXN ECD remaining in the supernatant would reveal the binding affinity between the NLGN and NRXN isoforms. However, the dissociation constants (K_D) for bound NRXN and NLGN isoforms are fairly low (30-100 nM; Comoletti et al., 2003; Leone et al., 2010). initial concentrations of NRXN for this assay would need to be below the K_D, and final concentrations of free NRXN would be lower still (Pollard,

2010; Lapetina and Gil-Henn, 2017). To quantify the remaining NRXN, a colloidal Coomassie gel stain could be utilized, which has a detection limit down to ~5 ng per band, significantly lower than the standard 30 ng per band of traditional Coomassie stains (Dyballa and Metzger, 2009). Alternatively, introducing an additional epitope tag to the NRXN ECD construct could allow for quantitative immunoblotting of the unbound NRXN remaining in the supernatant.

Overall, while mechanistic and detailed inquiries could still be pursued, the initial N-linked glycosylation of NLGNs is critical for the expression of NLGNs on the cell surface. Autism-associated mutations proximal to the conserved N-glycan Site I may inhibit its initial glycosylation, as suggested by the glycoprotein maturation and surface expression phenotypes of both NLGN4-R101Q and NLGN4-N102A, and of analogous mutations in NLGN1-3. Moreover, while it remains unclear whether NLGNs are explicitly required to traffic through the Golgi in each region of the brain, it is possible that sialidase sensitivity in Fig. 1.1, like insensitivity to EndoH, could indicate differences in NLGN1 secretory trafficking in these regions. Lastly, it remains unclear the extent to which N-linked glycosylation affects the molecular interactions of NLGN2, 3, and 4 with NRXN beyond the indirect effects imposed by trafficking defects.

In summary of this dissertation, N-linked glycosylation controls glycoprotein maturation and ER export of all four major NLGN isoforms in humans. While insubstantially affecting protein stability or the ability of NLGN proteins to interact with NRXN, N-glycosylation indirectly promotes the availability of NLGNs to interact with the presynapses by regulating the proteins' secretory trafficking. This effect is convergent on that of an ASD-associated variant, NLGN4-R101Q, which is also improperly glycosylated and mistrafficked. For the proband in whom this mutation was discovered, reduced availability of the R101Q variant vs. WT is likely causative for their autistic phenotype by disrupting the E/I balance of the CNS through altered abundance of AMPARs at excitatory postsynapses (Marro et al., 2019; Cast et al., 2021). The loss-of-function

phenotype of NLGN4-R101Q results in reduced excitatory synaptogenesis in both spontaneously differentiated and TF-induced human neurons. And based on both pharmacological inhibition of N-glycan maturation and alanine substitution of N102, it is likely that the R101Q variant impairs the initial transfer of the polysaccharide to N102.

REFERENCES

Aman MG (1994) Aberrant Behavior Checklist. Community (ABC).

An H, Gip P, Kim J, Wu S, Park K, McVaugh C, Schaffer D, Bertozzi C, Lebrilla C (2012) Extensive determination of glycan heterogeneity reveals an unusual abundance of high mannose glycans in enriched plasma membranes of human embryonic stem cells. Molecular & cellular proteomics : MCP 11.

Antonelli R, Pizzarelli R, Pedroni A, Fritschy J-M, Del Sal G, Cherubini E, Zacchi P (2014) Pin1-dependent signalling negatively affects GABAergic transmission by modulating neuroligin2/gephyrin interaction. Nature Communications 5:5066.

Arac D, Boucard AA, Ozkan E, Strop P, Newell E, Sudhof TC, Brunger AT (2007) Structures of neuroligin-1 and the neuroligin-1/neurexin-1 beta complex reveal specific protein-protein and protein-Ca2+ interactions. Neuron 56:992-1003.

Banerjee A, Lang J-Y, Hung M-C, Sengupta K, Banerjee SK, Baksi K, Banerjee DK (2011) Unfolded Protein Response Is Required in nu/nu Mice Microvasculature for Treating Breast Tumor with Tunicamycin. Journal of Biological Chemistry 286:29127-29138.

Batool S, Raza H, Zaidi J, Riaz S, Hasan S, Syed NI (2019) Synapse formation: from cellular and molecular mechanisms to neurodevelopmental and neurodegenerative disorders. Journal of Neurophysiology 121:1381-1397.

Beaudet AL (2007) Autism: highly heritable but not inherited. In: Nat Med, pp 534-536. United States.

Bemben MA, Nguyen QA, Wang T, Li Y, Nicoll RA, Roche KW (2015) Autism-associated mutation inhibits protein kinase C-mediated neuroligin-4X enhancement of excitatory synapses. Proc Natl Acad Sci U S A 112:2551-2556.

Bemben MA, Shipman SL, Hirai T, Herring BE, Li Y, Badger JD, Nicoll RA, Diamond JS, Roche KW (2014) CaMKII phosphorylation of neuroligin-1 regulates excitatory synapses. Nature Neuroscience 17:56-64.

Ben-Ari Y (2002) Excitatory actions of gaba during development: the nature of the nurture. Nature Reviews Neuroscience 3:728-739.

Ben-Dor S, Esterman N, Rubin E, Sharon N (2004) Biases and complex patterns in the residues flanking protein N-glycosylation sites. Glycobiology 14.

Bhide GP, Colley KJ (2017) Sialylation of N-glycans: mechanism, cellular compartmentalization and function. Histochemistry and Cell Biology 147:149-174.

Bieberich E (2014) Synthesis, Processing, and Function of N-glycans in N-glycoproteins. In: Advances in Neurobiology, pp 47-70: Springer New York.

Biederer T, Kaeser PS, Blanpied TA (2017) Transcellular Nanoalignment of Synaptic Function. Neuron 96:680-696.

Bliss TVP, Collingridge GL (1993) A synaptic model of memory: long-term potentiation in the hippocampus. Nature 361:31-39.

Blundell J, Blaiss CA, Etherton MR, Espinosa F, Tabuchi K, Walz C, Bolliger MF, Südhof TC, Powell CM (2010) Neuroligin-1 Deletion Results in Impaired Spatial Memory and Increased Repetitive Behavior. The Journal of Neuroscience 30:2115-2129.

Bolliger MF, Pei J, Maxeiner S, Boucard AA, Grishin NV, Sudhof TC (2008) Unusually rapid evolution of Neuroligin-4 in mice. Proc Natl Acad Sci U S A 105:6421-6426.

Boucard AA, Chubykin AA, Comoletti D, Taylor P, Südhof TC (2005) A Splice Code for trans-Synaptic Cell Adhesion Mediated by Binding of Neuroligin 1 to α- and β-Neurexins. Neuron 48:229-236.

Bourke AM, Schwartz SL, Bowen AB, Kleinjan MS, Winborn CS, Kareemo DJ, Gutnick A, Schwarz TL, Kennedy MJ (2021) zapERtrap: A light-regulated ER release system reveals unexpected neuronal trafficking pathways. Journal of Cell Biology 220.
Bowen AB, Bourke AM, Hiester BG, Hanus C, Kennedy MJ (2017) Golgi-independent secretory trafficking through recycling endosomes in neuronal dendrites and spines. eLife 6.
Bruining H, Hardstone R, Juarez-Martinez EL, Sprengers J, Avramiea A-E, Simpraga S, Houtman SJ, Poil S-S, Dallares E, Palva S, Oranje B, Matias Palva J, Mansvelder HD, Linkenkaer-Hansen K (2020) Measurement of excitation-inhibition ratio in autism spectrum disorder using critical brain dynamics. Scientific Reports 10.
Budreck EC, Scheiffele P (2007) Neuroligin-3 is a neuronal adhesion protein at GABAergic and glutamatergic synapses. Eur J Neurosci 26:1738-1748.
Burrows EL, May C, Hill T, Churliov L, Johnson KA, Hannan AJ (2022) Mice with an autism-associated R451C mutation in neuroligin-3 show a cautious but accurate response style in touchscreen attention tasks. Genes, Brain and Behavior 21.
Burrows EL, Laskaris L, Koyama L, Churilov L, Bornstein JC, Hill-Yardin EL, Hannan AJ (2015) A neuroligin-3 mutation implicated in autism causes abnormal aggression and increases repetitive behavior in mice. Molecular Autism 6.
Burrows EL, Eastwood AF, May C, Kolbe SC, Hill T, Mclachlan NM, Churilov L, Hannan AJ (2017) Social Isolation Alters Social and Mating Behavior in the R451C Neuroligin Mouse Model of Autism. Neural Plasticity 2017:1-9.
Camporesi E, Lashley T, Gobom J, Lantero-Rodriguez J, Hansson O, Zetterberg H, Blennow K, Becker B (2021) Neuroligin-1 in brain and CSF of neurodegenerative disorders: investigation for synaptic biomarkers. Acta Neuropathologica Communications 9.
Capano V, Herrmann HJ, De Arcangelis L (2015) Optimal percentage of inhibitory synapses in multi-task learning. Scientific Reports 5:9895.
Cast TP, Boesch DJ, Smyth K, Shaw AE, Ghebrial M, Chanda S (2021) An Autism-Associated Mutation Impairs Neuroligin-4 Glycosylation and Enhances Excitatory Synaptic Transmission in Human Neurons. The Journal of Neuroscience 41:392-407.
Chambers SM, Fasano CA, Papapetrou EP, Tomishima M, Sadelain M, Studer L (2009) Highly efficient neural conversion of human ES and iPS cells by dual inhibition of SMAD signaling. Nat Biotechnol 27:275-280.
Chanda S, Aoto J, Lee SJ, Wernig M, Sudhof TC (2016) Pathogenic mechanism of an autism-associated neuroligin mutation involves altered AMPA-receptor trafficking. Mol Psychiatry 21:169-177.
Chanda S, Hale WD, Zhang B, Wernig M, Sudhof TC (2017) Unique versus Redundant Functions of Neuroligin Genes in Shaping Excitatory and Inhibitory Synapse Properties. J Neurosci 37:6816-6836.
Chanda S, Ang CE, Lee QY, Ghebrial M, Haag D, Shibuya Y, Wernig M, Sudhof TC (2019) Direct Reprogramming of Human Neurons Identifies MARCKSL1 as a Pathogenic Mediator of Valproic Acid-Induced Teratogenicity. Cell Stem Cell 25:103-119.e106.
Chang IJ, He M, Lam CT (2018) Congenital disorders of glycosylation. Annals of Translational Medicine 6:477-477.
Chang Y-H, Weng C-L, Lin K-I (2020) O-GlcNAcylation and its role in the immune system. Journal of Biomedical Science 27.
Chen C, Lee P, Liao H, Chang P (2017) Neuroligin 2 R215H Mutant Mice Manifest Anxiety, Increased Prepulse Inhibition, and Impaired Spatial Learning and Memory. Frontiers in psychiatry 8.
Cherepanova N, Shrimal S, Gilmore R (2016) N-linked glycosylation and homeostasis of the endoplasmic reticulum. Current Opinion in Cell Biology 41:57-65.

Cherepanova NA, Gilmore R (2016) Mammalian cells lacking either the cotranslational or posttranslocational oligosaccharyltransferase complex display substrate-dependent defects in asparagine linked glycosylation. Scientific Reports 6:20946.
Cherepanova NA, Venev SV, Leszyk JD, Shaffer SA, Gilmore R (2019) Quantitative glycoproteomics reveals new classes of STT3A- and STT3B-dependent N-glycosylation sites. Journal of Cell Biology 218:2782-2796.
Chih B, Gollan L, Scheiffele P (2006) Alternative Splicing Controls Selective Trans-Synaptic Interactions of the Neuroligin-Neurexin Complex. Neuron 51:171-178.
Chmielewska JJ, Kuzniewska B, Milek J, Urbanska K, Dziembowska M (2019) Neuroligin 1, 2, and 3 Regulation at the Synapse: FMRP-Dependent Translation and Activity-Induced Proteolytic Cleavage. Molecular Neurobiology 56:2741-2759.
Chocholska S, Rossier E, Barbi G, Kehrer-Sawatzki H (2006) Molecular cytogenetic analysis of a familial interstitial deletion Xp22.2-22.3 with a highly variable phenotype in female carriers. Am J Med Genet A 140:604-610.
Colgan LA, Yasuda R (2014) Plasticity of Dendritic Spines: Subcompartmentalization of Signaling. Annual Review of Physiology 76:365-385.
Comoletti D (2004) The Arg451Cys-Neuroligin-3 Mutation Associated with Autism Reveals a Defect in Protein Processing. Journal of Neuroscience 24:4889-4893.
Comoletti D, Flynn R, Jennings LL, Chubykin A, Matsumura T, Hasegawa H, Sudhof TC, Taylor P (2003) Characterization of the Interaction of a Recombinant Soluble Neuroligin-1 with Neurexin-1beta. J Biol Chem 278:50497-50505.
Constantino JN (2005) Social Responsiveness Scale™.
Constantino JN (2012) Social Responsiveness Scale, Second Edition.
Crosby KC, Gookin SE, Garcia JD, Hahm KM, Dell'Acqua ML, Smith KR (2019) Nanoscale Subsynaptic Domains Underlie the Organization of the Inhibitory Synapse. Cell Reports 26:3284-3297.e3283.
Crowder JM, Croucher MJ, Bradford HF, Collins JF (1987) Excitatory amino acid receptors and depolarization-induced Ca2+ influx into hippocampal slices. J Neurochem 48:1917-1924.
Dahlhaus R, Hines R, Eadie B, Kannangara T, Hines D, Brown C, Christie B, El-Husseini A (2010) Overexpression of the cell adhesion protein neuroligin-1 induces learning deficits and impairs synaptic plasticity by altering the ratio of excitation to inhibition in the hippocampus. Hippocampus 20.
De Jaco A, Lin MZ, Dubi N, Comoletti D, Miller MT, Camp S, Ellisman M, Butko MT, Tsien RY, Taylor P (2010) Neuroligin Trafficking Deficiencies Arising from Mutations in the α/β-Hydrolase Fold Protein Family. Journal of Biological Chemistry 285:28674-28682.
Diering GH, Huganir RL (2018) The AMPA Receptor Code of Synaptic Plasticity. Neuron 100:314-329.
DSM-V APA (2013) Diagnostic and statistical manual of mental disorders - V, 5 Edition. Washington, DC: American Psychiatric Association.
Dufort-Gervais J, Provost C, Charbonneau L, Norris CM, Calon F, Mongrain V, Brouillette J (2020) Neuroligin-1 is altered in the hippocampus of Alzheimer's disease patients and mouse models, and modulates the toxicity of amyloid-beta oligomers. Scientific Reports 10.
Durieux A, J H, Petrinovic M (2016) Neuroligin-2 and the tightrope of excitation/inhibition balance in the prefrontal cortex. Journal of neurophysiology 115.
Dyballa N, Metzger S (2009) Fast and Sensitive Colloidal Coomassie G-250 Staining for Proteins in Polyacrylamide Gels. Journal of Visualized Experiments.
Elegheert J, Cvetkovska V, Clayton AJ, Heroven C, Vennekens KM, Smukowski SN, Regan MC, Jia W, Smith AC, Furukawa H, Savas JN, De Wit J, Begbie J, Craig AM, Aricescu AR (2017) Structural Mechanism for Modulation of Synaptic Neuroligin-Neurexin Signaling by MDGA Proteins. Neuron 95:896-913.e810.

Etherton M, Foldy C, Sharma M, Tabuchi K, Liu X, Shamloo M, Malenka RC, Sudhof TC (2011) Autism-linked neuroligin-3 R451C mutation differentially alters hippocampal and cortical synaptic function. Proceedings of the National Academy of Sciences 108:13764-13769.
Fabrichny IP, Leone P, Sulzenbacher G, Comoletti D, Miller MT, Taylor P, Bourne Y, Marchot P (2007) Structural Analysis of the Synaptic Protein Neuroligin and Its β-Neurexin Complex: Determinants for Folding and Cell Adhesion. Neuron 56:979-991.
Ferris SP, Kodali VK, Kaufman RJ (2014) Glycoprotein folding and quality-control mechanisms in protein-folding diseases. Disease Models & Mechanisms 7:331-341.
Fogel AI, Akins MR, Krupp AJ, Stagi M, Stein V, Biederer T (2007) SynCAMs Organize Synapses through Heterophilic Adhesion. The Journal of Neuroscience 27:12516-12530.
Fogel AI, Li Y, Giza J, Wang Q, Lam TT, Modis Y, Biederer T (2010) N-Glycosylation at the SynCAM (Synaptic Cell Adhesion Molecule) Immunoglobulin Interface Modulates Synaptic Adhesion. Journal of Biological Chemistry 285:34864-34874.
Fries GR, Saldana VA, Finnstein J, Rein T (2023) Molecular pathways of major depressive disorder converge on the synapse. Molecular Psychiatry 28:284-297.
Friligou I, Gassner J, Knoblauch D, Kagerer G, Popp F, Voit S, Engel AM, Leinenbach A, Steffen W, Haberger M, Tabarés G (2021) Glycosylation of recombinant rabbit immunoglobulins influences protease susceptibility as shown by comprehensive mass spectrometric glycan analysis. Glycobiology 31:762-771.
Fritschy J (2008) Epilepsy, E/I Balance and GABA(A) Receptor Plasticity. Frontiers in molecular neuroscience 1.
Fukata Y, Dimitrov A, Boncompain G, Vielemeyer O, Perez F, Fukata M (2013) Local palmitoylation cycles define activity-regulated postsynaptic subdomains. Journal of Cell Biology 202:145-161.
Fukata Y, Chen X, Chiken S, Hirano Y, Yamagata A, Inahashi H, Sanbo M, Sano H, Goto T, Hirabayashi M, Kornau H-C, Prüss H, Nambu A, Fukai S, Nicoll RA, Fukata M (2021) LGI1–ADAM22–MAGUK configures transsynaptic nanoalignment for synaptic transmission and epilepsy prevention. Proceedings of the National Academy of Sciences 118:e2022580118.
Gabriel L, Wu S, Melikian H (2014) Brain slice biotinylation: an ex vivo approach to measure region-specific plasma membrane protein trafficking in adult neurons. Journal of visualized experiments : JoVE.
Gallagher JT, Morris A, Dexter TM (1985) Identification of two binding sites for wheat-germ agglutinin on polylactosamine-type oligosaccharides. Biochemical Journal 231:115-122.
Gangwar SP, Zhong X, Seshadrinathan S, Chen H, Machius M, Rudenko G (2017) Molecular Mechanism of MDGA1: Regulation of Neuroligin 2:Neurexin Trans-synaptic Bridges. Neuron 94:1132-1141.e1134.
Gassmann M, Bettler B (2012) Regulation of neuronal GABAB receptor functions by subunit composition. Nature Reviews Neuroscience 13:380-394.
Gavel Y, von Heijne G (1990) Sequence differences between glycosylated and non-glycosylated Asn-X-Thr/Ser acceptor sites: implications for protein engineering. Protein engineering 3.
Giannone G, Mondin M, Grillo-Bosch D, Tessier B, Saint-Michel E, Czöndör K, Sainlos M, Choquet D, Thoumine O (2013) Neurexin-1β Binding to Neuroligin-1 Triggers the Preferential Recruitment of PSD-95 versus Gephyrin through Tyrosine Phosphorylation of Neuroligin-1. Cell Reports 3:1996-2007.
Giovedí S, Corradi A, Fassio A, Benfenati F (2014) Involvement of synaptic genes in the pathogenesis of autism spectrum disorders: the case of synapsins. Frontiers in pediatrics 2.

Gizaw ST, Koda T, Amano M, Kamimura K, Ohashi T, Hinou H, Nishimura S-I (2015) A comprehensive glycome profiling of Huntington's disease transgenic mice. Biochimica et Biophysica Acta (BBA) - General Subjects 1850:1704-1718.
Glessner J et al. (2009) Autism genome-wide copy number variation reveals ubiquitin and neuronal genes. Nature 459.
Glozman R, Okiyoneda T, Mulvihill CM, Rini JM, Barriere H, Lukacs GL (2009) N-glycans are direct determinants of CFTR folding and stability in secretory and endocytic membrane traffic. Journal of Cell Biology 184:847-862.
Graf ER, Zhang X, Jin S-X, Linhoff MW, Craig AM (2004) Neurexins Induce Differentiation of GABA and Glutamate Postsynaptic Specializations via Neuroligins. Cell 119:1013-1026.
Guang S, Pang N, Deng X, Yang L, He F, Wu L, Chen C, Yin F, Peng J (2018) Synaptopathology Involved in Autism Spectrum Disorder. Frontiers in cellular neuroscience 12.
Haas KT, Compans B, Letellier M, Bartol TM, Grillo-Bosch D, Sejnowski TJ, Sainlos M, Choquet D, Thoumine O, Hosy E (2018) Pre-post synaptic alignment through neuroligin-1 tunes synaptic transmission efficiency. eLife 7.
Halff E, Hannan S, Kwanthongdee J, Lesept F, Smart T, Kittler J (2022) Phosphorylation of neuroligin-2 by PKA regulates its cell surface abundance and synaptic stabilization. Science signaling 15.
Halff EF, Szulc BR, Lesept F, Kittler JT (2019) SNX27-Mediated Recycling of Neuroligin-2 Regulates Inhibitory Signaling. Cell Reports 29:2599-2607.e2596.
Hanus C, Geptin H, Tushev G, Garg S, Alvarez-Castelao B, Sambandan S, Kochen L, Hafner A-S, Langer JD, Schuman EM (2016) Unconventional secretory processing diversifies neuronal ion channel properties. eLife 5.
Heise C, Preuss J, Schroeder J, Battaglia C, Kolibius J, Schmid R, Kreutz M, Kas M, Burbach J, Boeckers T (2018) Heterogeneity of Cell Surface Glutamate and GABA Receptor Expression in Shank and CNTN4 Autism Mouse Models. Frontiers in molecular neuroscience 11.
Helenius A, Aebi M (2004) Roles of N-Linked Glycans in the Endoplasmic Reticulum. Annual Review of Biochemistry 73:1019-1049.
Herscovics A (1999) Importance of glycosidases in mammalian glycoprotein biosynthesis. Biochimica et biophysica acta 1473.
Heupel K, Sargsyan V, Plomp JJ, Rickmann M, Varoqueaux F, Zhang W, Krieglstein K (2008) Loss of transforming growth factor-beta 2 leads to impairment of central synapse function. Neural Development 3:25.
Hines RM, Wu L, Hines DJ, Steenland H, Mansour S, Dahlhaus R, Singaraja RR, Cao X, Sammler E, Hormuzdi SG, Zhuo M, El-Husseini A (2008) Synaptic Imbalance, Stereotypies, and Impaired Social Interactions in Mice with Altered Neuroligin 2 Expression. Journal of Neuroscience 28:6055-6067.
Hodgkin AL, Huxley AF (1952a) The components of membrane conductance in the giant axon of *Loligo*. The Journal of Physiology 116:473-496.
Hodgkin AL, Huxley AF (1952b) The dual effect of membrane potential on sodium conductance in the giant axon of *Loligo*. The Journal of Physiology 116:497-506.
Hodgkin AL, Huxley AF (1952c) Currents carried by sodium and potassium ions through the membrane of the giant axon of *Loligo*. The Journal of Physiology 116:449-472.
Hoffman RC, Jennings LL, Tsigelny I, Comoletti D, Flynn RE, Sudhof TC, Taylor P (2004) Structural Characterization of Recombinant Soluble Rat Neuroligin 1: Mapping of Secondary Structure and Glycosylation by Mass Spectrometry. Biochemistry 43:1496-1506.
Hoon M, Soykan T, Falkenburger B, Hammer M, Patrizi A, Schmidt KF, Sassoe-Pognetto M, Lowel S, Moser T, Taschenberger H, Brose N, Varoqueaux F (2011) Neuroligin-4 is

localized to glycinergic postsynapses and regulates inhibition in the retina. Proc Natl Acad Sci U S A 108:3053-3058.
Hu X, Luo J-H, Xu J (2015) The Interplay between Synaptic Activity and Neuroligin Function in the CNS. BioMed Research International 2015:1-13.
Huang Y-W, Yang H-I, Wu Y-T, Hsu T-L, Lin T-W, Kelly JW, Wong C-H (2017) Residues Comprising the Enhanced Aromatic Sequon Influence Protein N-Glycosylation Efficiency. Journal of the American Chemical Society 139:12947-12955.
Huganir L, Richard, Nicoll A, Roger (2013) AMPARs and Synaptic Plasticity: The Last 25 Years. Neuron 80:704-717.
Hülsmeier AJ, Paesold-Burda P, Hennet T (2007) N-Glycosylation Site Occupancy in Serum Glycoproteins Using Multiple Reaction Monitoring Liquid Chromatography-Mass Spectrometry. Molecular & Cellular Proteomics 6:2132-2138.
Hülsmeier AJ, Tobler M, Burda P, Hennet T (2016) Glycosylation site occupancy in health, congenital disorder of glycosylation and fatty liver disease. Scientific Reports 6:33927.
Ichtchenko K, Hata Y, Nguyen T, Ullrich B, Missler M, Moomaw C, Sudhof TC (1995) Neuroligin 1: a splice site-specific ligand for beta-neurexins. Cell 81:435-443.
Irie M, Hata Y, Takeuchi M, Ichtchenko K, Toyoda A, Hirao K, Takai Y, Rosahl TW, Sudhof TC (1997) Binding of neuroligins to PSD-95. Science 277:1511-1515.
Isaacson S, Jeffry, Scanziani M (2011) How Inhibition Shapes Cortical Activity. Neuron 72:231-243.
Jacob TC, Moss SJ, Jurd R (2008) GABAA receptor trafficking and its role in the dynamic modulation of neuronal inhibition. Nature Reviews Neuroscience 9:331-343.
Jaeken J, Matthijs G (2007) Congenital Disorders of Glycosylation: A Rapidly Expanding Disease Family. Annual Review of Genomics and Human Genetics 8:261-278.
Jamain S, Quach H, Betancur C, Råstam M, Colineaux C, Gillberg IC, Soderstrom H, Giros B, Leboyer M, Gillberg C, Bourgeron T (2003) Mutations of the X-linked genes encoding neuroligins NLGN3 and NLGN4 are associated with autism. Nature Genetics 34:27-29.
Jeong J, Paskus JD, Roche KW (2017) Posttranslational modifications of neuroligins regulate neuronal and glial signaling. Current Opinion in Neurobiology 45:130-138.
Jiang D-Y, Wu Z, Forsyth CT, Hu Y, Yee S-P, Chen G (2018) GABAergic deficits and schizophrenia-like behaviors in a mouse model carrying patient-derived neuroligin-2 R215H mutation. Molecular Brain 11.
Johnston G (1996) GABAA receptor pharmacology. Pharmacology & therapeutics 69.
Ju A, Hammerschmidt K, Tantra M, Krueger D, Brose N, Ehrenreich H (2014) Juvenile manifestation of ultrasound communication deficits in the neuroligin-4 null mutant mouse model of autism. Behav Brain Res 270:159-164.
Kandel MB, Yamamoto S, Midorikawa R, Morise J, Wakazono Y, Oka S, Takamiya K (2018) N-glycosylation of the AMPA-type glutamate receptor regulates cell surface expression and tetramer formation affecting channel function. Journal of Neurochemistry 147:730-747.
Kennedy MJ, Hanus C (2019) Architecture and Dynamics of the Neuronal Secretory Network. Annual Review of Cell and Developmental Biology 35:543-566.
Kim J, Jung S-Y, Lee YK, Park S, Choi J-S, Lee CJ, Kim H-S, Choi Y-B, Scheiffele P, Bailey CH, Kandel ER, Kim J-H (2008) Neuroligin-1 is required for normal expression of LTP and associative fear memory in the amygdala of adult animals. Proceedings of the National Academy of Sciences 105:9087-9092.
Klarić TS, Lauc G (2022) The dynamic brain N-glycome. Glycoconjugate Journal 39:443-471.
Ko J, Zhang C, Arac D, Boucard AA, Brunger AT, Südhof TC (2009) Neuroligin-1 performs neurexin-dependent and neurexin-independent functions in synapse validation. The EMBO Journal 28:3244-3255.

Koehnke J, Katsamba PS, Ahlsen G, Bahna F, Vendome J, Honig B, Shapiro L, Jin X (2010) Splice Form Dependence of β-Neurexin/Neuroligin Binding Interactions. Neuron 67:61-74.
Lam NH, Borduqui T, Hallak J, Roque A, Anticevic A, Krystal JH, Wang X-J, Murray JD (2022) Effects of Altered Excitation-Inhibition Balance on Decision Making in a Cortical Circuit Model. The Journal of Neuroscience 42:1035-1053.
Lapetina S, Gil-Henn H (2017) A guide to simple, direct, and quantitative in vitro binding assays. Journal of Biological Methods 4:e62.
Laumonnier F, Bonnet-Brilhault F, Gomot M, Blanc R, David A, Moizard MP, Raynaud M, Ronce N, Lemonnier E, Calvas P, Laudier B, Chelly J, Fryns JP, Ropers HH, Hamel BC, Andres C, Barthelemy C, Moraine C, Briault S (2004) X-linked mental retardation and autism are associated with a mutation in the NLGN4 gene, a member of the neuroligin family. Am J Hum Genet 74:552-557.
Lawson-Yuen A, Saldivar JS, Sommer S, Picker J (2008) Familial deletion within NLGN4 associated with autism and Tourette syndrome. Eur J Hum Genet 16:614-618.
Leone P, Comoletti D, Ferracci G, Conrod S, Garcia SU, Taylor P, Bourne Y, Marchot P (2010) Structural insights into the exquisite selectivity of neurexin/neuroligin synaptic interactions. The EMBO Journal 29:2461-2471.
Letellier M, Lagardère M, Tessier B, Janovjak H, Thoumine O (2020) Optogenetic control of excitatory post-synaptic differentiation through neuroligin-1 tyrosine phosphorylation. eLife 9.
Letellier M, Szíber Z, Chamma I, Saphy C, Papasideri I, Tessier B, Sainlos M, Czöndör K, Thoumine O (2018) A unique intracellular tyrosine in neuroligin-1 regulates AMPA receptor recruitment during synapse differentiation and potentiation. Nature Communications 9.
Li L, Guan W, Zhang G, Wu Z, Yu H, Chen X, Wang P (2020) Microarray analyses of closely related glycoforms reveal different accessibilities of glycan determinants on N-glycan branches. Glycobiology 30.
Lichnerova K, Kaniakova M, Park SP, Skrenkova K, Wang Y-X, Petralia RS, Suh YH, Horak M (2015) Two N-glycosylation Sites in the GluN1 Subunit Are Essential for Releasing N-methyl-d-aspartate (NMDA) Receptors from the Endoplasmic Reticulum. Journal of Biological Chemistry 290:18379-18390.
Liu H, Gaza-Bulseco G, Xiang T, Chumsae C (2008) Structural effect of deglycosylation and methionine oxidation on a recombinant monoclonal antibody. Molecular immunology 45.
Liu Y, Ouyang P, Zheng Y, Mi L, Zhao J, Ning Y, Guo W (2021) A Selective Review of the Excitatory-Inhibitory Imbalance in Schizophrenia: Underlying Biology, Genetics, Microcircuits, and Symptoms. Frontiers in cell and developmental biology 9.
Lizak C, Gerber S, Numao S, Aebi M, Locher KP (2011) X-ray structure of a bacterial oligosaccharyltransferase. Nature 474:350-355.
Lu W, Shi Y, Jackson AC, Bjorgan K, During MJ, Sprengel R, Seeburg PH, Nicoll RA (2009) Subunit composition of synaptic AMPA receptors revealed by a single-cell genetic approach. Neuron 62:254-268.
MacGillavry D, Harold, Song Y, Raghavachari S, Blanpied A, Thomas (2013) Nanoscale Scaffolding Domains within the Postsynaptic Density Concentrate Synaptic AMPA Receptors. Neuron 78:615-622.
Maenner MJ et al. (2023) Prevalence and Characteristics of Autism Spectrum Disorder Among Children Aged 8 Years — Autism and Developmental Disabilities Monitoring Network, 11 Sites, United States, 2020. MMWR Surveillance Summaries 72:1-14.
Marro SG, Chanda S, Yang N, Janas JA, Valperga G, Trotter J, Zhou B, Merrill S, Yousif I, Shelby H, Vogel H, Kalani MYS, Südhof TC, Wernig M (2019) Neuroligin-4 Regulates Excitatory Synaptic Transmission in Human Neurons. Neuron 103:617-626.e616.

Maxeiner S, Benseler F, Brose N, Krasteva-Christ G (2022) Of Humans and Gerbils-Independent Diversification of Neuroligin-4 Into X- and Y-Specific Genes in Primates and Rodents. Frontiers in molecular neuroscience 15.
Maxeiner S, Benseler F, Krasteva-Christ G, Brose N, Sudhof TC (2020) Evolution of the Autism-Associated Neuroligin-4 Gene Reveals Broad Erosion of Pseudoautosomal Regions in Rodents. Mol Biol Evol.
Melikian H, Ramamoorthy S, Tate C, Blakely R (1996) Inability to N-glycosylate the human norepinephrine transporter reduces protein stability, surface trafficking, and transport activity but not ligand recognition. Molecular pharmacology 50.
Meyer D, Bonhoeffer T, Scheuss V (2014) Balance and Stability of Synaptic Structures during Synaptic Plasticity. Neuron 82:430-443.
Meyer G, Varoqueaux F, Neeb A, Oschlies M, Brose N (2004) The complexity of PDZ domain-mediated interactions at glutamatergic synapses: a case study on neuroligin. Neuropharmacology 47:724-733.
Micheva KD, Busse B, Weiler NC, O'Rourke N, Smith SJ (2010) Single-Synapse Analysis of a Diverse Synapse Population: Proteomic Imaging Methods and Markers. Neuron 68:639-653.
Missler M, Sudhof TC, Biederer T (2012) Synaptic Cell Adhesion. Cold Spring Harbor Perspectives in Biology 4:a005694-a005694.
Mitra N, Sinha S, Ramya T, Surolia A (2006) N-linked oligosaccharides as outfitters for glycoprotein folding, form and function. Trends in biochemical sciences 31.
Mohorko E, Owen L, Robin, Malojčić G, Brozzo S, Maurice, Aebi M, Glockshuber R (2014) Structural Basis of Substrate Specificity of Human Oligosaccharyl Transferase Subunit N33/Tusc3 and Its Role in Regulating Protein N-Glycosylation. Structure 22:590-601.
Mondin M, Labrousse V, Hosy E, Heine M, Tessier B, Levet F, Poujol C, Blanchet C, Choquet D, Thoumine O (2011) Neurexin-neuroligin adhesions capture surface-diffusing AMPA receptors through PSD-95 scaffolds. J Neurosci 31:13500-13515.
Monteiro P, Feng G (2017) SHANK proteins: roles at the synapse and in autism spectrum disorder. Nature Reviews Neuroscience 18:147-157.
Moremen KW, Tiemeyer M, Nairn AV (2012) Vertebrate protein glycosylation: diversity, synthesis and function. Nature Reviews Molecular Cell Biology 13:448-462.
Morise J, Yamamoto S, Midorikawa R, Takamiya K, Nonaka M, Takematsu H, Oka S (2020) Distinct Cell Surface Expression Patterns of N-Glycosylation Site Mutants of AMPA-Type Glutamate Receptor under the Homo-Oligomeric Expression Conditions. International Journal of Molecular Sciences 21:5101.
Murray N, Amber, Chen W, Antonopoulos A, Hanson R, Sarah, Wiseman L, R., Dell A, Haslam M, Stuart, Powers L, David, Powers T, Evan, Kelly W, Jeffery (2015) Enhanced Aromatic Sequons Increase Oligosaccharyltransferase Glycosylation Efficiency and Glycan Homogeneity. Chemistry & Biology 22:1052-1062.
Nakanishi M, Nomura J, Ji X, Tamada K, Arai T, Takahashi E, Bućan M, Takumi T (2017) Functional significance of rare neuroligin 1 variants found in autism. PLoS genetics 13.
Nguyen Q-A, Horn ME, Nicoll RA (2016) Distinct roles for extracellular and intracellular domains in neuroligin function at inhibitory synapses. eLife 5.
Nguyen TA, Wu K, Pandey S, Lehr AW, Li Y, Bemben MA, Badger JDI, Lauzon JL, Wang T, Zaghloul KA, Thurm A, Jain M, Lu W, Roche KW (2020) A Cluster of Autism-Associated Variants on X-Linked NLGN4X Functionally Resemble NLGN4Y. Neuron 106:759- 768.
NIH GaRDIC (2023) Congenital disorders of glycosylation - About the Disease. In.
Niwa T, Uemura E, Matsuno Y, Taguchi H (2019) Translation-coupled protein folding assay using a protease to monitor the folding status. Protein Science.

Oinam L, Hayashi R, Hiemori K, Kiyoi K, Sage-Ono K, Miura K, Ono M, Tateno H (2022) Quantitative evaluation of glycan-binding specificity of recombinant concanavalin A produced in lettuce (*Lactuca sativa*). Biotechnology and Bioengineering 119:1781-1791.
Pampanos A, Volaki K, Kanavakis E, Papandreou O, Youroukos S, Thomaidis L, Karkelis S, Tzetis M, Kitsiou-Tzeli S (2009) A substitution involving the NLGN4 gene associated with autistic behavior in the Greek population. Genet Test Mol Biomarkers 13:611-615.
Parente DJ, Garriga C, Baskin B, Douglas G, Cho MT, Araujo GC, Shinawi M (2017) Neuroligin 2 nonsense variant associated with anxiety, autism, intellectual disability, hyperphagia, and obesity. American Journal of Medical Genetics Part A 173:213-216.
Park DH, Park S, Song JM, Kang M, Lee S, Horak M, Suh YH (2020) N-linked glycosylation of the mGlu7 receptor regulates the forward trafficking and transsynaptic interaction with Elfn1. The FASEB Journal 34:14977-14996.
Perova Z, Delevich K, Li B (2015) Depression of Excitatory Synapses onto Parvalbumin Interneurons in the Medial Prefrontal Cortex in Susceptibility to Stress. The Journal of Neuroscience 35:3201-3206.
Petrescu A, Milac A, Petrescu S, Dwek R, Wormald M (2004) Statistical analysis of the protein environment of N-glycosylation sites: implications for occupancy, structure, and folding. Glycobiology 14.
Pollard TD (2010) A Guide to Simple and Informative Binding Assays. Molecular Biology of the Cell 21:4061-4067.
Poulopoulos A, Soykan T, Tuffy LP, Hammer M, Varoqueaux F, Brose N (2012) Homodimerization and isoform-specific heterodimerization of neuroligins. Biochem J 446:321-330.
Poulopoulos A, Aramuni G, Meyer G, Soykan T, Hoon M, Papadopoulos T, Zhang M, Paarmann I, Fuchs C, Harvey K, Jedlicka P, Schwarzacher SW, Betz H, Harvey RJ, Brose N, Zhang W, Varoqueaux F (2009) Neuroligin 2 drives postsynaptic assembly at perisomatic inhibitory synapses through gephyrin and collybistin. Neuron 63:628-642.
Ramsey A, Tang A, LeGates T, Gou X, Carbone B, Thompson S, Biederer T, Blanpied T (2021) Subsynaptic positioning of AMPARs by LRRTM2 controls synaptic strength. Science advances 7.
Romero M, Aguilar J, Del-Rey-Mejías Á, Mayoral F, Rapado M, Peciña M, Barbancho M, Ruiz-Veguilla M, Lara J (2016) Psychiatric comorbidities in autism spectrum disorder: A comparative study between DSM-IV-TR and DSM-5 diagnosis. International journal of clinical and health psychology : IJCHP 16.
Rosnoblet C, Peanne R, Legrand D, Foulquier F (2013) Glycosylation disorders of membrane trafficking. Glycoconjugate Journal 30:23-31.
Samelson AJ, Jensen MK, Soto RA, Cate JHD, Marqusee S (2016) Quantitative determination of ribosome nascent chain stability. Proceedings of the National Academy of Sciences 113:13402-13407.
Savtchenko LP, Rusakov DA (2014) Moderate AMPA receptor clustering on the nanoscale can efficiently potentiate synaptic current. Philosophical Transactions of the Royal Society B: Biological Sciences 369:20130167.
Scheiffele P, Fan J, Choih J, Fetter R, Serafini T (2000) Neuroligin Expressed in Nonneuronal Cells Triggers Presynaptic Development in Contacting Axons. Cell 101:657-669.
Schopler E, Van Bourgondien ME (2010) Childhood Autism Rating Scale™, Second Edition.
Schulz BL, Stirnimann CU, Grimshaw JPA, Brozzo MS, Fritsch F, Mohorko E, Capitani G, Glockshuber R, Grütter MG, Aebi M (2009) Oxidoreductase activity of oligosaccharyltransferase subunits Ost3p and Ost6p defines site-specific glycosylation efficiency. Proceedings of the National Academy of Sciences 106:11061-11066.
Sebat J et al. (2007) Strong association of de novo copy number mutations with autism. Science 316:445-449.

SFARI G (2021a) NLGN4X. In.
SFARI G (2021b) NLGN1. In.
Shepherd JD, Huganir RL (2007) The cell biology of synaptic plasticity: AMPA receptor trafficking. Annu Rev Cell Dev Biol 23:613-643.
Shipman SL, Nicoll RA (2012) Dimerization of postsynaptic neuroligin drives synaptic assembly via transsynaptic clustering of neurexin. Proceedings of the National Academy of Sciences 109:19432-19437.
Shrimal S, Cherepanova NA, Gilmore R (2015) Cotranslational and posttranslocational N-glycosylation of proteins in the endoplasmic reticulum. Seminars in Cell & Developmental Biology 41:71-78.
Shrimal S, Ng BG, Losfeld M-E, Gilmore R, Freeze HH (2013) Mutations in STT3A and STT3B cause two congenital disorders of glycosylation. Human Molecular Genetics 22:4638-4645.
Song JY, Ichtchenko K, Sudhof TC, Brose N (1999) Neuroligin 1 is a postsynaptic cell-adhesion molecule of excitatory synapses. Proc Natl Acad Sci U S A 96:1100-1105.
Sparrow S, Cicchetti D, Saulnier C (2016) Vineland Adaptive Behavior Scales Third Edition, 3 Edition: Pearson.
Spence S, Schneider M (2009) The role of epilepsy and epileptiform EEGs in autism spectrum disorders. Pediatric research 65.
Stanley P (2011) Golgi Glycosylation. Cold Spring Harbor Perspectives in Biology 3:a005199-a005199.
Stanley P, Moremen K, Lewis N, Taniguchi N, Aebi M (2022) N-Glycans.
Stessman HAF et al. (2017) Targeted sequencing identifies 91 neurodevelopmental-disorder risk genes with autism and developmental-disability biases. Nature Genetics 49:515-526.
Stuart G, Spruston N, Sakmann B, Häusser M (1997) Action potential initiation and backpropagation in neurons of the mammalian CNS. Trends in neurosciences 20.
Sudhof TC (2018) Towards an Understanding of Synapse Formation. Neuron 100:276-293.
Sun C, Cheng M-C, Qin R, Liao D-L, Chen T-T, Koong F-J, Chen G, Chen C-H (2011) Identification and functional characterization of rare mutations of the neuroligin-2 gene (NLGN2) associated with schizophrenia. Human Molecular Genetics 20:3042-3051.
Südhof C, Thomas (2012) The Presynaptic Active Zone. Neuron 75:11-25.
Südhof TC (2008) Neuroligins and neurexins link synaptic function to cognitive disease. Nature 455:903-911.
Südhof TC (2021) The cell biology of synapse formation. Journal of Cell Biology 220.
Tabuchi K, Blundell J, Etherton MR, Hammer RE, Liu X, Powell CM, SüDhof TC (2007) A Neuroligin-3 Mutation Implicated in Autism Increases Inhibitory Synaptic Transmission in Mice. Science 318:71-76.
Taguchi Y, Yamasaki T, Ishikawa M, Kawasaki Y, Yukimura R, Mitani M, Hirata K, Kohda D (2021) The structure of an archaeal oligosaccharyltransferase provides insight into the strict exclusion of proline from the N-glycosylation sequon. Communications Biology 4.
Takeuchi Y, Morise J, Morita I, Takematsu H, Oka S (2015) Role of Site-Specific N-Glycans Expressed on GluA2 in the Regulation of Cell Surface Expression of AMPA-Type Glutamate Receptors. PLOS ONE 10:e0135644.
Tarentino AL, Gomez CM, Plummer TH (1985) Deglycosylation of asparagine-linked glycans by peptide:N-glycosidase F. Biochemistry 24:4665-4671.
Taylor L, Swerdfeger A, Eslick G (2014) Vaccines are not associated with autism: an evidence-based meta-analysis of case-control and cohort studies. Vaccine 32.
Toghi Eshghi S, Yang S, Wang X, Shah P, Li X, Zhang H (2014) Imaging of N-Linked Glycans from Formalin-Fixed Paraffin-Embedded Tissue Sections Using MALDI Mass Spectrometry. ACS Chemical Biology 9:2149-2156.

Troyano-Rodriguez E, Wirsig-Wiechmann CR, Ahmad M (2019) Neuroligin-2 Determines Inhibitory Synaptic Transmission in the Lateral Septum to Optimize Stress-Induced Neuronal Activation and Avoidance Behavior. Biological Psychiatry 85:1046-1055.
Tucholski J, Pinner AL, Simmons MS, Meador-Woodruff JH (2014) Evolutionarily Conserved Pattern of AMPA Receptor Subunit Glycosylation in Mammalian Frontal Cortex. PLoS ONE 9:e94255.
Tulsiani D, Harris T, Touster O (1982) Swainsonine inhibits the biosynthesis of complex glycoproteins by inhibition of Golgi mannosidase II. The Journal of biological chemistry 257.
Unichenko P, Yang JW, Kirischuk S, Kolbaev S, Kilb W, Hammer M, Krueger-Burg D, Brose N, Luhmann HJ (2018) Autism Related Neuroligin-4 Knockout Impairs Intracortical Processing but not Sensory Inputs in Mouse Barrel Cortex. Cereb Cortex 28:2873-2886.
Van den Steen P, Rudd P, Dwek R, Opdenakker G (1998) Concepts and principles of O-linked glycosylation. Critical reviews in biochemistry and molecular biology 33.
Varoqueaux F, Jamain S, Brose N (2004) Neuroligin 2 is exclusively localized to inhibitory synapses. Eur J Cell Biol 83:449-456.
Varoqueaux F, Aramuni G, Rawson RL, Mohrmann R, Missler M, Gottmann K, Zhang W, Sudhof TC, Brose N (2006) Neuroligins determine synapse maturation and function. Neuron 51:741-754.
Vitiazeva V, Kattla JJ, Flowers SA, Lindén SK, Premaratne P, Weijdegård B, Sundfeldt K, Karlsson NG (2015) The O-Linked Glycome and Blood Group Antigens ABO on Mucin-Type Glycoproteins in Mucinous and Serous Epithelial Ovarian Tumors. PLOS ONE 10:e0130197.
Wandall HH, Nielsen MAI, King-Smith S, De Haan N, Bagdonaite I (2021) Global functions of O-glycosylation: promises and challenges in O-glycobiology. The FEBS Journal 288:7183-7212.
Wang C, Ward ME, Chen R, Liu K, Tracy TE, Chen X, Xie M, Sohn PD, Ludwig C, Meyer-Franke A, Karch CM, Ding S, Gan L (2017) Scalable Production of iPSC-Derived Human Neurons to Identify Tau-Lowering Compounds by High-Content Screening. Stem Cell Reports 9:1221-1233.
Wang L, Mirabella V, Dai R, Su X, Xu R, Jadali A, Bernabucci M, Singh I, Chen Y, Tian J, Jiang P, Kwan K, Pak C, Liu C, Comoletti D, Hart R, Chen C, Südhof T, Pang Z (2022) Analyses of the autism-associated neuroligin-3 R451C mutation in human neurons reveal a gain-of-function synaptic mechanism. Molecular psychiatry.
Wilkinson H, Saldova R (2020) Current Methods for the Characterization of O-Glycans. Journal of Proteome Research 19:3890-3905.
Williams SE, Noel M, Lehoux S, Cetinbas M, Xavier RJ, Sadreyev RI, Scolnick EM, Smoller JW, Cummings RD, Mealer RG (2022) Mammalian brain glycoproteins exhibit diminished glycan complexity compared to other tissues. Nature Communications 13.
Wormald MR, Petrescu AJ, Pao Y-L, Glithero A, Elliott T, Dwek RA (2002) Conformational Studies of Oligosaccharides and Glycopeptides: Complementarity of NMR, X-ray Crystallography, and Molecular Modelling. Chemical Reviews 102:371-386.
Wu A, Wu J, Singh T, Lai L, Yang Z, Herp A (2006) Recognition factors of Ricinus communis agglutinin 1 (RCA(1)). Molecular immunology 43.
Wu X, Morishita WK, Riley AM, Hale WD, Südhof TC, Malenka RC (2019) Neuroligin-1 Signaling Controls LTP and NMDA Receptors by Distinct Molecular Pathways. Neuron 102:621-635.e623.
Xu C, Ng DTW (2015) Glycosylation-directed quality control of protein folding. Nature Reviews Molecular Cell Biology 16:742-752.
Xu X, Hu Z, Zhang L, Liu H, Cheng Y, Xia K, Zhang X (2017) Not all neuroligin 3 and 4X missense variants lead to significant functional inactivation. Brain Behav 7:e00793.

Xu X, Xiong Z, Zhang L, Liu Y, Lu L, Peng Y, Guo H, Zhao J, Xia K, Hu Z (2014) Variations analysis of NLGN3 and NLGN4X gene in Chinese autism patients. Molecular Biology Reports 41:4133-4140.
Xu-Friedman M, Regehr W (2004) Structural contributions to short-term synaptic plasticity. Physiological reviews 84.
Yan J, Oliveira G, Coutinho A, Yang C, Feng J, Katz C, Sram J, Bockholt A, Jones IR, Craddock N, Cook EH, Vicente A, Sommer SS (2005) Analysis of the neuroligin 3 and 4 genes in autism and other neuropsychiatric patients. Molecular Psychiatry 10:329-332.
Yoshida T et al. (2021) Canonical versus non-canonical transsynaptic signaling of neuroligin 3 tunes development of sociality in mice. Nature Communications 12.
Zhang C, Milunsky JM, Newton S, Ko J, Zhao G, Maher TA, Tager-Flusberg H, Bolliger MF, Carter AS, Boucard AA, Powell CM, Südhof TC (2009) A Neuroligin-4 Missense Mutation Associated with Autism Impairs Neuroligin-4 Folding and Endoplasmic Reticulum Export. The Journal of Neuroscience 29:10843-10854.
Zhang Y, Pak C, Han Y, Ahlenius H, Zhang Z, Chanda S, Marro S, Patzke C, Acuna C, Covy J, Xu W, Yang N, Danko T, Chen L, Wernig M, Südhof TC (2013) Rapid single-step induction of functional neurons from human pluripotent stem cells. Neuron 78:785-798.
Zhang Z, Yu H, Jiang S, Liao J, Lu T, Wang L, Zhang D, Yue W (2015) Evidence for Association of Cell Adhesion Molecules Pathway and NLGN1 Polymorphisms with Schizophrenia in Chinese Han Population. PLOS ONE 10:e0144719.
Zheng K, Bantog C, Bayer R (2011) The impact of glycosylation on monoclonal antibody conformation and stability. mAbs 3:568-576.
Zhu Z, Go EP, Desaire H (2014) Absolute Quantitation of Glycosylation Site Occupancy Using Isotopically Labeled Standards and LC-MS. Journal of the American Society for Mass Spectrometry 25:1012-1017.